Vol. 67 • No. 1
January 2024

Microwave® Journal

horizon house®
Founded in 1958
mwjournal.com

DC TO 86 GHz

Filter Technologies

For Every Application

Selection and Solutions

- 1500+ in-stock models
- Low pass, high pass, band pass, band stop, diplexers and triplexers
- In-house design and manufacturing capability
- Fast, affordable custom capabilities

LEARN MORE

Cavity

- Passbands to 43.5 GHz
- Stopbands to 57 GHz
- Bandwidths as narrow as 1%
- 100+ dB rejection

Ceramic Resonator

- Fractional bandwidths from 0.5 to 40%
- Excellent power handling, up to 20W
- High Q in miniature SMT package

Lumped L-C

- Wide catalog selection
- Several package options including aqueous washable
- Variety of filter topologies

LTCC

- Tiny size, as small as 0202
- Industry's widest selection of mmWave LTCC filters
- Proprietary designs with stopband rejection up to 100 dB

Microstrip

- Connectorized designs with 4 to 40% fractional bandwidth
- Power handling up to 10W
- Flat group delay

MMIC Reflectionless

- Patented topology absorbs and internally terminates stopband signals
- Perfect for pairing with amplifiers, mixers, multipliers, ADC/DACs & more
- Cascadable with other filter technologies

Rectangular Waveguide

- WR-12, WR-15 and WR-28 interfaces
- Passbands up to 87 GHz
- High stopband rejection, 40 dB

Suspended Substrate

- Ultra-wide passbands up to 26 GHz
- Wide stopbands up to 40 GHz
- High Q

Thin Film on Alumina

- Passbands from DC to 40 GHz
- High rejection with wide passband
- Miniature SMT package


RF-LAMBDA
THE LEADER OF RF BROADBAND SOLUTIONS
BROADBAND SSPA / EMC BENCHTOP
SOLID STATE POWER AMPLIFIER
0.1-22GHZ
ULTRA BROADBAND SSPA
RFLUPA01M22GA
4W 0.1-22GHZ
RFLUPA0218GB
20W 1-19GHZ
300W 6-18GHZ SOLID STATE BROADBAND
400W 8-11GHZ
SOLID STATE BROADBAND
0. 1-6GHZ VHZ,
UHF, L, S, C BAND
RFLUPA02G06GC
100W 2-6GHZ
RFLUPA0706GD
30W 0.7-6GHZ
MADE IN USA
6-18GHZ C, X, KU BAND
RFLUPA08G11GA
50W 8-11GHZ
RFLUPA0618GD
60W 6-18GHZ
RFLUPA06G12GB
25W 6-12GHZ
18-50GHZ K, KA, V BAND
RFLUPA18G47GC
2W 18-47GHZ
RFLUPA27G34GB
15W 27-34GHZ
RFLUPA47G53GA2
10W 47-53GHZ
RFLUPA27G34GB
30W 18-40GHZ
BENCHTOP RF MICROWAVE SYSTEM POWER AMPLIFIER
RAMP00G06GA- 30W 0.01-6GHZ
RAMP39G48GA- 4W 39-48GHZ
RAMP01G22GA- 8W 1-22GHZ
RAMP27G34GA- 8W 27-34GHZ
www.rflambda.com
sales@rflambda.com
1-888-976-8880
1-972-767-5998
San Diego, CA, US
Carrollton, TX, US
Ottawa, ONT, Canada
Frankfurt, Germany

SCi BLOCKS™

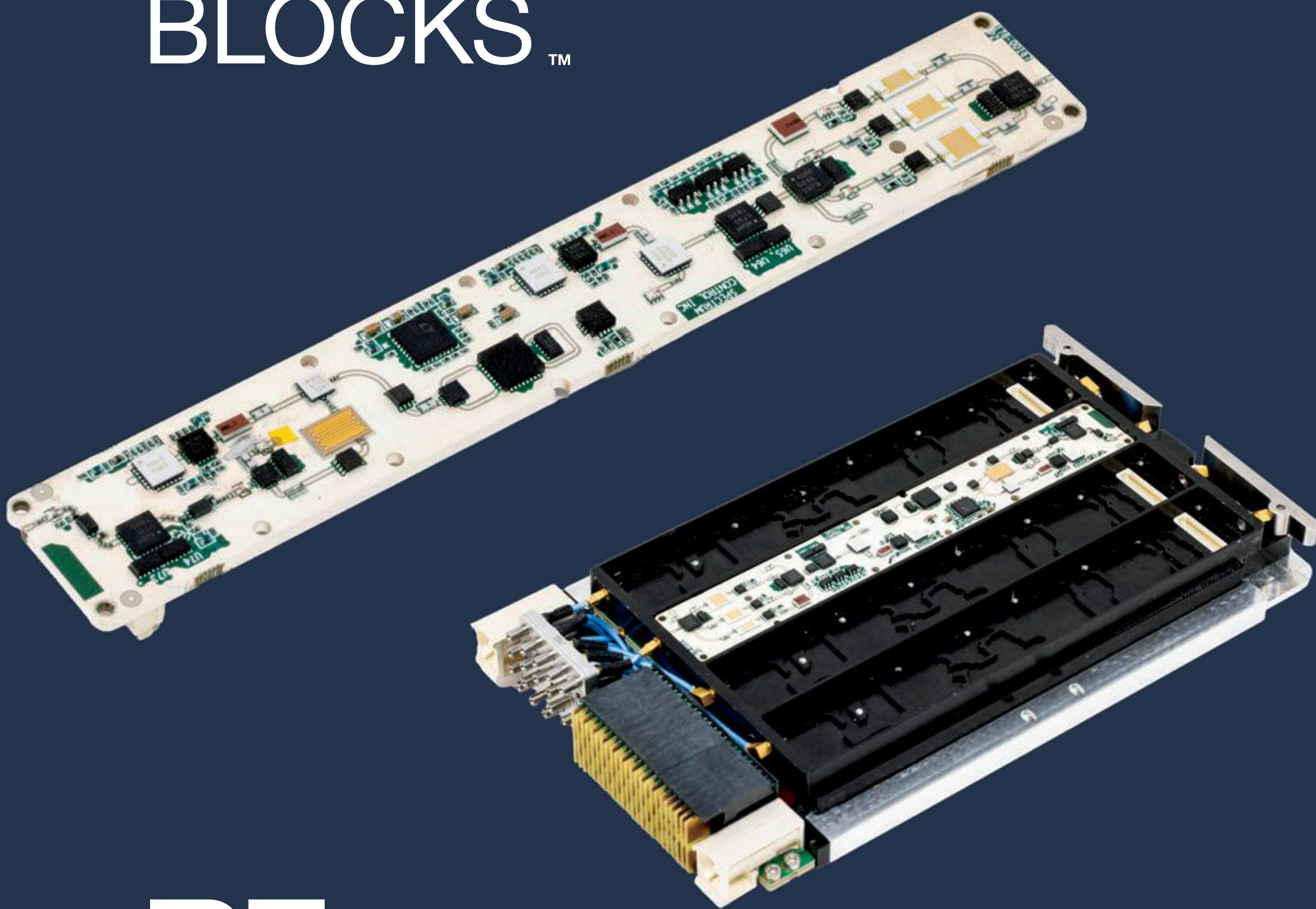

RF first.

The world has been waiting for an RF company to deliver wideband fidelity in an ultra-miniature, lightweight package. The wait is over.

SCi Blocks ("sky blocks") are revolutionary RF + digital building blocks for the next generation of EW, SIGINT, ISR, and ELINT.

Let us show you how you can meet your mission goals using this disruptive technology. See our demo at AOC booth 1202 or visit us at spectrumcontrol.com/sci-blocks

SPECTRUM CONTROL™

SpectrumControl.com


ara
ANTENNA RESEARCH ASSOCIATES (ARA)
A NEW ERA OF INNOVATION
VERSATILITY MEETS PRECISION
From specialized antennas to leading the charge in multi-band, multi-function and multi-mission defense technologies, ARA's latest products are an evolution in advanced defense and communications capabilities.
DISCOVER HOW ARA IS SHAPING TOMORROW'S DEFENSE SOLUTIONS TODAY.
www.ara-inc.com
sales@ara-inc.com
(877) ARA-SALE
USA (MA, MD, NH)

Microwave Journal

CONTENTS

January 2024
Vol. 67 • No. 1
Radar & Antennas
mwjournal.com

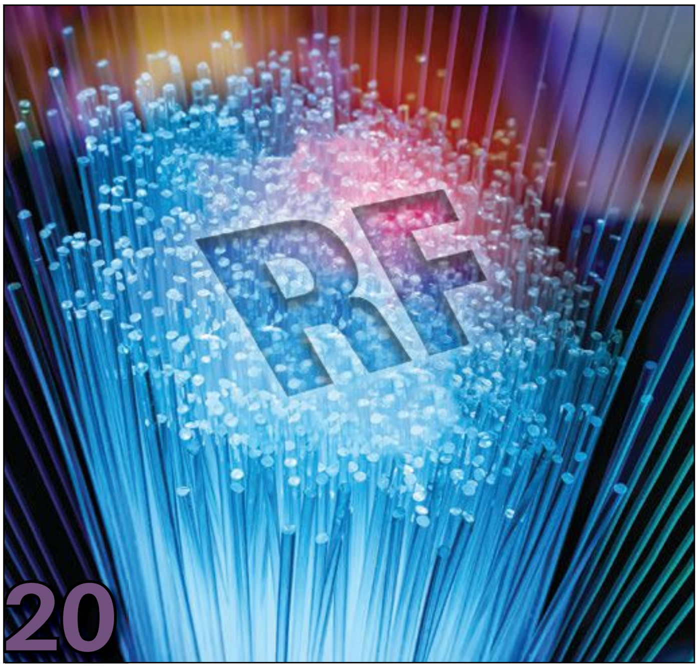

Look for this month's exclusive article online at mwjournal.com

Measurement and Analysis of a 230 to 330 GHz Terahertz Reflection Channel Based on PXI

Hongcheng Yang, Pandeng Wang, Wenyi Zhang, Cuiling Zhang, Cunlin Zhang, Bo Su, Jingsuo He

Key Laboratory of Terahertz Optoelectronics, Ministry of Education; Beijing Key Laboratory for Terahertz Spectroscopy and Imaging; Beijing Advanced Innovation Center for Imaging Theory and Technology; Department of Physics, Capital Normal University

67 YEARS OF PUBLISHING EXCELLENCE

MILLER MMIC

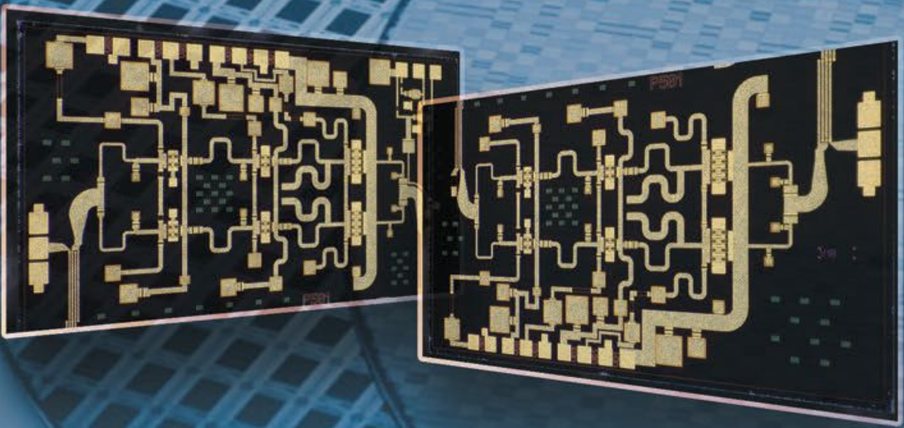

Miller MMIC is a global provider of RF semiconductor solutions with expertise in GaAs and GaN processes. We offer a diverse range of products tailored to various wireless applications. Our product lineup encompasses a wide array of offerings, including Low Noise Amplifiers, Distributed Amplifiers, Power Amplifiers, Driver Amplifiers, RF Switches, RF PIN Diode Switches, and numerous other voltage- and digitally-controllable RF components.

RF Distributed Low Noise Amplifiers

PN	Freq Low (GHz)	Freq High (GHz)	Gain (dB)	NF(dB)	P1dB (dBm)	Voltage (VDC)	Current (mA)	Package
MMW001T	DC	20.0	17~19	1~3.5	23 @ 10GHz	8.0	145	die
MMW4FP	DC	50.00	16.00	4.00	24.00	10	200	die
MMW507	0.20	22.0	14.0	4 - 6	28.0	10.0	350	die
MMW508	DC	30.0	14.0	2.5dB @ 15GHz	24.5	10.0	200	die
MMW509	30KHz	45.0	15.0		20.0	6.0	190	die
MMW510	DC	45.0	11.0	4.5	15.5	6.0	100	die
MMW510F	DC	30.00	20.00	2.50	22.00			die
MMW511	0.04	65.0	10.0	9.0	18.0	8.0	250	die
MMW512	DC	65.0	10.0	5.0	14.5	4.5	85	die
MMW5FN	DC	67.00	14.00	2.00	19.00	4.5	81	die
MMW5FP	DC	67.00	14.00	4.00	21.00	8	140	die
MMW011	DC	12.0	14.0		30.5	12.0	350	die

Low Noise Amplifiers

PN	Freq Low (GHz)	Freq High (GHz)	Gain (dB)	NF(dB)	P1dB (dBm)	Voltage (VDC)	Current (mA)	Package
MML040	6.0	18.0	24.0	1.5	14.0	5.0	35	die
MML058	1.0	18.0	15.0	1.7	17.0	5.0	35	die
MML063	18.0	40.0	11.0	2.9	15.0	5.0	52	die
MML080	0.8	18.0	16.5/15.5	1.9/1.7	18/17.5	5.0	65/40	die
MML081	2.0	18.0	25/23	1.0/1.0	16/9.5	5.0	37/24	die
MML083	0.1	20.0	23.0	1.6	11.0	5.0	58	die

RF Driver Amplifier

PN	Freq Low (GHz)	Freq High (GHz)	Gain (dB)	NF(dB)	P1dB (dBm)	Voltage (VDC)	Current (mA)	Package
MM3006	2.0	20.0	19.5	2.5	22.0	7.0	130	die
MM3014	6.0	20.0	15.0	-	19.5	5.0	107	die
MM3017T	17.0	43.0	25.0		22.0	5.0	140	die
MM3031T	20.0	43.0	20.0		24.0	5.0	480	die
MM3051	17.0	24.0	25.0	-	25.0	5.0	220	die
MM3058	18.0	40.0	20/19.5	2.5/2.3	16/14	5/4	69/52	die
MM3059	18.0	40.0	16/16	2.5/2.3	16/15	5/4	67/50	die

GaAs Medium Power Amplifier

PN	Freq Low (GHz)	Freq High (GHz)	Gain (dB)	P1dB (dBm)	Psat (dBm)	Voltage (VDC)	Current (mA)	Package
MMP107	17.0	21.0	19.0	30.0	30.0	6.0	400	die
MMP108	18.0	28.0	14.0	31.5	31.0	6.0	650	die
MMP111	26.0	34.0	25.5	33.5	33.5	6.0	1300	die
MMP112	2.0	6.0	20.0	31.5	32.0	8.0	365	die
MMP501	20.0	44.0	15.0	27 -- 32	29 - 34	5.0	1200	die
MMP502	18.0	47.0	14.0	28.0	30.0	5.0	1500	die

PN: MMW5FP
RF GaAs MMIC DC-67GHz

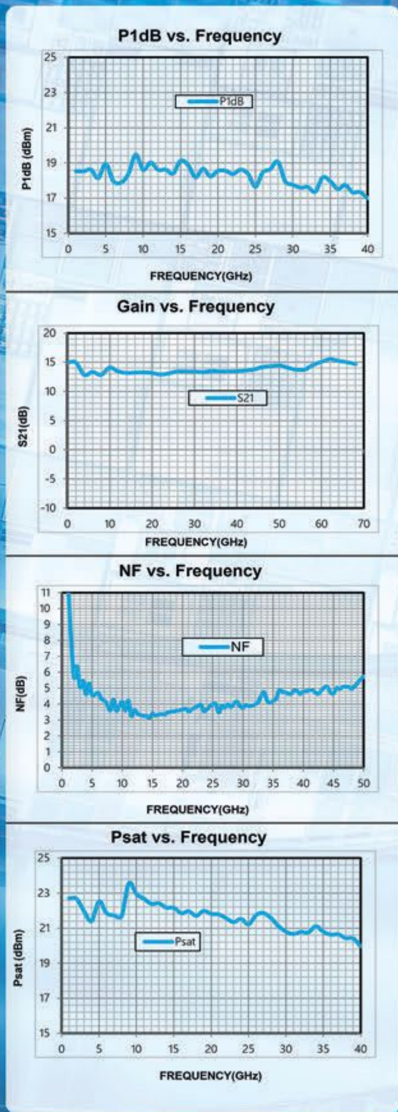

CALL US 1-833-2MILLER(264-5537)
WWW.MILLERMMIC.COM
sales@millermmic.com
support@millermmic.com

Microwave Journal CONTENTS

mwjournal.com

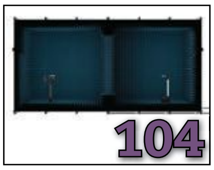

STAFF

Group Director: Carl Sheffres
Associate Publisher: Michael Hallman
Media Director: Patrick Hindle
Brand & Content Director: Jennifer DiMarco
Technical Editor: Eric Higham
Associate Technical Editor: Cliff Drubin
Editorial & Media Specialist: Kelley Roche
Associate Editor: Kaitlyn Joyner
Multimedia Staff Editor: Barbara Walsh
Electronic Marketing Manager: Chris Stanfa
Senior Digital Content Specialist: Lauren Tully
Digital Content Specialist: Vincent Carrabino
Audience Development Manager: Carol Spach
Director of Production & Distribution: Edward Kiessling
Art Director: Janice Levenson
Graphic Designer: Ann Pierce

EUROPE

Office Manager: Nina Plesu

CORPORATE STAFF

CEO: William M. Bazzy
President: Ivar Bazzy
Vice President: Jared Bazzy

EXECUTIVE EDITORIAL OFFICE
685 Canton Street, Norwood, MA 02062
Tel: (781) 769-9750
FAX: (781) 769-5037
e-mail: mwj@mwjournal.com

EUROPEAN EDITORIAL OFFICE
16 Sussex Street, London SW1V 4RW, England
Tel: Editorial: +44 207 596 8730 Sales: +44 207 596 8740
FAX: +44 207 596 8749

SUBSCRIPTION SERVICES
Send subscription inquiries and address changes to:
Tel: (978) 671-0446
e-mail: mwj@e-circ.net

www.mwjournal.com

Printed in the USA

Microwave Journal (USPS 396-250) (ISSN 0192-6225) is published monthly by Horizon House Publications Inc., 685 Canton St., Norwood, MA 02062. Periodicals postage paid at Norwood, MA 02062 and additional mailing offices.

POSTMASTER: Send address corrections to Microwave Journal, PO Box 1028, Lowell, MA 01853 or e-mail mwj@e-circ.net.com. Subscription information: (978) 671-0446. This journal is issued without charge upon written request to qualified persons working in the RF & microwave industry. Other subscriptions are: domestic, $130.00 per year, two-year subscriptions, $200.00; foreign, $225.00 per year, two-year subscriptions, $400.00; back issues (if available) and single copies, $20.00 domestic and $30.00 foreign. Claims for missing issues must be filed within 90 days of date of issue for complimentary replacement.

Microwave Journal ONLINE .COM

E LEARNING CENTER

Access webinars on-demand from the archived webinars and events page at www.mwjournal.com/events

Catch *Frequency Matters*, the industry update from *Microwave Journal*,
microwavejournal.com/FrequencyMatters

Executive Interview

Dr. Pierre-Yves Lesaicherre, CEO of **Finwave** talks about his new position, the origins of the company and how Finwave plans to differentiate their 3D GaN technology for the 5G market.

WHITE PAPERS

Coilcraft — Key Parameters for Selecting RF Inductors

ROHDE&SCHWARZ Make ideas real — E-Guide Testing RF Power Amplifier Designs

Join Us Online

Follow us
@Pathindle
@MWJEric
@MWJEditor

Join us at the RF and Microwave Community

Become a fan at facebook.com/microwavejournal

Microwave Journal PODCASTS

mmWave Security Scanning with R&S

NB-IoT Connectivity from Space with Sateliot

Frequency Matters: Radar & Antennas Issue

Visit us @ mwjournal.com

DC TO 50 GHz

MMIC Amplifiers

300+ Models Designed in House

Options for Every Requirement

CATV (75Ω)

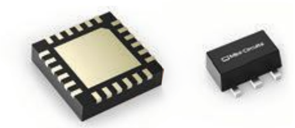

Supporting DOCSIS® 3.1 and 4.0 requirements

Dual Matched

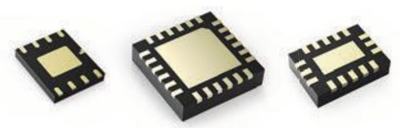

Save space in balanced and push-pull configurations

Hi-Rel

Rugged ceramic package meets MIL requirements for harsh operating conditions

High Linearity

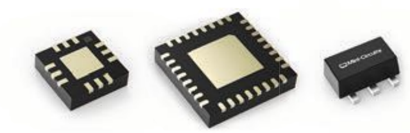

High dynamic range over wide bandwidths up to 45 GHz

Low Noise

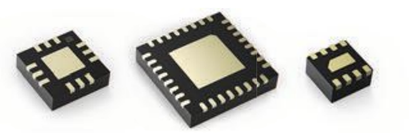

NF as low as 0.38 dB for sensitive receiver applications

Low Additive Phase Noise

As low as -173 dBc/Hz @ 10 kHz offset

RF Transistors

<1 dB NF with footprints as small as 1.18 x 1.42mm

Variable Gain

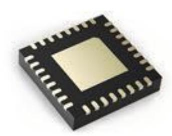

Up to 31.5 dB digital gain control

Wideband Gain Blocks

Flat gain for broadband and multi-band use

Mini-Circuits®

MARK YOUR CALENDAR

STAY CONNECTED TO COMING EVENTS

JANUARY

21-24
ARFTG
San Antonio, Texas
www.arftg.org

21-24
RWW 2024
San Antonio, Texas
www.radiowirelessweek.org

30-2/1
DesignCon
Santa Clara, Calif.
www.designcon.com

FEBRUARY

21-23
IMFW 2024
Cocoa Beach, Fla.
https://imfw-ieee.org

26-29
MWC Barcelona
Barcelona, Spain
www.mwcbarcelona.com

MARCH

12-14
emv 2024
Cologne, Germany
https://emv.mesago.com

17-22
EuCAP 2024
Glasgow, Scotland
www.eucap2024.org

18-21
SATELLITE
Washington, DC
www.satshow.com

APRIL

3-4
IEEE Texas Symposium
Waco, Texas
https://texassymposium.org

15-16
WAMICON 2024
Clearwater Beach, Fla.
www.ieeewamicon.org

ONLINE PANEL SERIES

3/26
Will Flat Panel Beamsteering Arrays Meet the SATCOM Challenge?

Call for Papers Deadlines

2/9	WAMICON
3/17	EuMW
5/13	IEEE Phased Array

FOR DETAILS VISIT MWJOURNAL.COM/EVENTS

On Our Radar...

Carl Sheffres
Microwave Journal *Publisher*

We kick off 2024 with our traditional "Radar and Antennas" issue, with a cover feature titled: "The Role of RFoF in an Autonomous Military Future," provided by Optical Zonu. Articles by IMST, Mitron, Imec, Analog Devices, ANTENNEX B.V. and others provide expert insights in a variety of technical topics. The editors have some excellent content lined up for this year in print, digital and online formats, so stay tuned.

You may have seen our recent 5G Special Focus eBook. This eBook, part of the November 2023 5G/6G and IoT issue, focuses on 5G. This new feature transitions select content from the print/digital issue to an eBook format, providing targeted content for readers and lead generation for advertisers. We will be showcasing this new feature with "Special Focus" sections in March (Cables & Connectors), May (5G/6G), August (mmWave Technology) and November (IoT).

The popular MWJ "Online Panel Series" continues this year with four select topics, beginning on March 26 with a panel titled: "Will Flat Panel Beamsteering Arrays Meet the SATCOM Challenge?" Watch for additional panel sessions in June, September and November.

The Frequency Matters video series continues to bring bi-monthly industry updates, interviews and new product launches to a growing audience. If you haven't caught an episode yet, I highly recommend it. For podcast enthusiasts, the "B&S on Aerospace and Defense" podcast featuring Bryan Goldstein of Analog Devices and Sean Darcy of Infineon is a must listen.

EDI CON Online continues to inform and educate thousands of professionals with a combination of keynotes, technical presentations and workshops. We have spread the tracks throughout the year for easier consumption. Our EDI CON Educational Days in 2024: "PCB/Interconnect/EMC-EMI" track will take place on April 10, the "5G-6G/Wi-Fi/IoT" track is May 22, the "Signal Integrity/Power Integrity" is on August 21 and the "Radar/Automotive/SATCOM" track is October 23. In a recent survey of attendees, 97% said that they would attend EDI CON Online sessions again and 97% would recommend the event to friends or colleagues. You can even earn IEEE Continuing Education credits for free by attending.

Speaking of events, we will be exhibiting at or attending numerous in-person events again this year. We start with DesignCon at the end of this month in Santa Clara, Calif., followed by Mobile World Congress in Barcelona in February and SATELLITE in Washington, DC, in March. IMS also takes place in Washington, DC, this June. This is the year to exhibit if your company has not yet signed on. The IEEE EMC & SIPI event visits Phoenix this summer, followed by European Microwave Week in September. EuMW returns to Paris, always a good venue for business and pleasure. I found this past EuMW in Berlin to be most productive. Find us this fall at AMTA in October and AOC in December.

I have recently returned from AOC as of this writing. It was so nice to catch up with old friends and colleagues. It reminds me why live events are so important for networking and establishing new relationships. We have such a tightknit community that these events sometimes feel like a big family reunion, and I look forward to seeing many of you in the year ahead.

In the meantime, please take a few minutes to renew your subscription to *Microwave Journal* if you haven't done so recently. It saves us from hounding you and hopefully brings you value each month.

Wishing all of our readers a healthy and happy New Year. ■

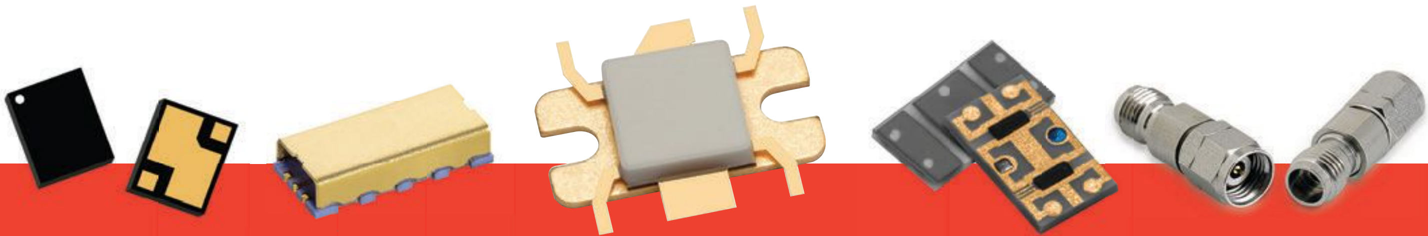

The Role of RFoF in an Autonomous Military Future

Meir Bartur
Optical Zonu, Van Nuys, Calif.

The presence of autonomous vehicles and weaponry in the military is set to grow at a significant rate, spurred by funding from the Department of Defense (DOD) in recent years. In 2021, the Pentagon received $7.5 billion to fund unmanned systems across the Air Force, Army and Navy.[1] Generally speaking, these are positive innovations that help the U.S. keep pace with the military advancement of other world powers, such as Russia and China, but they are not without significant risks to national security if the communication infrastructure supporting them is insufficient.

Unmanned vehicles and weapons rely heavily on continuous real-time communication, in addition to radar/LiDAR, as well as other passive sensors that are deployed without human involvement. Operational integrity is at risk if there is any communication failure or adversarial intervention based on emission profiles. Even autonomous mission-oriented apparatus that does not emit information, for the sole purpose of avoiding detection, relies on receiving signals. While always important, communication has never been on the "hot seat" quite like it is now when it determines whether our autonomous defenses work reliably. ***Figure 1*** shows a portion of the U.S. Naval fleet, a military domain containing some of the biggest sensor platforms in existence.

Fig. 1 **Naval ships at the ready.**

Exacerbating the issue are the high frequency RF signals that provide the low latency, high bandwidth communication necessary for automation. High frequencies tend to be less resilient and more easily disrupted by outside elements, of which there are many in military environments. This article examines the state of military communications and why radio frequency over fiber (RFoF) is important to safeguard autonomous military systems.

MILITARY COMMUNICATION AT A GLANCE

Military communication relies on a wide spectrum of RF bands, each serving specific purposes tailored to the demands of modern warfare. The choice of RF bands varies depending on factors such as geographic location, technology availability and operational requirements. What follows is a general overview of key RF bands used in military communication and their typical applications:

Ultra-High and Very High Frequency (UHF/VHF) Bands

The UHF (300 MHz to 3 GHz) and VHF (30 to 300 MHz) bands, often associated with "walkie-talkie" style communication, are essential for ground troops, vehicles and aircraft. VHF radios excel in line-of-sight communication over open terrain, providing reliable voice and data transmission. In contrast, UHF radios are preferable in congested or urban environments due to their shorter wavelengths and better signal penetration capabilities. UHF satellite communication facilitates secure and encrypted data transmission among military units, including ground stations, ships and aircraft.

L-Band (1 to 2 GHz)

L-Band is used for satellite communications, GPS and certain radar systems, offering a versatile spectrum for military applications. The ability of L-Band networks to penetrate atmospheric conditions and foliage enhances utility in scenarios where communication resilience is crucial. This makes it suitable for military command and control, intelligence gathering and communication of strategic information.

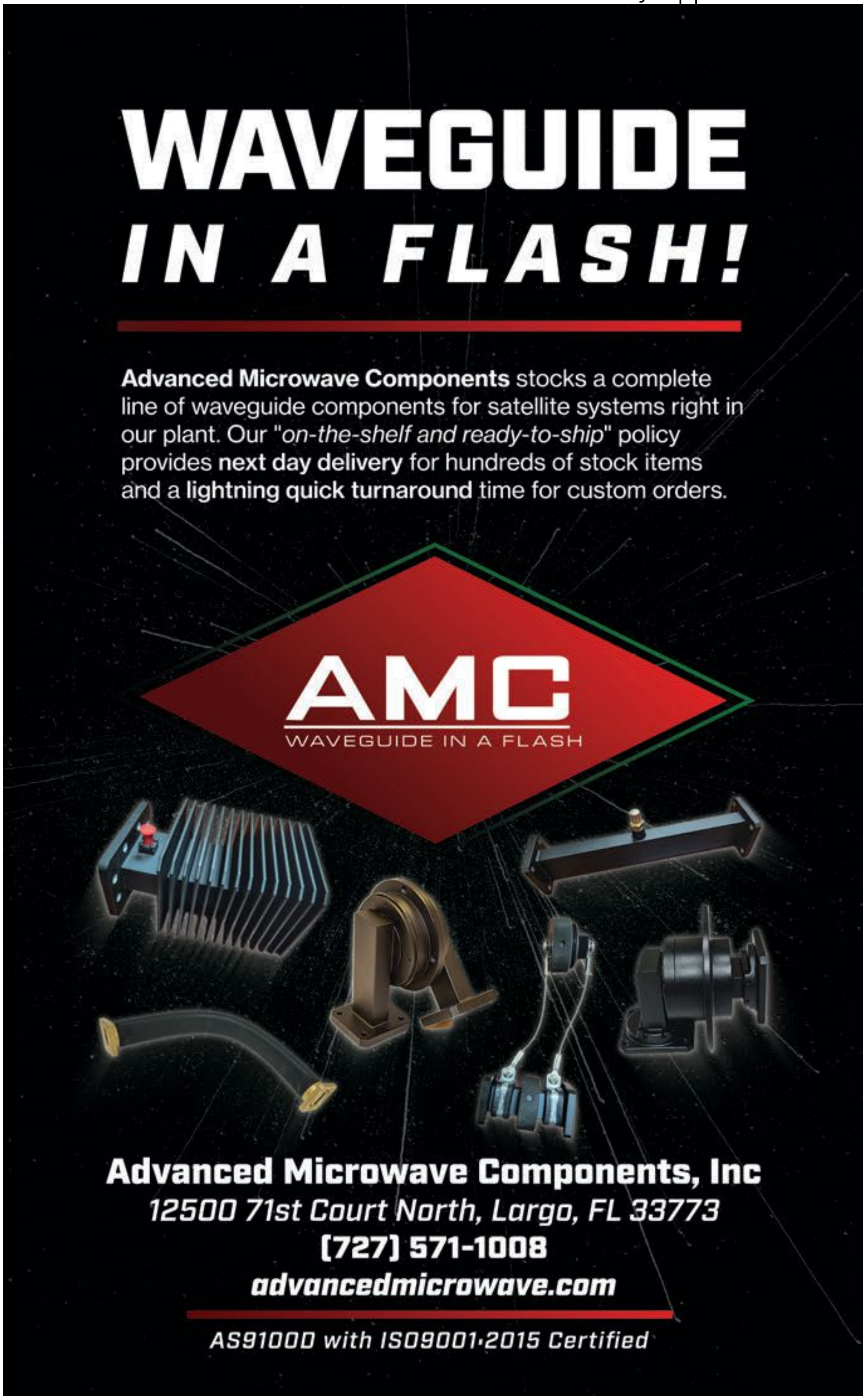

S-Band (2 to 4 GHz)

S-Band frequencies support long-range surveillance and tracking radars, as well as select satellite communication systems. Some overlap exists with Wi-Fi and cellular bands, as well as certain GPS applications.

C-Band (4 to 8 GHz)

C-Band is a versatile frequency range employed in radar systems, satellite communications and various weather radar applications. It offers a balanced compromise between the need for high-resolution and atmospheric penetration.

X-Band (8 to 12 GHz)

Military radar systems rely on X-Band for tasks like target identification, tracking and missile guidance. This band provides exceptional resolution and accuracy to improve situational awareness.

Ku-Band (12 to 18 GHz) and Ka-Band (26.5 to 40 GHz)

These higher frequency bands are crucial for military satellite communications, offering enhanced data transfer rates compared to lower frequencies. Ku-Band is widely used for communication between different U.S. military units.

While these RF bands are arguably the most common, frequency allocations and standards in military communication can vary globally and evolve with technological advancements. Additionally, classified or encrypted communication further complicates the disclosure of precise frequency bands and their applications.

THE BALANCING ACT OF DIGITAL AND ANALOG COMMUNICATIONS

The military has relied on communications since its inception. Even with network evolution, at the heart of contemporary military communications lies the fact that the na-

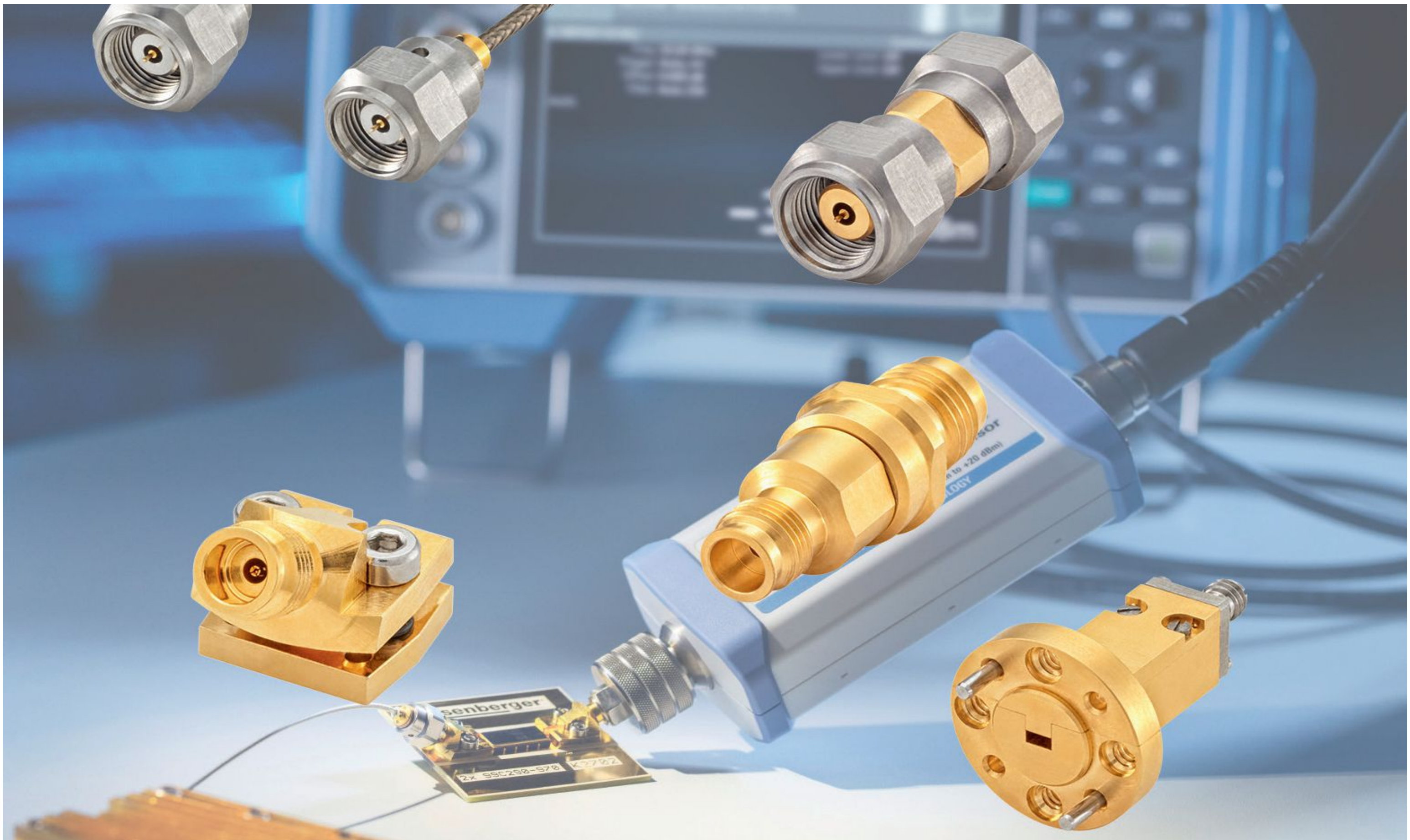

TEST & MEASUREMENT

Test, Measurement & Calibration

RF and microwave components from Rosenberger play a key role in a variety of test, measurement and calibration applications. RF high precision connectors, adaptors & devices, PCB connections, calibration kits, microwave test cables or VNA test port cables – the precision and quality of Rosenberger test and measurement products have been proven in various applications:

- Microwave measurements and VNA calibrations
- Lab testing, factory testing
- PCB connections
- Semiconductor test applications and high-speed digital testing
- Network testing
- Test and measurement equipment and devices

www.rosenberger.com

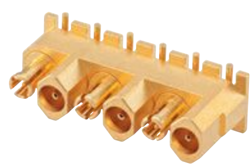

Rosenberger

ture of transportation over RF bands is analog. The receiver of the signal must have a wide dynamic range, so even systems deploying down-converters must have an analog transport section.

Digital communication systems are celebrated for their precision and reliability, boasting error correction capabilities, adaptability to various data types and better spectral efficiency. However, converting RF signals into digital formats introduces certain complexities. These conversions can lead to latency and jitter, along with creating vulnerabilities such as unauthorized interception, commonly known as "listening," by nefarious actors.

In contrast, analog technology is the primary medium for propagating signals through the air. Autonomous non-tethered military platforms, such as drones and unmanned aircraft, rely on analog components for receiving and transmitting signals. Since there is no need for conversion between endpoints and the transport medium, there is less latency and it drastically reduces the chance of detection. While cabled communication via fiber or CAT cables is principally digital, coaxial and waveguide transport is almost always analog. Each technology has its strengths and weaknesses, making their combination essential for effective and secure communication.

A persistent concern in military communication is the potential detection of electromagnetic radiation by adversaries. To enhance survivability, military strategists often opt for remote antennas, distancing them from sensitive command centers or main platforms. For instance, an unmanned ship may house its processing and command center below deck while needing to communicate with remote antennas on its exterior. This practice creates a foundation for resiliency, as it reduces the risk of mission failure due to antenna damage or compromise. It is also the reason that RFoF is so critical for autonomous military systems.

WHAT IS RFOF?

As currently deployed and widely used in many market segments, RFoF is a technology that transfers electromagnetic signals over fiber-optic links via amplitude modulation. A basic link consists of a transmitter at one end, composed of a semiconductor laser and a matching circuit that controls the light intensity according to an input signal and an optical receiver at the other end. The receiver is a photodetector aligned with an optical fiber and a circuit that amplifies the signal and drives the output. Fiber-optic technology is widely used for the Ethernet backbone and all digital data networks. The same fibers that inherently have very low optical losses transport the light modulated by the transmitter over a significant range, often at distances up to tens of kilometers. The modern RFoF systems are modular and offer significant signal grooming/matching and control for higher frequencies. Transport at 40 GHz is routine and transport systems operating at 60 GHz have been demonstrated. A simplified block diagram for RFoF network transmission is shown in ***Figure 2***.

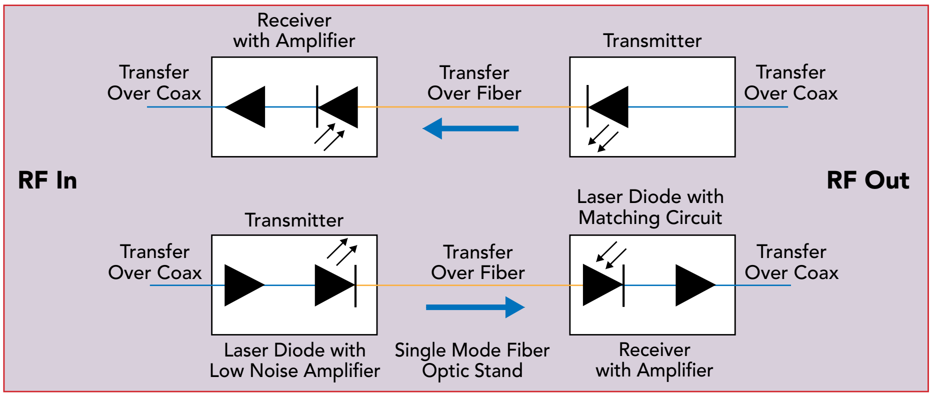

Fig. 2 **Bi-directional RF signal transport over fiber.**

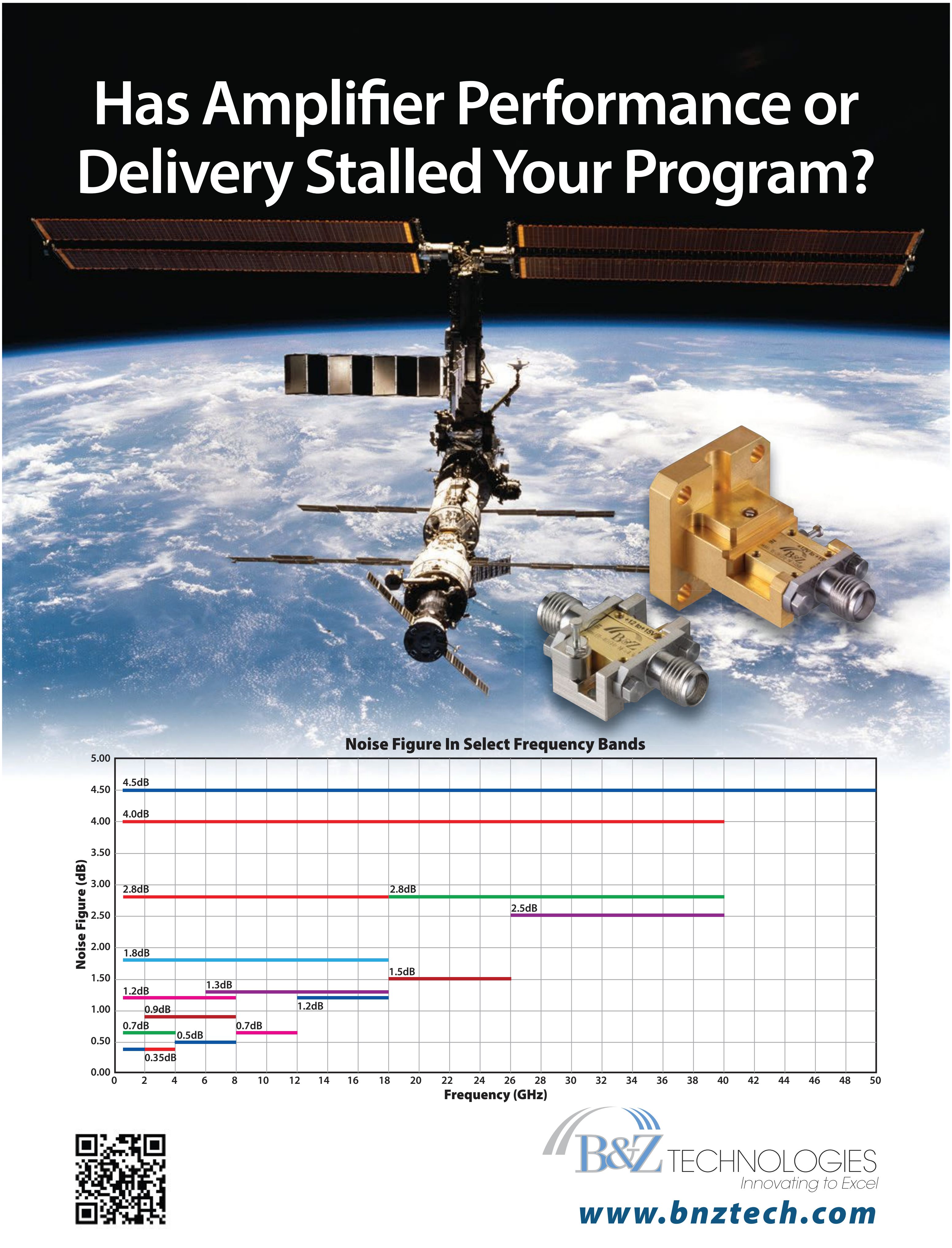
Has Amplifier Performance or
Delivery Stalled Your Program?
Noise Figure In Select Frequency Bands
Noise Figure (dB)
5.00
4.50
4.00
3.50
3.00
2.50
2.00
1.50
1.00
0.50
0.00
4.5dB
4.0dB
2.8dB
2.8dB
2.5dB
1.8dB
1.5dB
1.3dB
1.2dB
1.2dB
0.9dB
0.7dB
0.7dB
0.5dB
0.35dB
0 2 4 6 8 10 12 14 16 18 20 22 24 26 28 30 32 34 36 38 40 42 44 46 48 50
Frequency (GHz)
B&Z TECHNOLOGIES
Innovating to Excel
www.bnztech.com

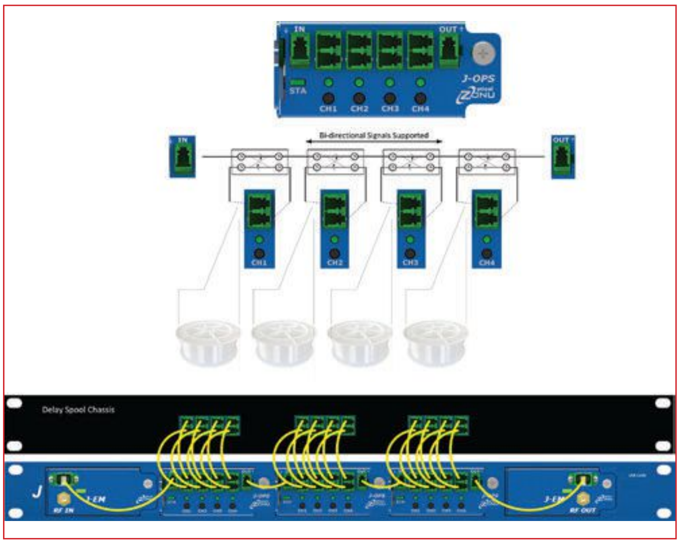

Fig. 3 **Programmable RFoF time delay system for radar simulation and testing.**

The scalability and adaptability of RFoF systems contribute to their efficacy in evolving technological landscapes. These systems can be easily integrated into existing infrastructure, offering seamless upgrades and expansions without the need for extensive overhauls. The modular nature of RFoF allows for the incorporation of advanced features and functionalities, enhancing signal processing, minimizing latency and optimizing performance. This adaptability is important for telecommunications and big data sectors, where the demand for higher bandwidths and improved signal integrity continues to grow. Despite how vital this technology has become for many industries; it comes from humble beginnings.

BRIEF HISTORY

RFoF emerged during the second generation of CATV distribution, a period when TV channels were transmitted through analog modulation across the nation. In the 1990s, the original equipment, initially operating up to 800 MHz and later expanding to 1 GHz, utilized RFoF technology to deliver video signals. These signals were transmitted to a node and then distributed to individual subscribers' homes via coaxial cables.

During this era, CATV served as the primary market application for RFoF. As the demand for VHF transport increased, RFoF found applications in various niche sectors. RFoF technology began to play a crucial role in satellite communication, ground stations, telemetry, audio/video distribution in studios and impromptu events. The technology also contributed to enhancing cellular network coverage in key locations such as airports, stadiums and campuses.

RFoF applications also extended to unique instrumentation scenarios, where programmable time delay became widely adopted for radar testing. This adaptability showcased the capability of the technology to meet the specific needs of various industries and settings. ***Figure 3*** shows a programmable RFoF time delay system for radar simulation and testing.

As technology advances, RFoF continues to evolve, with improvements in bandwidth, reliability and efficiency. The 1990s laid the foundation, but subsequent decades witnessed the refinement and expansion of RFoF applications, making it an integral part of modern telecommunications and broadcasting infrastructure. The journey from its inception in CATV applications to becoming a crucial component in diverse sectors exemplifies RFoF's capacity to evolve and address the ever-changing demands of the telecommunications landscape.

WHY RFOF IS BECOMING INCREASINGLY IMPORTANT TO THE MILITARY

For military applications, RFoF plays a vital role as a replacement for coaxial cables or waveguides, enhancing the efficiency and versatility of communication systems. RFoF uses analog signals to modulate the light intensity of specific wavelengths, effectively converting electrical RF signals into an optical format. The signal then traverses a

single-mode fiber for resilient and efficient low loss transmission and upon reaching its destination, it is converted back into an RF output to enable precise control and utilization. A significant feature of RFoF transmission is its ability to carry high dynamic range broadband signals over a single link and multiplex multiple wavelengths over a single strand of fiber for high density transport.

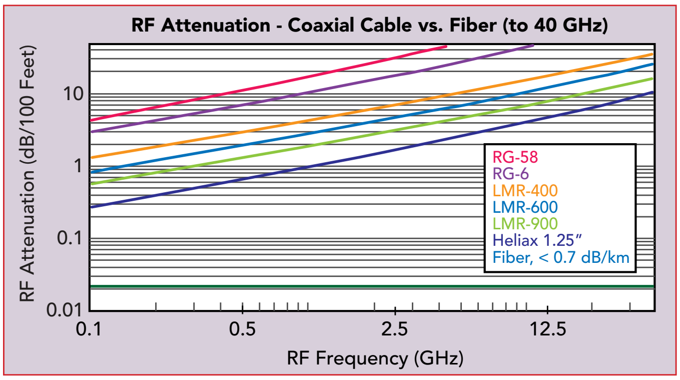

Fig. 4 RF attenuation to 40 GHz.

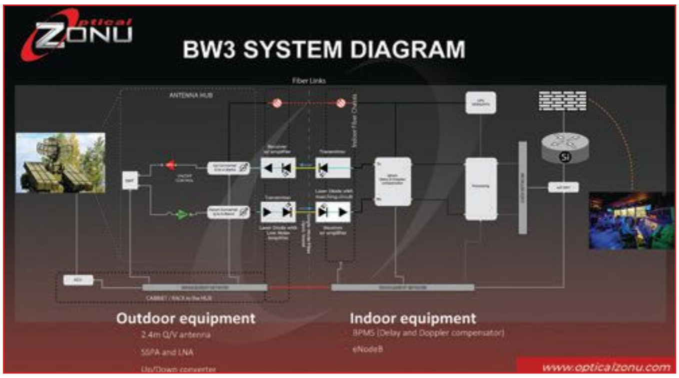

Fig. 5 Antenna remoting with RFoF link.

Fiber-optic cables have minimal signal loss over long distances, ensuring that data can be transmitted reliably, even across extended military networks. Coaxial cables, in contrast, are more susceptible to signal degradation over distance, necessitating signal boosters or repeaters. The difference in RF attenuation for coaxial cables and fiber is illustrated in ***Figure 4***.

In addition to higher loss, coaxial cables are susceptible to electromagnetic interference that can disrupt or degrade signal quality. Fiber is also inherently more secure than coaxial cables since it does not emit electromagnetic radiation that can be easily intercepted. This feature makes the transport method resistant to electronic eavesdropping and signal interception by adversaries. This is why the military uses fiber for antenna remoting to separate mission-critical systems from its communication transmitter/receiver. RFoF will be a critical element of all military communications as electronic warfare becomes a growing and increasingly sophisticated issue.

There are a significant number of military-focused use cases for antenna remoting with RFoF. ***Figure 5*** shows a simplified functional block diagram for what takes place between the control center and the remote antenna. Many applications are making more use of antenna remoting:

- **Satellite Communication:** Military satellite communication systems rely on remote antenna installations to establish and maintain connections with satellites in geostationary or low earth orbit. These antennas are often placed on ships, aircraft or in remote locations to ensure a reliable link with satellites.
- **Radar Systems:** Military radar systems, including ground-based, naval and airborne radar utilize phased array antenna technology. Control of signal phase and delay over fiber provides an advantage over coax cables or waveguides. Fiber-based radar simulators are used for calibration and training purposes.
- **Covert Surveillance:** Remote antenna systems can be camouflaged or hidden to conduct covert surveillance and intelligence gathering operations. These antennas are placed in concealed locations to avoid detection by adversaries.

Optimize Wireless Communication Coverage with Wireless InSite®

Now with Engineered Electromagnetic Surface Modeling

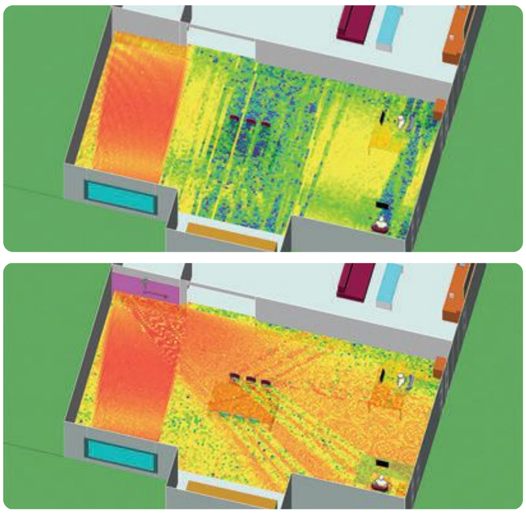

Wireless InSite simulates propagation in a scene with sub-optimal signal coverage (top) and reveals the improvement with the addition of an EES (bottom).

Model passive metasurfaces designed to optimize wireless communication coverage by manipulating how signals propagate through a scene.

Evaluate how the EES modifies the propagation environment to improve connectivity.

Learn more and request a demonstration at **www.remcom.com/wireless-insite**

REMCOM®

+1.888.7.REMCOM (US/CAN) | +1.814.861.1299 | **www.remcom.com**

Improve the design process | Reduce development costs | Deliver superior results

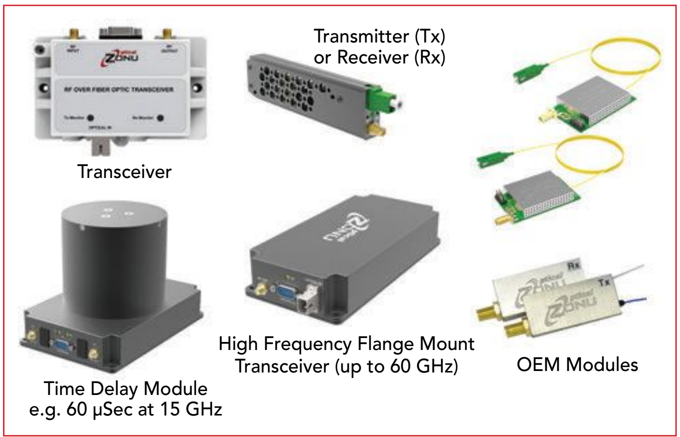

Fig. 6 **RFoF components.**

Fig. 8 **Antenna remoting use case.**

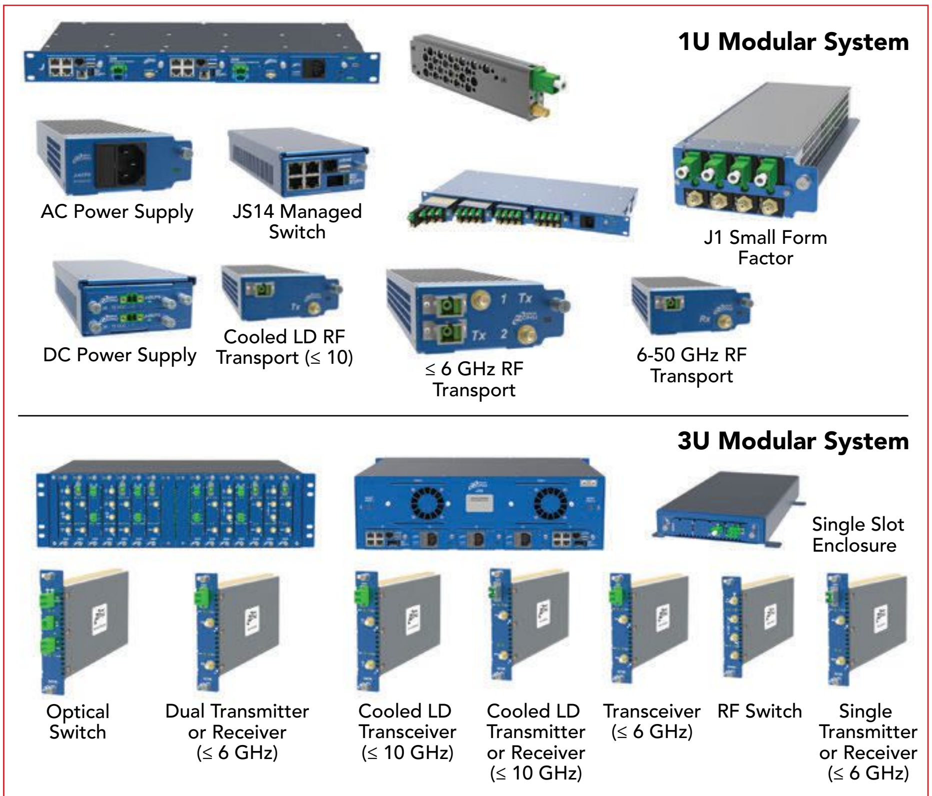

Fig. 7 **RFoF subsystems.**

- **Secure Wi-Fi:** Antenna remoting enables secure Wi-Fi in sensitive compartmented information facilities (SCIFs) by physically separating the external antennas from the secure facility. Fiber-optic connections are used to transmit signals and implement a controlled and secure internal Wi-Fi network. This approach prevents unauthorized access and eavesdropping while providing secure and reliable Wi-Fi access to authorized personnel within the SCIF. The same platform can also be used for full spectrum monitoring of the area covered by the Wi-Fi service.

It is important to note that the electronics in RFoF systems do not look substantially different than what would be expected in legacy systems. Only the transport medium looks different. ***Figure 6*** shows RFoF components for a variety of system functions. ***Figure 7*** shows the sub-system implementations for RFoF networks.

Fiber is also lighter weight with a smaller form factor. In military communications, size and weight matter, particularly in airborne applications like aerostats and drones. The size and weight of fiber cables make them easier to transport and install in military operations. They are also well-suited for field deployments where mobility and rapid setup are critical. Beyond size and weight, fiber is more durable than coaxial cable. It is less susceptible to environmental factors such as moisture, temperature fluctuations and corrosion.

U.S. NAVY CASE EXAMPLE

While using RFoF for autonomous military assets may feel like futuristic, many of these problems are being discovered and solved today. A compelling case study of the application of RFoF technology on autonomous vehicles for the military is exemplified by the U.S. Navy's utilization of unmanned surface vessels (USVs). Ku-Band Common Data Link (CDL) communications payloads are routinely transported between radomes mounted high above USV decks and equipment rooms nestled within the ship's hulls via antenna remoting.

Currently, waveguide and coaxial cables are used for such tasks, but they present significant RF losses and logistical difficulties. Coaxial cables are inherently inflexible and highly susceptible to mechanical stress like shock or vibration. Their fragility necessitates meticulous maintenance, a particularly daunting task during prolonged deployments at sea or in oceanic conditions. Service disruptions require extra time and resources to repair and may even create the need for the ship to go back to port for repairs.

Even minimal moisture or minute traces of dirt or salt can detrimentally impact waveform transmission and subsequently degrade RF per-

Metal-flange /

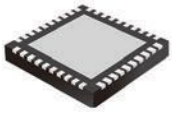

QFN /

Die

ASX
AGN family
ABX

HPA

Radar, up to 35 W

Internally Matched MMIC

S-, C-band

AGN0343MC	3.2~4.2	20 W
AGN0540MC	4.2~5.2	12 W
AGN0542DC/Q/MC	4.4~5.6	20 W
AGN0642DC/MC	5~7	18 W
AGN0743MC	5.8~8.5	22 W

Ku-, Ka-band

AGN1440DC/MC	13~16.5	12 W
ASX1436	13.75~14.5	3 W
ASX1437	13.5~14.5	5 W
ASX1536	13.5~16	5 W
ASX2731D/Q35P	27.5~31	3 W

X-band

ASX0837HG	7.5~8.5	4 W
ASX1037HG	8.5~10.5	4 W
ASX1037	8.5~10.5	5 W
AGN0940DC	7.7~10.7	12 W
AGN0942D/Q	7.7~10.7	14 W
AGN0943DC/Q	7.7~10.7	20 W
AGN0944DC/Q/MC	8.5~10	25 W
AGN0945DC/Q	8.5~10.5	35 W

Wide-band

ABX0618Q	6~18	1 W

ISO 9001
ISO 14001
IATF 16949
www.asb.co.kr

ASB

formance. To mitigate moisture-related issues, waveguides are often filled with dried air or purified nitrogen, but any corrosion or oxidation of the inner metal surfaces further compromises their performance. In one instance, water entered the hull even with the nitrogen present and disrupted the RF signal.

To counter this issue, the Optical Zonu team worked with the U.S. Navy to successfully deploy fiber cables as a replacement for waveguides to fix the lingering issues. Fiber-optic technology demonstrated several key advantages over waveguides, including superior long-term performance and lower overall lifetime costs. The technology also proved to be much more flexible and easier to install with a bend radius of less than 1 in. ***Figure 8*** shows the RFoF fiber run and location for the aircraft carrier.

The fiber-optic transport links proved capable of meeting and exceeding CDL requirements. They offered low loss transport, support for all CDL-compliant waveforms, symmetric/asymmetric data rates and comprehensive audio/video transport. These fiber-optic links enable Ku-Band RF transport over much longer distances than could be supported by waveguide technology.

CONCLUSION

The rapid expansion of autonomous vehicles and weapons within the military, driven by substantial funding from the DOD, represents a pivotal step in maintaining the U.S.' military edge. However, this transformative shift is not without its challenges, chief among them being the resilience of the communication infrastructure that underpins these innovative systems. As unmanned military assets become increasingly integral to operations, their reliance on continuous, real-time communication, alongside advanced sensor technologies, becomes paramount. The potential for communication failures or adversarial detection poses a direct threat to operational integrity. Compounding these challenges is the vulnerability of higher frequencies, which support the low latency, high bandwidth communication networks essential for automation.

RFoF is emerging as a critical solution to safeguard and enable autonomous military systems. RFoF technology not only offers enhanced security and resilience but also addresses the evolving demands of modern warfare, ensuring that the U.S. can maintain its military capabilities in an increasingly complex and connected world. As the landscape of military technology continues to evolve, the strength of our communication infrastructure becomes a decisive factor in the success and reliability of our national defense systems. ■

Reference

1. "Pentagon Gets $7.5 Billion for Unmanned Systems," *National Defense Magazine*, May 2021, Web: nationaldefensemagazine.org/articles/2021/5/27/pentagon-gets-$7-5-billion-for-unmanned-systems.

RF-LAMBDA

MADE IN USA

THE LEADER OF RF BROADBAND SOLUTIONS

EMC Broadband RF Power Amplifier

High Power Solid State

HUNDREDS IN STOCK

FAST SHIPPING

FREQUENCY UP TO 90GHZ

POWER UP TO 2KW CW

REMC06G18GG

6-18GHZ 300W

- AUTOMATIC BUILT IN SELF CALIBRATION AND BIAS ADJUSTMENT.
- OVER TEMPERATURE, CURRENT, INPUT POWER PROTECTION.
- VSWR MEASUREMENT AND OPEN CIRCUIT PROTECTION.
- USER FRIENDLY CONTROL INTERFACE.
- REMOTE ETHERNET CONTROL AND FIRMWARE UPDATE.
- HIGH POWER EFFICIENCY AND LIGHTWEIGHT.

RAMP42G47GA 42-47GHZ 8W

REMC02G06GE 2-6GHZ 500W

RAMP18G40GB-U 18-40G 20W

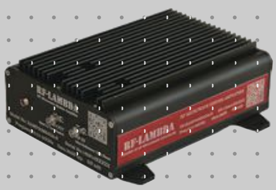

RAMP05M80GC 0.5-80GHZ

REMC08G11GE 8-11GHZ 400W

RF Amplifiers and Sub-Assemblies for Every Application

Delivery from Stock to 2 Weeks ARO from the catalog or built to your specifications!

- Competitive Pricing & Fast Delivery
- Military Reliability & Qualification
- Various Options: Temperature Compensation, Input Limiter Protection, Detectors/TTL & More
- Unconditionally Stable (100% tested)

ISO 9001:2000 and AS9100B CERTIFIED

OCTAVE BAND LOW NOISE AMPLIFIERS

Model No.	Freq (GHz)	Gain (dB) MIN	Noise Figure (dB)	Power-out @ P1-dB	3rd Order ICP	VSWR
CA01-2110	0.5-1.0	28	1.0 MAX, 0.7 TYP	+10 MIN	+20 dBm	2.0:1
CA12-2110	1.0-2.0	30	1.0 MAX, 0.7 TYP	+10 MIN	+20 dBm	2.0:1
CA24-2111	2.0-4.0	29	1.1 MAX, 0.95 TYP	+10 MIN	+20 dBm	2.0:1
CA48-2111	4.0-8.0	29	1.3 MAX, 1.0 TYP	+10 MIN	+20 dBm	2.0:1
CA812-3111	8.0-12.0	27	1.6 MAX, 1.4 TYP	+10 MIN	+20 dBm	2.0:1
CA1218-4111	12.0-18.0	25	1.9 MAX, 1.7 TYP	+10 MIN	+20 dBm	2.0:1
CA1826-2110	18.0-26.5	32	3.0 MAX, 2.5 TYP	+10 MIN	+20 dBm	2.0:1

NARROW BAND LOW NOISE AND MEDIUM POWER AMPLIFIERS

Model No.	Freq (GHz)	Gain (dB) MIN	Noise Figure (dB)	Power-out @ P1-dB	3rd Order ICP	VSWR
CA01-2111	0.4 - 0.5	28	0.6 MAX, 0.4 TYP	+10 MIN	+20 dBm	2.0:1
CA01-2113	0.8 - 1.0	28	0.6 MAX, 0.4 TYP	+10 MIN	+20 dBm	2.0:1
CA12-3117	1.2 - 1.6	25	0.6 MAX, 0.4 TYP	+10 MIN	+20 dBm	2.0:1
CA23-3111	2.2 - 2.4	30	0.6 MAX, 0.45 TYP	+10 MIN	+20 dBm	2.0:1
CA23-3116	2.7 - 2.9	29	0.7 MAX, 0.5 TYP	+10 MIN	+20 dBm	2.0:1
CA34-2110	3.7 - 4.2	28	1.0 MAX, 0.5 TYP	+10 MIN	+20 dBm	2.0:1
CA56-3110	5.4 - 5.9	40	1.0 MAX, 0.5 TYP	+10 MIN	+20 dBm	2.0:1
CA78-4110	7.25 - 7.75	32	1.2 MAX, 1.0 TYP	+10 MIN	+20 dBm	2.0:1
CA910-3110	9.0 - 10.6	25	1.4 MAX, 1.2 TYP	+10 MIN	+20 dBm	2.0:1
CA1315-3110	13.75 - 15.4	25	1.6 MAX, 1.4 TYP	+10 MIN	+20 dBm	2.0:1
CA12-3114	1.35 - 1.85	30	4.0 MAX, 3.0 TYP	+33 MIN	+41 dBm	2.0:1
CA34-6116	3.1 - 3.5	40	4.5 MAX, 3.5 TYP	+35 MIN	+43 dBm	2.0:1
CA56-5114	5.9 - 6.4	30	5.0 MAX, 4.0 TYP	+30 MIN	+40 dBm	2.0:1
CA812-6115	8.0 - 12.0	30	4.5 MAX, 3.5 TYP	+30 MIN	+40 dBm	2.0:1
CA812-6116	8.0 - 12.0	30	5.0 MAX, 4.0 TYP	+33 MIN	+41 dBm	2.0:1
CA1213-7110	12.2 - 13.25	28	6.0 MAX, 5.5 TYP	+33 MIN	+42 dBm	2.0:1
CA1415-7110	14.0 - 15.0	30	5.0 MAX, 4.0 TYP	+30 MIN	+40 dBm	2.0:1
CA1722-4110	17.0 - 22.0	25	3.5 MAX, 2.8 TYP	+21 MIN	+31 dBm	2.0:1

ULTRA-BROADBAND & MULTI-OCTAVE BAND AMPLIFIERS

Model No.	Freq (GHz)	Gain (dB) MIN	Noise Figure (dB)	Power-out @ P1-dB	3rd Order ICP	VSWR
CA0102-3111	0.1-2.0	28	1.6 Max, 1.2 TYP	+10 MIN	+20 dBm	2.0:1
CA0106-3111	0.1-6.0	28	1.9 Max, 1.5 TYP	+10 MIN	+20 dBm	2.0:1
CA0108-3110	0.1-8.0	26	2.2 Max, 1.8 TYP	+10 MIN	+20 dBm	2.0:1
CA0108-4112	0.1-8.0	32	3.0 MAX, 1.8 TYP	+22 MIN	+32 dBm	2.0:1
CA02-3112	0.5-2.0	36	4.5 MAX, 2.5 TYP	+30 MIN	+40 dBm	2.0:1
CA26-3110	2.0-6.0	26	2.0 MAX, 1.5 TYP	+10 MIN	+20 dBm	2.0:1
CA26-4114	2.0-6.0	22	5.0 MAX, 3.5 TYP	+30 MIN	+40 dBm	2.0:1
CA618-4112	6.0-18.0	25	5.0 MAX, 3.5 TYP	+23 MIN	+33 dBm	2.0:1
CA618-6114	6.0-18.0	35	5.0 MAX, 3.5 TYP	+30 MIN	+40 dBm	2.0:1
CA218-4116	2.0-18.0	30	3.5 MAX, 2.8 TYP	+10 MIN	+20 dBm	2.0:1
CA218-4110	2.0-18.0	30	5.0 MAX, 3.5 TYP	+20 MIN	+30 dBm	2.0:1
CA218-4112	2.0-18.0	29	5.0 MAX, 3.5 TYP	+24 MIN	+34 dBm	2.0:1

LIMITING AMPLIFIERS

Model No.	Freq (GHz)	Input Dynamic Range	Output Power Range Psat	Power Flatness dB	VSWR
CLA24-4001	2.0 - 4.0	-28 to +10 dBm	+7 to +11 dBm	+/- 1.5 MAX	2.0:1
CLA26-8001	2.0 - 6.0	-50 to +20 dBm	+14 to +18 dBm	+/- 1.5 MAX	2.0:1
CLA712-5001	7.0 - 12.4	-21 to +10 dBm	+14 to +19 dBm	+/- 1.5 MAX	2.0:1
CLA618-1201	6.0 - 18.0	-50 to +20 dBm	+14 to +19 dBm	+/- 1.5 MAX	2.0:1

AMPLIFIERS WITH INTEGRATED GAIN ATTENUATION

Model No.	Freq (GHz)	Gain (dB) MIN	Noise Figure (dB)	Power-out @ P1-dB	Gain Attenuation Range	VSWR
CA001-2511A	0.025-0.150	21	5.0 MAX, 3.5 TYP	+12 MIN	30 dB MIN	2.0:1
CA05-3110A	0.5-5.5	23	2.5 MAX, 1.5 TYP	+18 MIN	20 dB MIN	2.0:1
CA56-3110A	5.85-6.425	28	2.5 MAX, 1.5 TYP	+16 MIN	22 dB MIN	1.8:1
CA612-4110A	6.0-12.0	24	2.5 MAX, 1.5 TYP	+12 MIN	15 dB MIN	1.9:1
CA1315-4110A	13.75-15.4	25	2.2 MAX, 1.6 TYP	+16 MIN	20 dB MIN	1.8:1
CA1518-4110A	15.0-18.0	30	3.0 MAX, 2.0 TYP	+18 MIN	20 dB MIN	1.85:1

LOW FREQUENCY AMPLIFIERS

Model No.	Freq (GHz)	Gain (dB) MIN	Noise Figure dB	Power-out @ P1-dB	3rd Order ICP	VSWR
CA001-2110	0.01-0.10	18	4.0 MAX, 2.2 TYP	+10 MIN	+20 dBm	2.0:1
CA001-2211	0.04-0.15	24	3.5 MAX, 2.2 TYP	+13 MIN	+23 dBm	2.0:1
CA001-2215	0.04-0.15	23	4.0 MAX, 2.2 TYP	+23 MIN	+33 dBm	2.0:1
CA001-3113	0.01-1.0	28	4.0 MAX, 2.8 TYP	+17 MIN	+27 dBm	2.0:1
CA002-3114	0.01-2.0	27	4.0 MAX, 2.8 TYP	+20 MIN	+30 dBm	2.0:1
CA003-3116	0.01-3.0	18	4.0 MAX, 2.8 TYP	+25 MIN	+35 dBm	2.0:1
CA004-3112	0.01-4.0	32	4.0 MAX, 2.8 TYP	+15 MIN	+25 dBm	2.0:1

CIAO Wireless can easily modify any of its standard models to meet your "exact" requirements at the Catalog Pricing.

Visit our web site at www.ciaowireless.com for our complete product offering.

Ciao Wireless, Inc. 4000 Via Pescador, Camarillo, CA 93012

Tel (805) 389-3224 Fax (805) 389-3629 sales@ciaowireless.com

Revolutionizing GaN Technology for Improved RF Sensors

RTX has been awarded a four-year, $15 million contract from DARPA to increase the electronic capability of RF sensors with high power density GaN transistors. The improved transistors will have 16x higher output power than traditional GaN with no increase in operating temperature.

Raytheon is a leading manufacturer of military-grade GaN, a cutting-edge semiconductor technology that, when used in radar systems, improves range and radar resource management handling. This new prototyping work is being performed under DARPA's Technologies for Heat Removal in Electronics at the Device Scale program, known as THREADS.

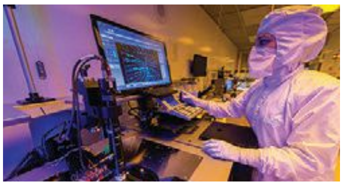

THREADS (Source: RTX)

Raytheon is partnering with the Naval Research Laboratory, Stanford University and Diamond Foundry to grow diamond, the world's best thermal conductor, for integration with military-grade GaN transistors and circuits. Cornell University, Michigan State University, the University of Maryland and Penn State University also provide technology and performance analysis.

Microelectronics for Next-Generation Radar, EW and Communication

The Office of Naval Research (ONR) has awarded BAE Systems' FAST Labs research and development organization a $5 million contract for the Common-architecture Amplifier for Low-cost, Efficient, SWaP-Constrained Environments (COALESCE) program.

In this effort, BAE Systems' FAST Labs will develop advanced GaN-based MMIC and module electronics. The program's objective is to develop the world's highest efficiency high power amplifier module in its frequency band. The RF modules will then transition to small form factor U.S. Navy payloads, enabling longer range and greater effectiveness in active electronic warfare (EW) applications.

"The COALESCE program closes the gap between commercial electronics and customized electronics to meet the Department of Defense's space and power requirements and enable next-generation solutions," said Ben McMahon, technology development manager at BAE Systems' FAST Labs. "Together with the ONR, we will deliver these electronic solutions to increase survivability for our warfighters."

COALESCE (Source: BAE Systems)

BAE Systems will provide capabilities above and beyond what can be found commercially, and its solution is designed specifically for harsh Department of Defense operating environments. The technology's high power and ultra-small form factor will enable next-generation radar, EW and communication applications.

NATO Strengthens Situational Awareness

NATO has selected its next-generation command and control aircraft as the Alliance's existing Airborne Warning and Control (AWACS) fleet nears retirement. Production of the six new Boeing's E-7A Wedgetail aircraft is set to begin in the coming years, with the first aircraft expected to be ready for operational duty by 2031. A consortium of Allies gave their approval to the project, one of NATO's biggest-ever capability purchases, in November.

"Surveillance and control aircraft are crucial for NATO's collective defense and I welcome Allies' commitment to investing in high-end capabilities," said NATO Secretary General Jens Stoltenberg. "By pooling resources, Allies can buy and operate major assets collectively that would be too expensive for individual countries to purchase. This investment in state-of-the-art technology shows the strength of transatlantic defense cooperation as we continue to adapt to a more unstable world."

NATO AWACS (Source: NATO)

The E-7 Wedgetail is an advanced early warning and control aircraft that provides situational awareness and command and control functions. Equipped with a powerful radar, the aircraft can detect hostile aircraft, missiles and ships at great distances and can direct NATO fighter jets to their targets. The U.S., the U.K. and Turkey also either fly the Wedgetail or plan to operate it. It is based on a militarized version of the 737 jetliner.

NATO has operated a fleet of E-3A AWACS aircraft since the 1980s. Based at Geilenkirchen airbase in Germany, the AWACS have flown in every major NATO operation, including the fight against ISIS as well as on NATO's eastern flank following Russia's invasion of Ukraine. The E-7 is expected to have its main base at Geilenkirchen and could operate from several forward locations across Europe. The Wedgetail will be part of

For More Information Visit mwjournal.com for more defense news.

the Alliance's future surveillance and control project which will field NATO's next-generation surveillance systems from the mid-2030s.

GA-ASI Demos Short Takeoff/Landing of a UAS on UK Carrier

General Atomics Aeronautical Systems, Inc. (GA-ASI) conducted a first-of-its-kind demonstration of its short takeoff and landing (STOL) capability on the HMS Prince of Wales, a Royal Navy aircraft carrier, using the Mojave Unmanned Aircraft System (UAS). The demonstration took place in November when the Prince of Wales was underway off the East Coast of the U.S. and the Mojave was controlled by an aircrew within a control station onboard the ship. The demonstration included takeoff, circuits and approaches and ended with a landing back onto the carrier.

Mojave is a short takeoff and landing UAS demonstrator originally developed to prove STOL operations at unprepared landing sites. While Mojave shares common systems and components with GA-ASI's Gray Eagle model, a STOL wing set option is likewise being planned for the larger, more capable MQ-9B aircraft, which includes SkyGuardian®, SeaGuardian® and the

STOL Demo (Source: General Atomics)

new Protector RG Mk 1 currently being delivered to the U.K. Royal Air Force. The MQ-9B version, called MQ-9B STOL, is being considered by the Royal Navy and other navies that operate aircraft from large flat-deck warships without catapults and arresting gear.

Equipping UAS with STOL capability provides greater versatility and allows the aircraft to operate in areas previously deemed unsuitable for UAS operations, including landing onto and taking off from an aircraft carrier. MQ-9B STOL will be capable of carrying the same payloads and conducting the same missions as the SkyGuardian and SeaGuardian, including maritime surveillance, anti-submarine warfare, airborne early warning and surface strike.

DC TO 95 GHz

High-Frequency Products

For mmWave Test Applications

LEARN MORE

E-Band Amplifiers

ZVA-50953G+

E-Band Medium Power Amplifier

- 50 to 95 GHz
- +21 dBm P_{OUT} at Saturation
- 28 dB gain
- ±2.0 dB gain flatness
- Single supply voltage, +10 to +15V

ZVA-71863HP+

E-Band Medium Power Amplifier

- 71 to 86 GHz
- +24 dBm P_{OUT} at Saturation
- 38 dB gain
- ±1.5 dB gain flatness
- Single supply voltage, +10 to +15V

ZVA-71863LNX+

E-Band Low Noise Amplifier

- 71 to 86 GHz
- 4.5 dB noise figure
- 37 dB gain
- +13.8 dBm P1dB, +18 dBm P_{SAT}
- Single-supply voltage, +10 to +15V

K – V-Band Amplifiers

ZVA-35703+

Medium Power Amplifier

- 35 to 71 GHz
- +21 dBm P_{SAT}
- 17.5 dB gain
- ±1.5 dB gain flatness
- Single supply voltage, +10 to +15V

ZVA-543HP+

Medium Power Amplifier

- 18 to 54 GHz
- +29 dBm P_{SAT}
- High gain, 31 dB
- ±2.0 dB gain flatness
- Single supply voltage, +10 to +15V

ZVA-0.5W303G+

Medium Power Amplifier

- 10 MHz to 30 GHz
- 0.5W P_{OUT} at Saturation
- ±1.5 dB gain flatness
- 4.2 dB noise figure
- Single +12V bias voltage

More Products In Stock

BIAS TEES

DIGITAL STEP ATTENUATORS

I/Q MIXERS

MIXERS

MULTIPLIERS

POWER DETECTORS

SWITCHES

& MORE

Mini-Circuits®

6G – Now and in the Future

Every decade, a new telecom generation emerges, with 5G currently being commercialized, offering faster data rates, low latency and enhanced reliability. 6G is characterized by terabits per second (Tbps) data rates, microsecond latency and extensive network dependability. Operating in the THz spectrum, it extends to applications beyond connectivity, encompassing energy harvesting, sensing and more. Technological challenges, research trends, applications and market of 6G are covered in the IDTechEx market research report "6G Market 2023-2043: Technology, Trends, Forecasts, Players."

In the realm of 5G, the frequency band assigned includes the sub-6 GHz spectrum (3.5 to 6 GHz) and the mmWave band (24 to 40 GHz). As the focus shifts to 6G, the spectrum encompasses a range of frequencies. The candidates include the 7 to 20 GHz frequency band, followed by W-Band (75 to 110 GHz), D-Band (110 to 175 GHz), segments spanning 275 to 300 GHz and extending into the terahertz (THz) range (0.3 to 10 THz).

Incorporating the 7 to 20 GHz bands is strategic, driven by the demand for coverage that can support mobile applications and facilitate "on the go" applications for diverse 6G use cases. The W- and D-Bands hold significance not only for 6G access but also for networks like Xhaul, encompassing fronthaul and backhaul services. Solutions that effectively serve both these services are under consideration.

As of September 2022, global spectrum allocations have not extended beyond 275 GHz. However, the 275 to 450 GHz range has been earmarked for implementing land mobile and fixed service applications alongside radio astronomy, earth exploration, satellite services and space research services, spanning from 275 to 1000 GHz.

6G promises substantial advantages, most notably the potential for leveraging expansive bandwidth (GHz range) that can support peak data flow in the Tbps range, all while maintaining microsecond-level latency.

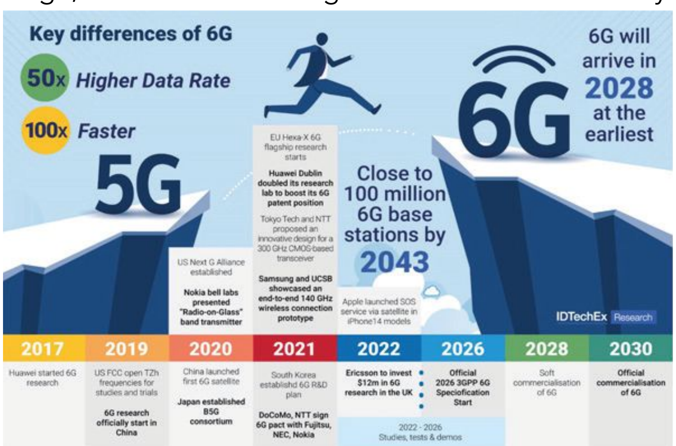

6G Roadmap (Source: IDTechEx)

However, despite the immense potential, the use of such high frequency spectra is not without its challenges.

The key challenges in 6G are very short signal propagation range (cm range for above 100 GHz frequency) and line-of-sight obstacles.

THz signals face severe limitations in how far they can travel due to substantial absorption in the air. This makes addressing signal decaying and establishing strong communication over reasonable distances a top priority for 6G. Likewise, the higher frequency nature of THz signals makes them highly sensitive to obstacles in their direct path.

To overcome this issue, improving the link budget of a communication device becomes essential to enhance signal propagation. Higher power is needed for greater link budget. The final power output results from both the antenna gain and the power amplifier gain.

The development of 6G technology has been rapidly advancing since its inception. In 2017, Huawei embarked on its 6G research and since 2019, key milestones have been achieved on multiple fronts. The U.S. FCC opened up THz frequencies for experimental studies and trials. China also formally initiated its 6G research. Global collaboration and consortiums gained traction, with the U.S. Next G Alliance, Japan's B5G consortium and the European Union's Hexa-X project.

Meanwhile, pioneering initiatives by companies from infrastructure suppliers to telecom operators showcased key strides in hardware innovation and continue to pump investment into 6G R&D, underlining their dedication to shaping the future of wireless communication.

Advancements were also seen in satellite-based services and wireless connections. China launched its first 6G satellite, Apple launched an SOS service via satellite in iPhone 14 models and Starlink has had worldwide connection apart from the poles since August 2021.

According to IDTechEx, the gradual introduction of 6G technology is likely to begin around 2028, with official commercialization anticipated by 2030. The standardization process, led by 3GPP, will be vital for ensuring the compatibility and adoption of this innovative technology, and it is set to commence in 2026.

Structural Health Monitoring Sensors for Critical Infrastructure to Reach 22.9M Connections by 2030

Governments are increasingly eager to address the escalating maintenance needs of aging critical infrastructure, including rail, bridges, mines, dams and older buildings. Safety concerns, amplified by disastrous incidents like the 2018 Morandi Bridge collapse, which resulted in 43 casualties and a staggering U.S.$450 million in damages, have sparked

For More Information Visit mwjournal.com for more commercial market news.

a preference for "predictive maintenance" over "maintenance after failure" approaches. The surge in extreme weather events linked to climate change has also laid bare additional vulnerabilities in aging and strained post-war infrastructure. A greater variety of sensor and connectivity types, alongside more advanced data analytics software platforms, is enabling the structural health monitoring (SHM) market to expand. According to ABI Research, SHM sensors will reach 22.9 million connections by 2030, with a compound annual growth rate of 18 percent for wired retrofitted sensors and 28 percent for wireless retrofitted sensors.

"The greater variety of IoT sensor hardware has made it much easier for asset owners to integrate sensors into their operations, shifting away from expensive and bulky implementations to lower cost and easy-to-install solutions," said Maryam Zafar, IoT markets analyst at ABI Research. "Vendors are increasingly investing in software and analytics platforms to extract meaningful information from large volumes of data. Enhanced software intelligence is key, offering actionable information that adds significant value and enables more efficient predictive maintenance."

Innovation is happening on two fronts in the SHM market. First, it is happening on the hardware edge with a shift to smaller data loggers and DAQs, greater edge processing capabilities and a more extensive variety of sensors and technologies. Second, it is happening with the software. Many companies seek an analytics platform, often compatible with other third-party sensors. Vendors also want to see how AI can improve predictive capabilities and generate more value for asset owners and managers. Companies that are leading the market and driving innovation include Worldsensing, Campbell Scientific, Encardio Rite, GEO-Instruments, Hottinger Bruel & Kjaer and Bentley Systems.

> Growth is enabled by a greater variety of sensor and connectivity types alongside more advanced data analytics software.

One of the biggest markets for SHM is the rail industry, as demand for rail transport is expected to double in the next two decades. As demand for passenger and freight travel increases, so does the need to prevent delays. By digitizing rail infrastructure and monitoring critical areas of concern, such as rail tracks, switches and slopes, rail operators know when failures will happen and can implement more efficient predictive maintenance strategies. Wireless sensor technology is essential here, with vendors like KONUX and Senceive making a mark in this market.

Around the **Circuit**

Barbara Walsh, Multimedia Staff Editor

MERGERS & ACQUISITIONS

Q Microwave Inc. announced its acquisition by **Amphenol Corporation**. The acquisition took place during the third quarter, which concluded in September 2023. Q Microwave will be included in Amphenol's Harsh Environment Solutions Segment. Founded over 25 years ago and headquartered in the vibrant wireless community of El Cajon, San Diego, Q Microwave has consistently empowered global military and space RF specialists with unmatched RF filter and sub-system solutions. The company's commitment to in-house technical expertise, innovation and customer-centric efficiency has solidified its position as a trusted partner in the industry.

COLLABORATIONS

Keysight Technologies Inc. and **MediaTek** have successfully completed 5G New Radio and 5G reduced capability (RedCap) interoperability development testing (IODT) based on the 3GPP Release 17 standard. The testing verified the latest MediaTek 5G modem technologies using Keysight's 5G Network Emulation Solutions. IODT, an important step in validating equipment using new 5G specifications, determines whether a base station and device can establish and maintain a 5G communication link based on prescribed test conditions. The RedCap interoperability testing conducted by Keysight and MediaTek validated that the MediaTek 5G modem technologies supports early identification, bandwidth part definition, user equipment capability, radio resource management relaxation, network control device-synchronization signal block and sounding reference signal enhancement.

Modelithics® and **RFMW** announce their collaboration to expand the resources readily available to engineering designers and suppliers. The RFMW and Modelithics collaboration offers engineering designers rapid access to obtain device components and technical information. This technical information includes device datasheets as well as highly accurate simulation models for industry-leading suppliers of RF, microwave and mmWave electronic devices, such as Qorvo, Marki Microwave, Smiths Interconnect, Knowles, Spectrum Control, Guerilla RF and more. Through the Modelithics Vendor Partner program, many suppliers are sponsoring free extended use of Modelithics models, for customers that do not already have access to the Modelithics COMPLETE Library or its customized vendor specific libraries.

In a significant development for the world of AME, **Jetted Additively Manufactured Electronics Sources (J.A.M.E.S)** announce a strategic partnership with **Advanced Printed Electronic Solutions (APES)**. This collaboration is set to drive innovation, amplify brand awareness and foster advancements in the field of 3D printed electronics. The partnership between J.A.M.E.S and APES opens doors to an array of collaborative projects aimed at advancing AME. Both companies bring unique strengths to the table, creating opportunities for mutual value creation. APES, with its focus on the North American market, complements J.A.M.E.S, which has a strong presence in Europe. This geographic synergy allows for a seamless exchange of support and market expansion.

Digital Nasional Berhad (DNB), **Telekom Malaysia Berhad (TM)** and **ZTE Corporation** have forged a strategic alliance to unveil the world's fastest 5G live trial which will deliver remarkable speeds up to 28 Gbps. This groundbreaking technology will reshape Malaysia's digital landscape and establish a new global standard in wireless communication. An expansion of DNB's commitment to driving 5G capabilities for the country, the partnership will leverage TM's established network infrastructure and digital expertise, as well as ZTE's state-of-the-art mmWave active antenna unit to deliver Malaysia's first standalone 5G core, complemented by an adaptable next-generation transport network.

Picocom, a 5G Open RAN baseband semiconductor and software specialist, announced that it has collaborated with **Texas Instruments (TI)** on a complete 5G Open RAN small cell radio unit reference design to help accelerate customers' time-to-market. The 5G small cell radio unit meets the O-RAN Alliance specification for a 5 W 4T4R 200 MHz 5G outdoor radio unit. It features TI's AFE7769D quad-channel RF transceiver integrating DPD/CFR with Picocom's PC802 5GNR/LTE PHY System-on-Chip. The reference design hardware is also LTE compatible.

SWISSto12 announced it is developing active electronically steerable antennas (AESAs) for airborne, land and maritime platforms in collaboration with **Thales**. SWISSto12's AESAs will use innovative 3D-printed miniature horn antennas instead of traditional patch antennas. These 3D-printed antenna apertures are of higher efficiency and overall performance (gain, axial ratio and bandwidth over scan volume) than patch antennas. These features are key to maintaining wide-angle scanning capabilities in AESAs. SWISSto12's 3D-printed antennas are mounted on planar beamformers provided by Thales, which will use the latest beamforming integrated circuits and innovative patented interconnection solutions.

Presto Engineering announced its collaboration with **Nokia** for the industrialization of new equipment designed to build the foundations of the next generation of microwave links as part of the DIMIT project, supported by the French Public Investment Bank. Through this collaboration, Presto Engineering and Nokia are addressing the challenge of RF application design and RF

For More Information For up-to-date news briefs, visit mwjournal.com

testing beyond 80 GHz. They intend to develop a new generation of microwave links that are more integrated with the 5G and future 6G markets. The DIMIT 5G project involves studying and industrializing new microwave transmission equipment to enable the densification and enhancement of 5G RAN networks.

NEW STARTS

Nullspace Inc. announced the launch of its Academic Partnership Program. This initiative is designed to empower and accelerate cutting-edge research in the field of electromagnetics (EM). Nullspace EM simulation software provides power and speed, enabling design and optimization of antennas, radars and other RF devices faster and with more flexibility than other EM simulation tools. Nullspace's Academic Program offers researchers access to Nullspace EM, Nullspace ES and Nullspace Prep software tools, helping to advance the understanding of EM, enabling successful publications and research projects and empowering researchers to push the boundaries of what is possible in EM design and analysis.

Astrodyne TDI, a technology leader in power electronics, power distribution units and EMI filters, announced the opening of its new state-of-the-art manufacturing facility in Penang, Malaysia. This development marks a significant milestone in the company's growth and commitment to serving its customers with leading-edge manufacturing capabilities. Affirming their dedication to delivering high-quality products and services to their valued customers worldwide, the new factory boasts 32,000 ft.^{2} of initial production space with a committed expansion to 75,000 ft.^{2} in 2024. Equipped with the latest cutting-edge technology and automation, including 3D automated optical inspection, the new facility is positioned to meet the growing demands of their customers and the market.

ACHIEVEMENTS

Antenna Research Associates (ARA) announced its 60th anniversary. Founded in 1963, the company has decades of experience designing, developing and manufacturing antennas and RF systems for both military and civilian applications across a multitude of industries including: communication networks, unmanned air systems satcom, radar, RF surveillance and jamming for electronic warfare, spectrum operations and border patrol, public safety networks and civilian markets. What began as an RF communications antenna business has grown to become an industry leader with cross market capabilities, a fleet of new innovations and over 50 patents for unique solutions to both civilian and military challenges.

Quantic Microwave Dynamics, a business of **Quantic® Electronics** and a manufacturer of high-precision microwave and mmWave solutions, celebrates 30 years of operation. Founded in 1993, Quantic Microwave Dynamics has consistently delivered cutting-edge solutions that ensure peak performance for demanding RF and microwave applications. Quantic Microwave Dynamic's products have found applications on land, sea, air and space, showcasing their ability to perform under the harshest conditions, including intense shock, vibration and high temperature variances.

CONTRACTS

Comtech announced the receipt of a $20 million order from the company's U.K.-based partners, **Spectra Group**. The order will allow Spectra Group, the appointed regional distributor of Comtech's Compact Over-the-Horizon Transportable Terminal (COMET), to service multiple orders already received and several expected follow-on orders from undisclosed customers in the NATO and European regions. Comtech's feature-rich, network agnostic COMET system is designed to be easily integrated with other Department of Defense and coalition tactical, mobile and fixed communications systems to provide resilient, secure beyond-line-of-sight (BLOS) capabilities in some of the world's most challenging environments. Each Comtech COMET is an end-to-end, rapidly deployable BLOS system that utilizes a single fully integrated Troposcatter hub, which includes the company's CS67PLUS Troposcatter radio.

Gilat Satellite Networks Ltd announced that the **U.S. Army** awarded a nearly $20 million contract to the company's U.S.-based subsidiary, Wavestream, for the continuation of a program to sustain anytime, anywhere satellite connectivity. Wavestream's solid-state power amplifier, ruggedized to withstand the harshest environments, enables the satellite transportable terminals used in this program to deliver a "Communications-on-the-Pause" solution across diverse climates and conditions around the globe.

Smiths Interconnect announced it has received £1,907,065 in funding from the **U.K. Space Agency** through its Space Clusters Infrastructure Fund (SCIF). Smiths Interconnect will use the funding to enhance its space qualification laboratory, a cutting-edge facility in Dundee that simulates the extreme conditions of space to assure the quality and durability of space components. From simulating the extreme vibration and shock environment of launch to surviving the extreme temperature swings experienced during space flight, the lab has a full range of capabilities in which it will be investing substantially through the SCIF grant.

Sypris Electronics LLC, a subsidiary of **Sypris Solutions Inc.**, announced that it has recently received two full rate production follow-on multimillion-dollar contract awards from a U.S. global defense contractor to manufacture advanced integrated electronic warfare and communications avionics system modules for one of the largest government Department of Defense programs. Production was expected to begin in 2023 and is planned to continue into mid-year 2025. Terms of the agreement were not disclosed. The program is for an American family of single-seat, single-engine, all-weather stealth multirole combat aircraft that is intended to perform both air superiority and strike missions.

Around the **Circuit**

PEOPLE

▲ *Chris Emerson*

ALL.SPACE announced the appointment of **Chris Emerson**, a respected former aerospace executive, as chairman of the Board. Emerson's rich leadership experience, proven in his previous senior executive roles at Airbus, as well as his current engagement in the space industry, will be key in guiding ALL.SPACE as it moves its fifth generation 'smart terminal' into initial production, set for release in Q4 2023. With a distinguished career in aerospace and defense, Emerson brings a wealth of experience to the company, having previously served as chairman and CEO of Airbus US Space and Defense and, prior, president of Airbus Helicopters Inc. His other executive roles included marketing, product strategy and finance.

▲ *Eric de Saintignon*
Nicolas Capet

Building on its recent commercial successes and the development of new innovative products, **Anywaves** continues its market expansion. Through EdSpace, **Eric de Saintignon** has been appointed as the general manager to support the space antenna specialist in its upward trajectory. This appointment will enable **Nicolas Capet**, the founder and president, to prepare the future of Anywaves through the Strategy Department, for which he assumes responsibility. With over 30 years of experience in the space industry, Eric de Saintignon has notably excelled by taking the helm of OneWeb Satellites at its inception in 2015.

▲ *Dr. Ajay Poddar*

The 2023 Radio Club of America Armstrong Medal has been presented to **Dr. Ajay Poddar** in recognition of his legacy of innovation and his many contributions to the art and science of radio. Dr. Ajay K. Poddar (SM 2005, Fellow 2015) is an IEEE Fellow and is a member of IEEE Eta-Kappa-Nu. He is the chief scientist at Synergy Microwave, responsible for the design and development of signal generation and signal processing electronics for industrial, medical and space applications. Poddar's work includes RF-MEMS and metamaterial-antenna/sensors/electronics. He also serves as a visiting professor at the University of Oradea, Romania, Indian Institute of Technology Jammu, India, and a guest lecturer at the Technical University Munich, Germany.

For more news and industry happenings, visit mwjournal.com daily.

INVITED PAPER

Selecting the Best ADC for Radar Phased Array Applications: Part 1

Benjamin Annino
Analog Devices, Wilmington, Mass.

Many papers discuss the system trade-offs and relative merits of digital, analog and hybrid beamforming.[1] Building on prior work, this article uses RF-to-analog-to-digital converter (ADC) cascade modeling to show dynamic range (linearity and noise) and sample rate trade-offs against DC power consumption in a multichannel system with varying channel summation in both the RF and digital realms. The optimal selection of sample rate, ADC effective number of bits (ENOB) and RF versus digital channel combining are weighed against DC power consumption. The Schreier and Walden ADC figures of merit (FOMs) are proposed as extensible to a multichannel system to express a single system FOM portraying optimal dynamic range normalized for DC power. Part 2 of this article will analyze the results and draw conclusions from system FOMs.

SYSTEM MODEL INTRODUCTION

In the phased array radar community, full digital beamforming gets a lot of attention. Significant government funding is leading to this capability rapidly evolving and the technique is an industry research hotbed. The promise of omnidirectional arrays with digital beamforming creating simultaneous beams enables software-defined multimission apertures and one array fits many missions. The appeal is multiple independent, simultaneous, software-configurable digital beams that improve detection and enable multifunction.[1]

In practice, there are multiple challenges to overcome; the biggest being DC power consumption. In elemental digital beamforming, the digitizer node (DAC/ADC) is distributed behind each element and must be of lower DC power than alternatives without sacrificing performance. Digitizer power is a function of dynamic range capability and sampling rate. Choosing the optimal ADC bit resolution and sampling rate, while being cognizant of RF performance, power consumption and digital versus analog beamforming capability is a complicated multidimensional puzzle for phased array system designers.

Thermal limits and size are also factors. Larger phased arrays often employ blades that put the electronics orthogonal to the antenna face, offering thermal and size flexibility. Some systems, especially those at higher frequencies, require electronics that are planar with the antenna and fit within the element lattice spacing. This creates challenging thermal and size problems. The electronics must get smaller and shed power without sacrificing performance.

SYSTEM FIGURES OF MERIT

Dynamic range, or spurious-free dynamic range (SFDR), is the most common receiver FOM and is a function of linearity and sensitivity. Receiver SFDR is different than ADC SFDR. ADC SFDR quantifies the maximum ADC spur among harmonics, interleaving spurs, clock leakage and intermodulation products and is not a direct representation of two-tone linearity. Receiver sensitivity is the minimum detectable signal level at some offset threshold from the noise floor. Considerations like waveform type and probability of detection determine the offset threshold, which is set to zero in this paper. Sensitivity does not consider linearity; it is solely a noise metric. A point of emphasis: radar and electronic warfare (EW) systems operate in blocker environments, so linearity (two-tone intermodulation) is as important as noise. Phased array systems are generally sub-octave and IMD3 distortion is most important. Conversely, EW systems are multi-octave

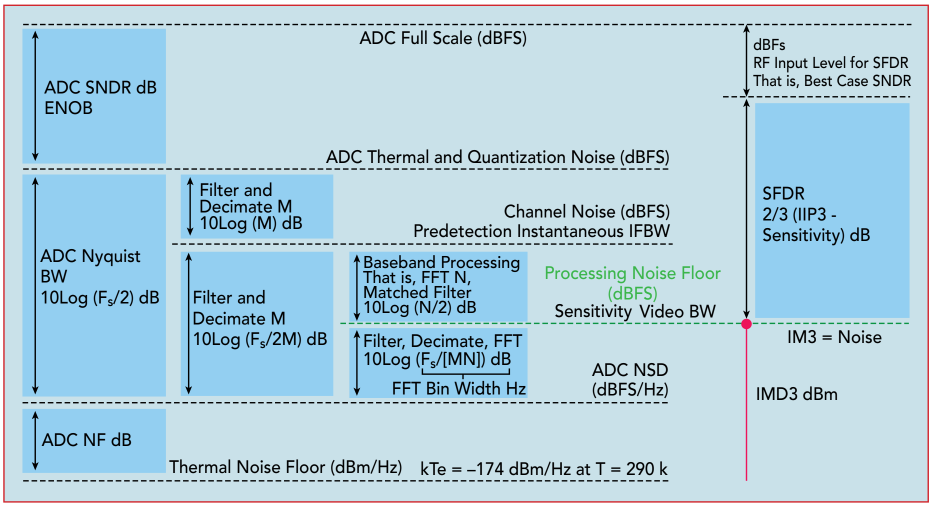

Fig. 1 **Noise contribution of ADC SNDR, NF, IFBW, IMD3 and SFDR.**[3]

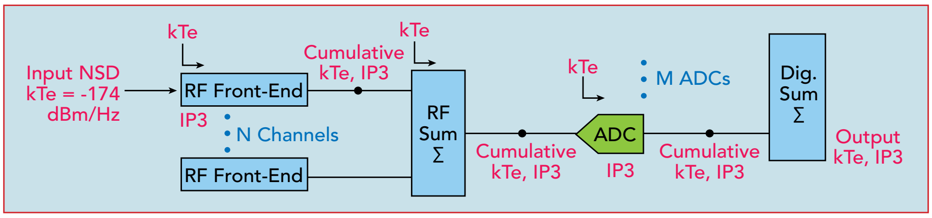

Fig. 2 **Phased array cascade model using analog and digital beamforming and summation.**

and IMD2 and IMD3 distortion is most important. A radar or EW receiver is typically not optimized only for sensitivity. Linearity is an important design goal and receiver SFDR is a handy FOM because it considers both sensitivity and linearity. ***Figure 1*** illustrates the noise contribution from various processes and components.

SFDR is a single-point FOM that expresses the best-case SNR and distortion at a singular best-case RF input power. This occurs when the IMD spurs are at the same level as the noise.[2] SFDR can be expressed as shown in Equation 1:

$$\text{SFDR}\left(\text{dB}\right) = 2/3 \left(\text{IIP3}\left(\text{dBm}\right) - \text{Sensitivity}\left(\text{dBm}\right)\right) \quad (1)$$

$$\text{Sensitivity}\left(\text{dBm}\right) = -174\ \text{dBm}/\text{Hz} + \text{NF} + 10\ \text{Log}\left(\text{IFBW}\right)$$

Where the processing bandwidth of the noise channel (IFBW), often set using a combination of IF and digital filtering and the thermal noise spectral density, is -174 dBm/Hz at T=290 K.

The model analyzes SFDR and sensitivity system performance FOMs. These metrics are processing bandwidth dependent and the processing bandwidth is set to IFBW=1 Hz. To adjust for the specific processing bandwidth:

- Add 10log(IFBW) to the sensitivity
- Subtract (2/3 x 10log(IFBW)) from SFDR

A receiver often has simultaneous sensitivity and SFDR requirements. Low RF front-end (RFFE) noise figure (NF) helps IP3 and SFDR, but gain helps sensitivity and hurts SFDR. A "Goldilocks" RFFE has enough gain to meet sensitivity requirements but not too much for fear of degrading SFDR. As a rule of thumb; never design a receiver with excess gain.

SYSTEM CASCADE MODEL

The objective is to build a simple Excel model that accommodates swept RF, digital beamforming ratios, ADC ENOB and DC power consumption derived from Murmann survey data. This data will be used to determine the best performance/DC power consumption solution. The cascade model includes the RFFE, channel summation, ADC and digital channel summation. ***Figure 2*** shows the modeled blocks and cascade metrics at each node.

The model uses the method for summed RF channel cascade analysis described by Delos et al.[4] The key to the model is to track device-additive and cumulative noise spectral density, kTe, at each node and account for signal gain and noise gain separately.

Using this model, it is possible to get a negative system NF with summed RF channels, which is exactly the desired advantage of coherent summation as shown in Equation 2:

$$\text{NF}_{\text{overall}}\text{dB} = \text{SNR}_{\text{in}} - \text{SNR}_{\text{out}}\text{dB} = \left[\text{signal}_{\text{in}} - \text{noise}_{\text{in}}\right] - \left[\text{signal}_{\text{out}} - \text{noise}_{\text{out}}\right]\text{dB}$$

$$\text{NF}_{\text{overall}}\text{dB} = \text{Gain}_{\text{signal}} - \text{Gain}_{\text{Noise}}\text{dB}$$

$$\text{Gain}_{\text{Noise}}\text{dB} = \text{NSD}_{\text{out}} - \text{NSD}_{\text{in}}\frac{\text{dBm}}{\text{Hz}}$$

$$\text{NSD}\frac{\text{dBm}}{\text{Hz}} = 10\log_{10}\left(\text{kTe}\right)$$

$$k = 1.38 \times 10^{-23}$$

$$T_e = k\left(F - 1\right) \quad (2)$$

Where F (noise factor)=$\text{SNR}_{\text{input}}/\text{SNR}_{\text{output}}$
NSD = noise spectral density.

The examples use a 64-channel subarray. When plots show channel summation, the horizontal axis ranges from 64-channel digital at the origin to 64-channel RF on the right of the axis, with a blend in between. The blend is called hybrid beamforming with increasing RF sum from left to right. ADC ENOB is swept in the analysis and presented in the plots. Trends in DC power and performance are analyzed as these parameters are swept.

MODELING THE RFFE

The RFFE model is an RF black box with gain, NF, IP3 and DC power that are functions of swept attributes. As the system model sweeps the RF, digital sum ratio and ADC ENOB, the RFFE attributes tune for the best cascade performance. ***Table 1*** provides the attribute function equations.

The model sets RFFE gain as a

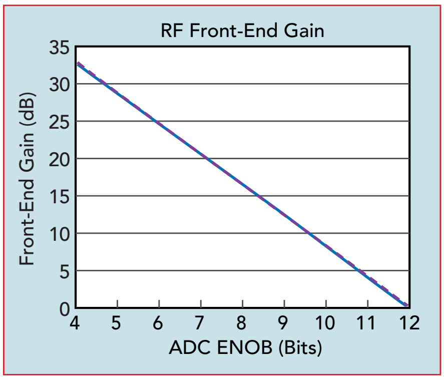

Fig. 3 RFFE gain vs. ADC_ENOB.

TABLE 1			
RFFE ATTRIBUTE EQUATIONS			
Block	**Model Attribute**	**Equation**	**Note**
RFFE	Gain	–4.2 × ADC_ ENOB + 50 dB	
	NF	5 dB	Nominal
	OIP3	ADC_IP3 + 8 – 7 LOG10(N)	N = RF sum ports
	DC power	(N = 1) m × OIP3 + b (mW)	M = 0.14, b = 0.02
		(N > 1) 2× (N = 1 case)	(model fit)

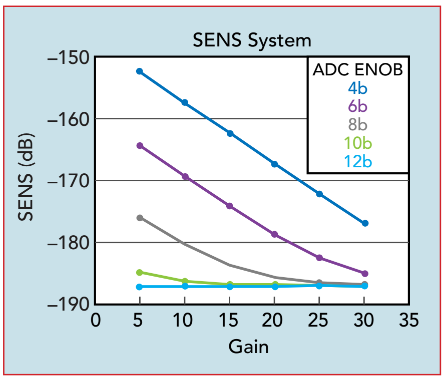

Fig. 4 Overall sensitivity vs. RFFE gain for varying ENOB.

function of ADC_ENOB, a swept parameter, as shown in ***Figure 3***. The model uses a linear equation to set a minimum viable gain for reasonable system kTe while seeking to maximize SFDR. RF gain reduces SFDR, so it should be minimized to just meet NF requirements. Lower-resolution ADCs have a much higher NF and require more RF gain to set acceptable system NF. In contrast, an ADC with ENOB=12 has excellent NF and requires no front-end gain. This provides a big dynamic range benefit, albeit at an ADC DC power penalty. The effect of sensitivity from RFFE gain and ADC ENOB is shown in ***Figure 4***. ***Figure 5*** shows the gain impact on SFDR for an ADC with ENOB=8 and ***Figure 6*** shows the same analysis for an ADC with ENOB=12. The ENOB=8 case sees improving sensitivity and neutral SFDR impact as the gain is increased to approximately 15 dB. Above 15 dB, SFDR begins to degrade. In contrast, the ENOB=12 case has superior ADC NF, requiring no gain in front. Putting the same 15 dB gain block in front would have a net negative impact on ENOB=12 performance.

For these simulations, the RFFE block is set to NF=5 dB and OIP3=30 to 40 dBm. These values are realistic and acknowledge the linearity trade-off. These simulations also assume RFFE filtering, switching, limiting and other loss elements.

The model sets RFFE OIP3 as a function of ADC_IP3 and the number of summed RF ports. The result where every element uses digital beamforming and ADC IP3=22 dBm is shown in ***Figure 7***. This shows that a single port requires an RFFE OIP3 of 30 dB, 8 dB higher than the ADC IP3, for a degradation to system-cascaded IP3 of approximately 0.8 dB. Summing up more RF channels eases the single-channel OIP3 requirement, which eases the RFFE DC power requirement.

DC power is an important consideration and the model sets RFFE DC power as a function of RFFE OIP3, which is a function of ADC IP3 and RF sum ports. For the case of RF=1, the RFFE is a variable gain stage with signal filtering. The RF > 1 case sums more than one RF path and the RFFE architecture requires time or phase delay and attenuation control for beamforming. The model assumes a time delay unit (TDU) and a variable attenuator (DATT) between two gain stages. The extra gain stage doubles the DC power, but it is required to overcome the TDU and DATT loss. The results of the analysis are shown in ***Figure 8***, where the doubling of DC power is evident. Figure 8 also shows increasing RFFE DC power with increasing ADC IP3.

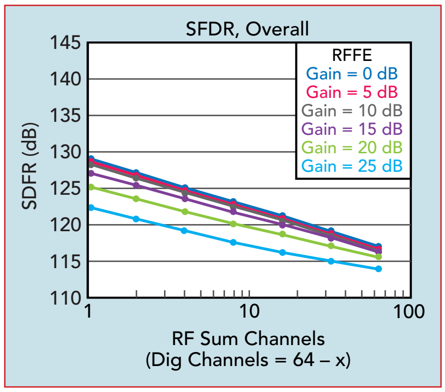

Fig. 5 RFFE gain impact on SFDR for ADC ENOB=8.

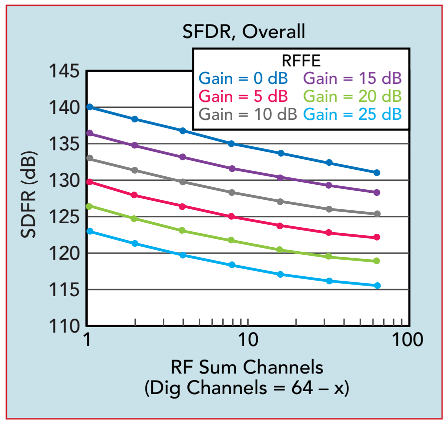

Fig. 6 RFFE gain impact on SFDR for ADC ENOB=12.

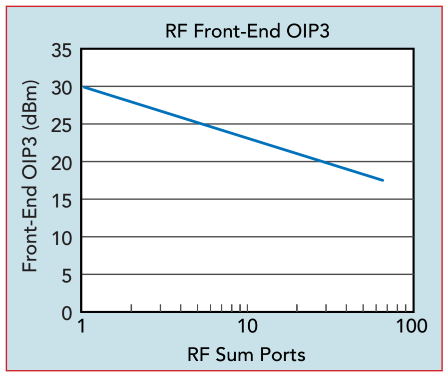

Fig. 7 RFFE OIP3 vs. the number of summed RF ports.

MODELING RF CHANNEL SUMMATION

RFFE single-channel OIP3 decreases with increasing RF channel summation. Summing RF channels improves SNR by coherently adding the signal and noncoherent Gaussian white noise. Improved SNR is an advantage, but this creates a larger signal before the nonlinear ADC than digitally summing channels after the ADC. The spur level resulting from multitone intermodulation is a

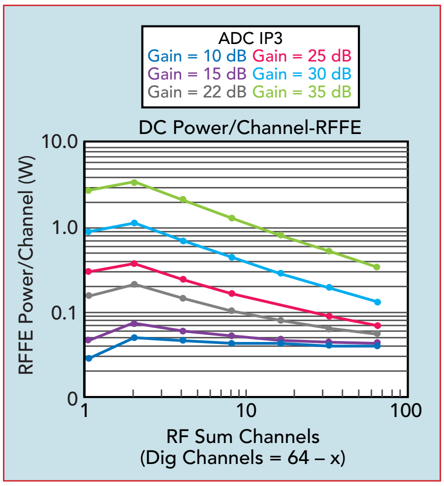

Fig. 8 RFFE DC power/channel.

TABLE 2		
RF SUMMATION ATTRIBUTE EQUATIONS		
Block	***Model Attribute***	***Equation***
RF Sum	Gain, signal	F {N, 'on' ports}
	Gain, noise	-sqrt(N) dB

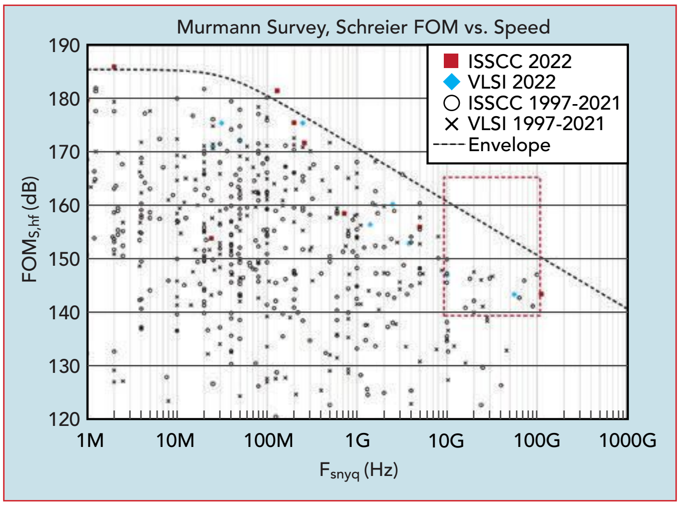

Fig. 9 Walden FOM from Murmann survey.

function of ADC IP3 and the signal level into the ADC. For two tones at the same level, Equation 3 specifies:

$$P_{IN,IM3}dBm = 3 \times P_{IN}dBm - 2 \times IIP3\ dBm \quad (3)$$

Summing before the ADC improves SNR but degrades the two-tone spurs due to ADC nonlinearity compared to the same N channels summed digitally after the ADC. The SFDR improves by digitally summing and computing the gain after the ADC. The ADC handles a lower signal and the SNR benefit is realized through the combination of digital data streams at the price of bit growth.

To understand the effects of summing channels, we use a method of passive RF summation developed by Analog Devices.[5] With passive summation, there is insertion loss but no additive noise and no impact on IP3. RF summation benefits SNR and has no impact on IP3 because intermodulation spurs add coherently across combined channels, like the signal. Because of RF combiner loss, the sensitivity degrades as the summed channels increase. This is modeled in Equation 4 as:

$$\text{the Insertion Loss}_{RF\ Sum}dB = \sqrt{\text{Number of RF Sum Channels dB}} \quad (4)$$

The RF sum attributes are shown in ***Table 2***.

MODELING THE ADC

The ADC model uses behavioral equations derived from Murmann's ADC survey population data.[6] For a valid comparison, near-peer data points from similar-class ADCs are selected using two separate, but similar, FOMs. A black box ADC model allowing swept attributes is created from fitting population data points. The analysis uses two FOMs from the Murmann survey. The Walden FOM (FOM_W) shown in ***Figure 9*** favors low-resolution ADCs as it moves 2× per bit. FOM_W is calculated in Equation 5 and a lower value is better.

$$FOM_W = \frac{Power}{2^{ENOB} \times f_{s,Nyq}} \left(\frac{fJ}{conv-step}\right)$$

$$ENOB = \frac{SNDR - 1.76}{6} \quad (5)$$

The Schreier FOM (FOM_S) shown in ***Figure 10*** favors high-resolution ADCs as they move 4× per bit. FOM_S is calculated in Equation 6,

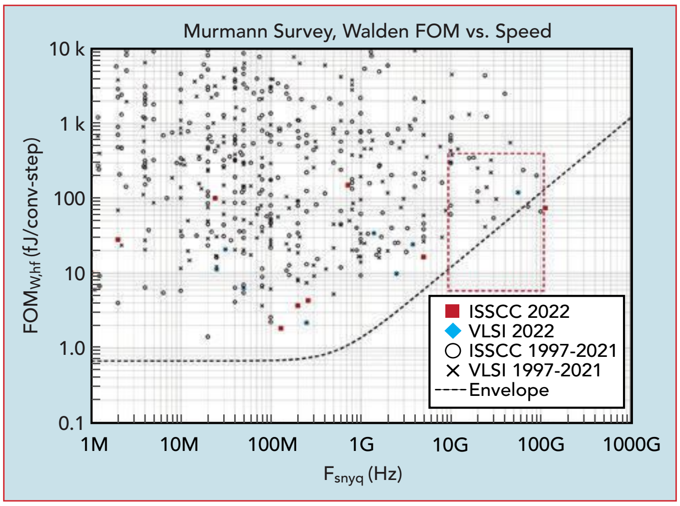

Fig. 10 **Schreier FOM from Murmann survey.**

and a higher value is better.

$$FOM_S = SNDR + 10Log\left[\frac{f_{s,Nyq}/2}{Power}\right] dB \qquad (6)$$

As an important rule of thumb, DC power is proportional to the sample rate and exponential with dynamic range for a fixed FOM value.

The points in Figures 9 and 10 represent ADC conference presentations. The dotted "Envelope" line in the charts represents the expectation of commercially available future performance. The most successful ADCs balance dynamic range, sampling rate and DC power requirements.

Rearranging the FOM equations results in Equation 7. This data is plotted as DC power versus ENOB for the Walden FOM in ***Figure 11*** and the Schreier FOM in ***Figure 12***. These charts show how to trade off power and ENOB to arrive at the same FOM.

$$FOM_W \times f_{s,Nyq} \times 2^{ENOB} = Power(Walden)$$

$$\frac{f_{s,Nyq}/2}{10^{[FOMs-SNDR]/10}} = Power(Schreier) \qquad (7)$$

The attractiveness of a high speed ADC in an application involves a trade-off of ENOB, ISBW and DC power. Simultaneously excelling in all is very difficult. For example, a maximum DC power limit of 100 mW per ADC requires a compromise in sampling rate and ENOB for the application. At 60 GSPS, a state-of-the-art ADC will be ENOB=6. Lowering the sampling rate to 10 GSPS increases the ADC dynamic range to ENOB=8.7. Both ADCs are considered state-of-the-art, but the best solution depends on system priorities.

High sampling rate converters offer benefits in areas like frequency planning, instantaneous coverage, software-defined digital tuning and RF simplification. To fully understand the implications, designers must also understand DC power consumption and ENOB. The dynamic range, sampling rate and DC power consumption "triangle" determine overall ADC merit. In a radar application, for example, 60 GSPS at ENOB=6 might not be a better solution than 10 GSPS at ENOB=8.7. A high sampling rate

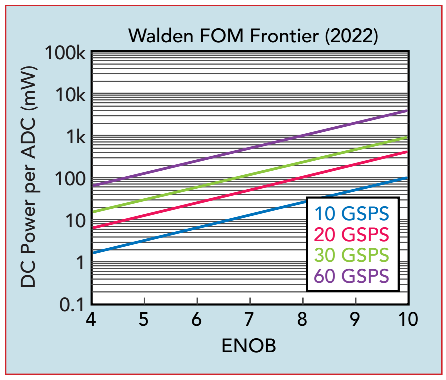

Fig. 11 **DC power vs. ENOB on the Walden envelope.**

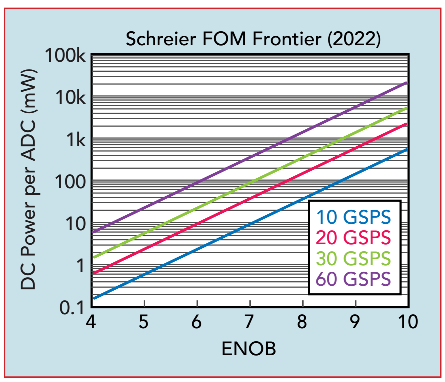

Fig. 12 **DC power vs. ENOB on the Schreier envelope.**

Introducing a Family of Tunable Impedance Insensitive Filters

Marki Microwave's new MFBT MMIC tunable filters allow users to create bandpass filters with variable center frequencies and % bandwidths for adaptive filtering applications. These impedance insensitive filters feature low return losses in both the passband and stopband, low insertion loss, high stopband rejection and high IP3. Available in a 4x4mm QFN package, these products are suited for LO tracking filters and replacing larger switched filter banks.

APPLICATIONS

- **Test & Measurement Equipment**
- **Radar/SATCOM**
- **Electronic Warfare Systems**
- **Digital Communications**

Contact: sales@markimicrowave.com
www.markimicrowave.com

The Trusted Leader When Performance Matters

Marki® microwave

TABLE 3 ADC ATTRIBUTE EQUATIONS

Block	Model Attribute	Equation
ADC	NF	F {f_S, ENOB, full scale}
	IP3	22 dBm
	DC power	F {ENOB}

might look attractive, but ENOB and power limit are often higher system priorities.

The ADC performance cascade model uses an RF black box with attributes NF, IP3 and DC power as shown in ***Table 3***. These ADC attributes change as the system model sweeps.

The ADC NF is a function of ENOB or SNR as shown in Equation 8:

$$NF_{ADC}dB = kTe_{ADC}\frac{dBm}{Hz} - \left(-174\right)\frac{dBm}{Hz}$$

Noise Spectral Density:

$$kTe_{ADC}\frac{dBm}{Hz} = FullScale_{ADC}dBm - SNR_{ADC}^{dB} - 10Log\left(\frac{f_s}{2}\right)Hz$$

$$SNR_{ADC}^{dB} = 6 \times ENOB_{ADC} + 1.76\ dB \qquad (8)$$

Noise spectral density, kTe (dBm/Hz), is equivalent to sensitivity (dBm) in a 1 Hz bandwidth. A 1 Hz bandwidth is assumed throughout, but this can be adjusted by adding a 10LogBW term. While this analysis focuses on noise, ADC two-tone IP3 performance is also important.

The ADC DC power model uses data summarized in the Murmann survey. ***Figure 13*** reduces the Murmann ADC survey data (rev20220719) to 20 members and filters for Analog Devices and industry peers, CMOS < 32 nm and f_S>=4 GSPS to show the data and extrapolation of DC power as a function of ENOB. The curves in Figure 13 come from substituting the values of ***Table 4*** into Equation 9.

$$\frac{Power_{DC}}{freq_{sample}} = ae^{k(ENOB)}pJ \qquad (9)$$

Using the selected set of Murmann data, the model derives a relation for ENOB as a function of bits as shown in Equation 10 and plotted in ***Figure 14***.

$$ENOB_{ADC} = 0.6 \times bits_{ADC} + 1 \qquad (10)$$

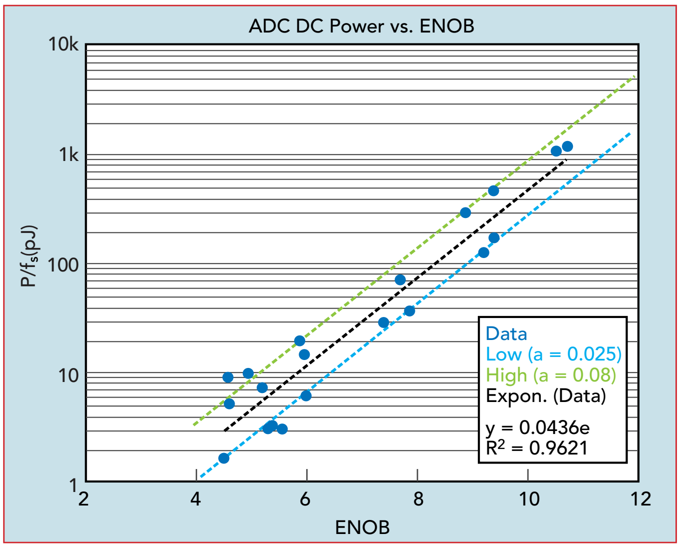

Fig. 13 ADC DC power vs. ENOB.

TABLE 4
ADC DC POWER VALUES

	a	k
Best fit	0.045	0.93
Low bound	0.025	0.93
High bound	0.08	0.93

These equations describe a DC power and RF attribute model for the ADC as a function of ENOB. This is shown in ***Figure 15***. ***Figure 16*** shows DC power/channel versus ENOB in a system using digital beamforming.

MODELING THE DIGITAL PAYLOAD

The high speed data payload and sum computation DC power are estimated from the transport energy per bit.[6] The digital payload transport power associated with the

ADC-to-digital sum node scales up as the number of digital sum channels and IBW increases. ***Table 5*** shows the digital sum model attributes and Equation 11 calculates the high speed interface physical link transport DC power.

$$Power_{Digital\,Sum\,Interface}\,W = \left[Energy_{Serializer} + Energy_{Deserializer}\,J/bit\right] \times Payload\ bits \times Dig.Sum\ Channels$$

$$Payload\ bits = Encode\ Rate\ Gbps \times Overhead_{JESD204C} \times bits_{ADC}$$

$$Encode\ Rate\ Gbps = IBW\ GHz \times 2\ bits \times 1.2$$

$$Overhead_{JESD204C} = 66/64 \qquad (11)$$

Equation 12 assumes a JESD link:

$$Energy_{Serializer} = 3\frac{pJ}{bit}$$

$$Energy_{Deserializer} = 4\frac{pJ}{bit} \qquad (12)$$

$$IBW = 1\,GHz$$

Figure 17 plots the DC power/channel including the interface versus summed RF channels for various ADCs.

CONCLUSION

Every phased array system has different beam attributes, sensitivity and dynamic range requirements for given DC power limits. A continuum of performance versus DC power solutions exists, but the best solution depends on the mission requirements. This article constructs an RF

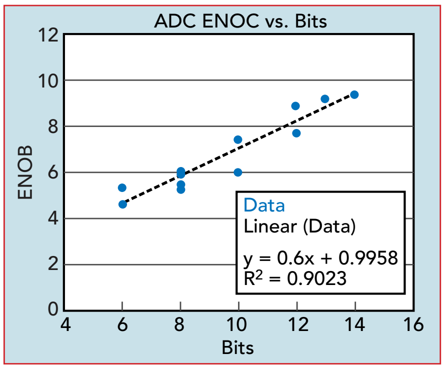

Fig. 14 ENOB vs. bits.

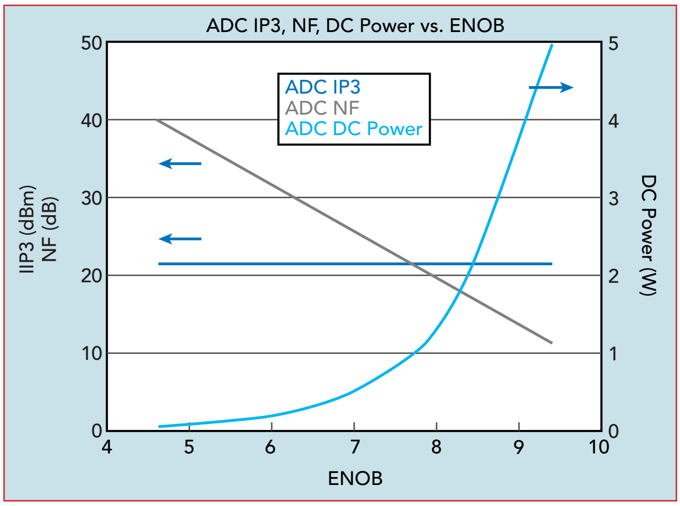

Fig. 15 ADC NF, DC power and ENOB.

TABLE 5 DIGITAL PAYLOAD DC POWER MODEL		
Block	**Model Attribute**	**Equation**
Digital sum	DC power	F {bits, IBW, lanes, pJ/b}

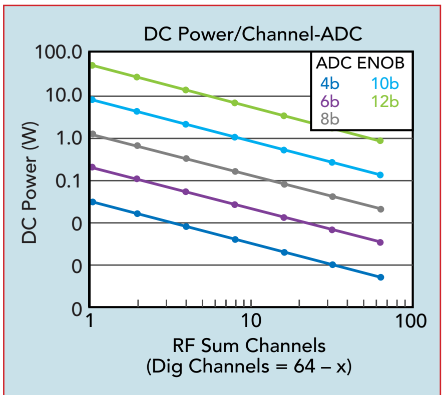

Fig. 16 **Beamforming trade-offs.**

cascade model for a phased array receiver that analyzes the impact of RF and digital channel summation on dynamic range and DC power. The Excel model includes:

- RFFE
- RF channel summation
- ADC
- High speed digital interface and compute
- Digital channel summation.

Part 2 will present and analyze model results, relate the results to system FOMs and draw conclusions. ■

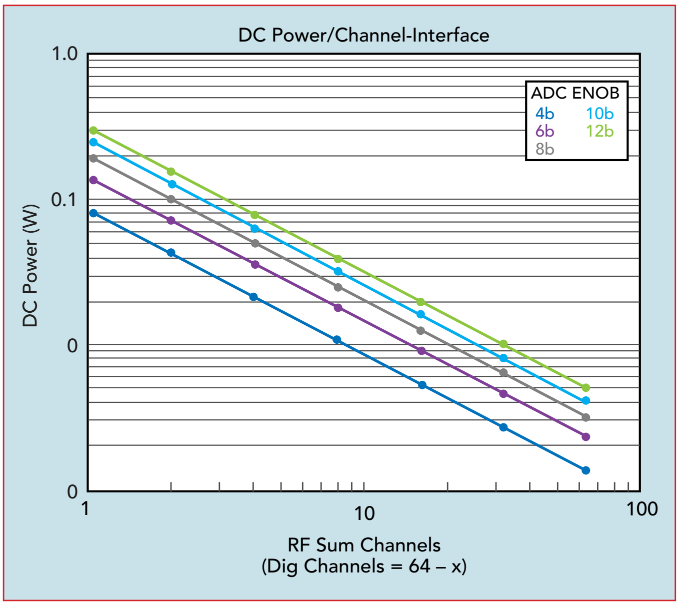

Fig. 17 **DC power response.**

References

1. T. H., Salvador, K.W. O'Haver, T. M. Comberiate, M. D. Sharp and O. F. Somerlock, "Benefits of Digital Phased Array Radars," *Proceedings of the IEEE*, Vol. 104, No. 3, February 2016.
2. W. F. Egan, "Practical RF System Design," *John Wiley & Sons.*
3. B. Annino, "SFDR Considerations in Multi-Octave Wideband Digital Receivers." *Analog Dialogue*, Vol. 55, No.1, January 2021.
4. P. Delos, S. Ringwood and M. Jones," Hybrid Beamforming Receiver Dynamic Range Theory to Practice," *Analog Devices, Inc.*, November 2022.
5. www.analog.com/en/technical-articles/hybrid-beamforming-receiver-dynamic-range.html.
6. B. Murmann, "ADC Performance Survey 1997–2022," *GitHub, Inc.*, 2023.

Welcome to our Team in New England.

Spotlight on Garrett Lynch

"Having lived in the city of Boston for over fourteen years, I have great access to my territory. My customer base with Bradford RF Sales includes metro Boston, southeastern MA, Rhode Island, and Connecticut. One day I could be visiting a large OEM customer in the morning and then working with a research lab in the afternoon. The diversity of my clients is probably the most intriguing part of my job. I really look forward to helping our customers and suppliers achieve success."

Garrett Lynch
Territory Sales Manager

"Garrett has been part of the Bradford RF Sales' team since mid-2018 and has consistently added design wins year after year. His area of coverage is challenging and he offers great support to a multitude of customers dealing with complex and varying needs."

Mike Crittenden
President/Owner

Bradford RF Sales has been finding new microwave/RF opportunities in the New England territory for over seventeen years. We help to match up and support our best-in-class suppliers with those design opportunities from concept through production.

Please visit us at **www.bradfordrfsales.com** to learn more.

Bradford RF Sales

Manufacturers' Representatives for New England
58 Beechwood Drive North Andover, MA 01845
www.bradfordrfsales.com

John Libby, Garrett Lynch, Mike Crittenden, Michael Wholley

Microwave, RF, and Electronic Products for Military & Commercial Applications

INVITED PAPER

Low Phase Noise mmWave Voltage-Controlled Oscillator

Indra Ghosh, Jan Buchholz, Horst Fischer, Ulrich Altmann, Jörg Berben, Jonas Lehmke, Ulrich Lewark, Uwe Gollor, Wolfgang Wischmann and Rüdiger Follmann
IMST GmbH, Kamp-Lintfort, Germany

Enrico Lia
European Space Agency, Noordwijk, The Netherlands

Stephen M. Hanham
University of Birmingham, Birmingham, U.K.

Benjamin Walter and Fuanki Bavedila
V-Micro SAS, Villeneuve d'Ascq, France

Leif Jensen
TopSil Global Wafers A/S, Frederikssund, Denmark

Marc Faucher
V-Micro SAS, Villeneuve d'Ascq, France, Univ. Lille, CNRS, Centrale Lille, Univ. Polytechnique Hauts-de-France, Lille, France

Local oscillators (LOs) are critical components in mmWave radar and communications systems. Dielectric resonator oscillators (DROs) are commonly used up to a maximum frequency near 30 GHz. Above that, the LO signal generation requires additional multiplier circuits and bandpass filters. These additional components can create adverse effects by increasing phase noise, circuit complexity, mass, power consumption and reducing reliability.

This article describes an mmWave oscillator using a high Q electromagnetic bandgap (EBG) resonator with a reduced dielectric filling factor. The measured results of the resonator demonstrate an unloaded room temperature Q-factor of 115,000 at 45 GHz. The active MMIC includes a two-stage loop amplifier, a coupler, an electronic phase shifter and an output amplifier. The oscillator has phase noise levels of -95, -120 and -143 dBc/Hz at offset frequencies of 1, 10 and 100 kHz, respectively. The authors believe these noise levels are the lowest reported values for electronic feedback oscillators without noise degeneration.

The LO is at the heart of any communications system or RF-sensing unit. Its frequency stability has a broad impact on achievable data rates or radar sensor sensitivity. Wideband communications now use bandwidths up to 1 GHz and higher-order QAM modulation to target data rates above 40 Gbps.[1] For low bit error rates in these applications, the error vector magnitude (EVM) needs to be sufficiently small. EVM impairments primarily originate from the LO phase error and to a lesser degree from power amplifier compression, AM-to-PM conversion and Johnson noise. Consequently, the phase error obtained by integrating the LO single-sideband (SSB) phase noise needs to be sufficiently small. In this context, the relevant frequency limits for integration range from the digital receiver frequency tracking bandwidth, typically 100 Hz to several kHz, as the lower limit to one-half the signal bandwidth as the upper limit.

For radar sensing applications, the echo, a Doppler-shifted radar pulse, is down-converted to baseband using the LO. A detectable signal needs to be larger than the LO phase noise at the relevant Doppler frequency. At 45 GHz, a target moving at 100 km/h creates a Doppler shift of 8.3 kHz. For 1000 km/h the offset frequency is 83.3 kHz. Therefore, the phase noise in the offset frequency range between 5 and 500 kHz should be minimized to maximize the radar sensitivity for relevant applications like space.

Generally, an oscillator consists of an active element, like an amplifier or Gunn diode and a resonator as the frequency-determining element. An electronic phase shifter is needed to adjust the feedback phase for constructive interference and enable phase stabilization as part of a PLL. This common feedback topology is depicted in ***Figure 1***.

The phase noise of a free-running oscillator is governed by Leeson's

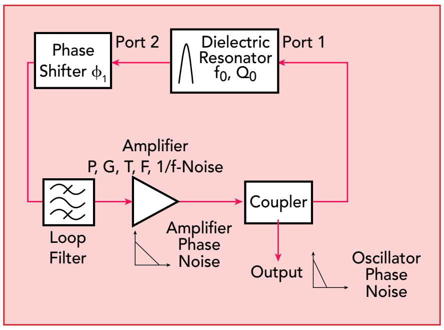

Fig. 1 Oscillator with feedback topology.

equation[2] as shown in Equation 1:

$$L_{ssb}(f) = 10 \cdot \log \left[\frac{1}{2} \cdot \left(1 + \frac{f_0^2}{4Q_l^2 f^2} \right) \cdot \left(1 + \frac{\alpha}{f} \right) \cdot \frac{GFkT}{P} \right] \quad (1)$$

where:
Q_l is the loaded Q-factor of the resonator
α is the 1/f flicker noise corner frequency of the active element
G is the gain of the active element of the oscillator
F is (large signal) noise figure
P is the available power at the loop amplifier output
k the Boltzmann constant
f_0 is the operating or carrier frequency
f is the phase noise offset frequency
T is the thermodynamic temperature.

At small offset frequencies, the phase noise increases quadratically with the operating frequency and decreases quadratically with the loaded Q-factor of the resonator used in the feedback loop. This increases the difficulty of building a low phase noise oscillator at mmWave frequencies. Traditionally, low phase noise quartz oscillators have been designed at lower frequencies, typically 100 MHz maximum and their output signal is subsequently multiplied to the target frequency. The drawback is this method increases the oscillator phase noise by 20 log (N) with N being the frequency multiplication factor. Moreover, low phase noise frequency multipliers consume a considerable amount of current.

For frequency generation directly at mmWave frequencies, DROs may use low loss ceramic materials such as BMT ($Ba(Mg_{1/3}Ta_{2/3})O_3$). This enables operation to around 30 GHz, but this material has a dielectric loss tangent of 2×10^{-4} at 45 GHz.[3] For a dielectric loss-limited resonator, the Q-factor is the inverse of the dielectric loss tangent, meaning that BMT can achieve a maximum Q-factor of 5000 and this is not sufficient.

High resistivity silicon (HRS) is an interesting alternative with dielectric losses described by Equation 2:

$$\tan\delta = \frac{\varepsilon''}{\varepsilon'} + \frac{1}{\rho\omega\varepsilon_0\varepsilon'},$$

$$\tan\delta_{diel} = \frac{\varepsilon''}{\varepsilon'} = 1.2 \times 10^{-5} \quad (2)$$

where:
ρ is the electrical resistivity of the material.
ω is the angular frequency.
ε' and ε'' are the real and imaginary parts of the dielectric constant, respectively.

The electrical resistivity depends on the purity of the material and typically varies between 10 kΩ•cm and 50 kΩ•cm for standard HRS. Values up to 416 kΩ•cm have been achieved with proton or neutron irradiation or Au-doping. At 45 GHz, the corresponding values of the HRS loss tangent are 8.1×10^{-5} (ρ =50 kΩ•cm) and 2.0×10^{-5} (ρ = 416 kΩ•cm), which are far lower than the BMT loss tangent.

The temperature variation of the permittivity is another important consideration when choosing the resonator base material. BMT has been designed to minimize the temperature variation with a permittivity gradient of $d\varepsilon'/dT = 5 \times 10^{-6}$/°C at room temperature. However, HRS is not temperature compensated and the gradient of the permittivity is much larger, with a value of 1.2×10^{-3}/°C at room temperature.[3] The temperature gradient of the resonance frequency can be calculated from the temperature gradient of the material permittivity as shown in Equation 3:

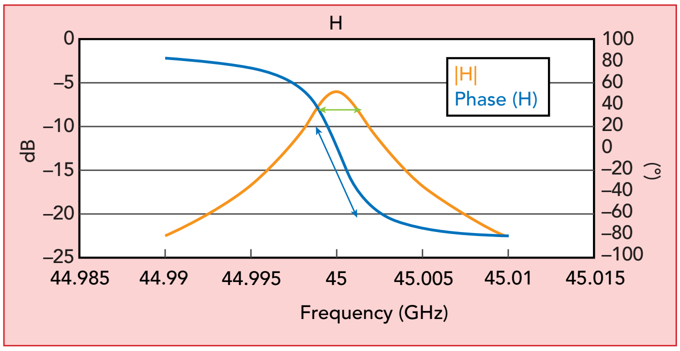

Fig. 2 Resonator transmission magnitude and phase.

$$\frac{df}{dT} = -\frac{1}{2}\frac{f}{\varepsilon'}\frac{d\varepsilon'}{dT} \quad (3)$$

This is 2.3 MHz/°C For HRS at 45 GHz.

For the oscillator, the electronic phase shifter in the feedback path in Figure 1 can compensate for the temperature-induced resonator frequency variation. The resonator phase shift is 90 degrees across its 3 dB bandwidth, as shown in ***Figure 2***. By adjusting the phase shifter by 90 degrees, the oscillator frequency can be adjusted by the amount of the 3 dB bandwidth. This is because the total oscillator open-loop phase is required to stay at a multiple of 360 degrees. As an example, for irradiated HRS, a Q_l of 50,000 is expected. In this case, the 3 dB bandwidth at 45 GHz is only 900 kHz. Consequently, the electronic phase shifter can correct for temperature changes of approximately 0.4°C, which equates to 900 kHz/2.3 MHz/°C. This compares to a 3 dB bandwidth of 9 MHz and a frequency gradient of just -5 kHz/°C for BMT. This shows that temperature stabilization is not required for BMT.

RESONATOR DESIGN

EBG resonators are formed from resonance-supporting defects created within metamaterials engineered to have an EBG. The metamaterial's EBG prohibits the propagation of electromagnetic (EM) waves in specific directions, allowing localization and confinement of a resonant defect mode. EBG metamaterials can be realized using periodic metal or dielectric structures and feature an EBG in one, two or three dimensions. This work considers a resonator made entirely from HRS with an

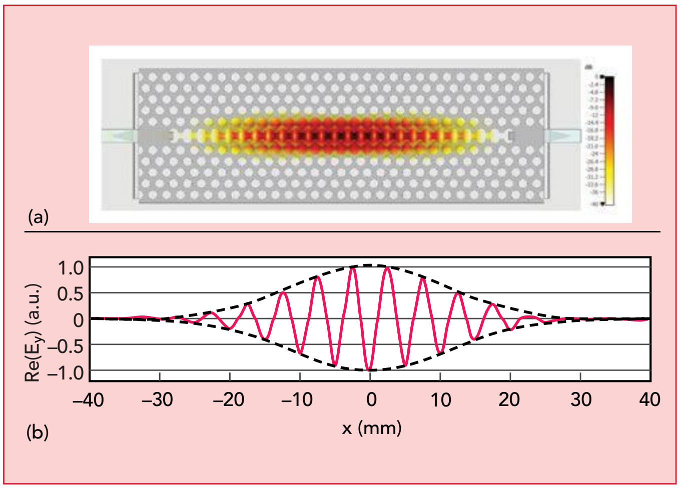

▲ Fig. 3 **(a) The resonator structure and electric field intensity. (b) Gaussian envelope of the resonant mode's electric field.**

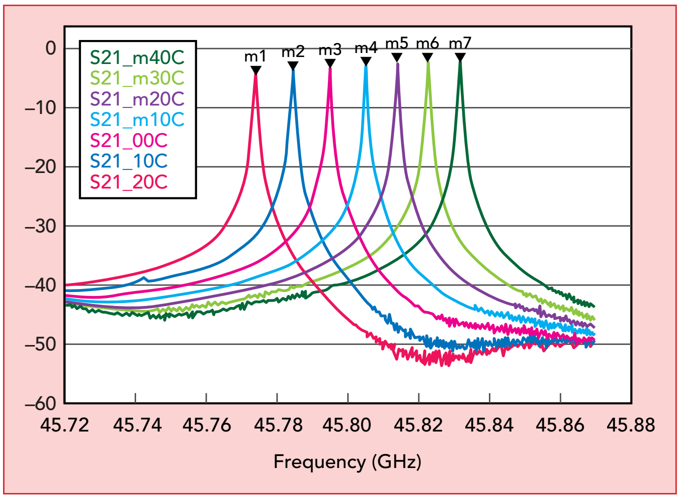

▲ Fig. 4 **Measured resonator insertion loss at different temperatures.**

engineered 2D EBG due to its ease of fabrication.

A common method for creating an EBG resonator is to construct a dielectric 2D EBG from a periodic lattice of air holes perforating a slab made from a high permittivity dielectric. The resonator is created by introducing a defect in the periodic lattice of air holes through the omission of several consecutive holes.[4,5] In this case, the achievable resonator Q-factor values are essentially limited by the dielectric loss of the base material. Further enhancement of the resonator Q-factor can be achieved by reducing the fraction of the resonant EM energy confined inside the dielectric and storing a larger fraction in air. In this case, the Q-factor can be expressed as Q=1/(ρ·tanδ) with tanδ being the loss tangent of the HRS substrate and ρ being the dielectric filling factor. The dielectric filling factor is defined as the fraction of the electric energy inside the silicon compared with the total stored electric energy of the resonant mode, as shown in Equation 4:

$$\rho = \frac{\iiint_{V_{si}} \varepsilon'_{si} |E|^2 dv}{\iiint_{V_t} \varepsilon'(v) |E|^2 dv} \qquad (4)$$

where:

V_{si} is the volume of the silicon forming the EBG resonator

V_t is the total volume containing the resonant mode

E is the electric field of the resonant mode

ε'_{si} is the dielectric constant of HRS

$\varepsilon'(v)$ is the position-dependent permittivity.

A reduction of the dielectric filling factor resulted from an air slot embedded in the middle of the EBG to contain the resonant mode. ***Figure 3(a)*** shows this air slot with the resonant mode's electric field intensity overlayed. To minimize radiation, the EM fields must be shaped in the resonator. ***Figure 3(b)*** shows a Gaussian envelope of the field created by linearly increasing reflection from the center to the outer unit cells. This is achieved by varying the horizontal period (width) of the unit cells quadratically with the distance in the ±x-directions. The simulated dielectric filling factor of the resonator is 47 percent. Further details can be found in work by E. Lia, et al.[6]

The resonator insertion loss as a function of temperature is shown in ***Figure 4***. The unloaded Q at room temperature is 115,000 and the resonance frequency is 45.77 GHz. The unloaded Q increases to 200,000 at -40°C upon cooling. Correspondingly, the insertion loss decreases to -3.6 dB at 40°C. Lowering the temperature below -10°C results in a relatively small increase in unloaded Q. This mirrors the temperature dependence of the HRS loss tangent.[3]

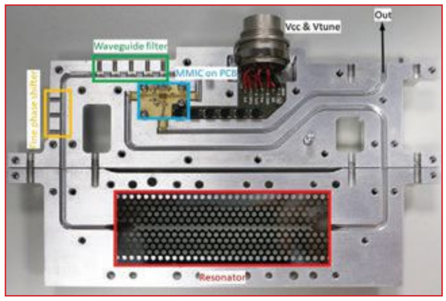

▲ Fig. 5 **Final MMIC VCO assembly.**

These results illustrate the low dielectric loss of the 1 mm thick neutron transmutation-doped HRS 6 in. wafers supplied by TopSil GlobalWafers A/S, along with the superior quality of the holes etched using the deep reactive-ion etching (DRIE) method carried out by V-Micro SAS. Maintaining hole sidewall angles very close to 90 degrees is key to achieving a high Q-factor. Due to the 1 mm thickness of the HRS wafers, maintaining straight sidewall angles across the thickness is a difficult task and requires significant DRIE process expertise.

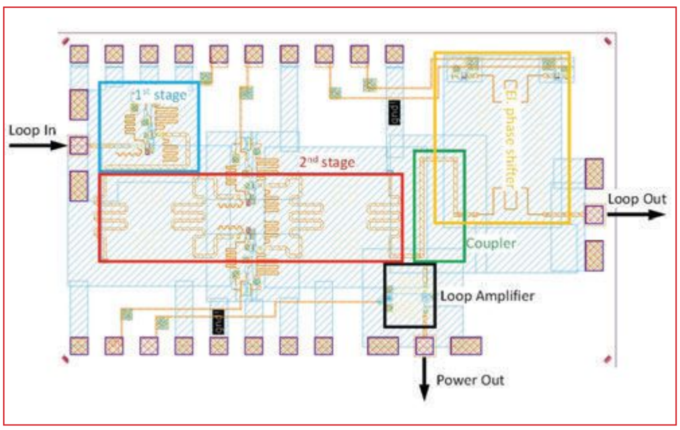

▲ Fig. 6 **MMIC VCO circuit layout.**

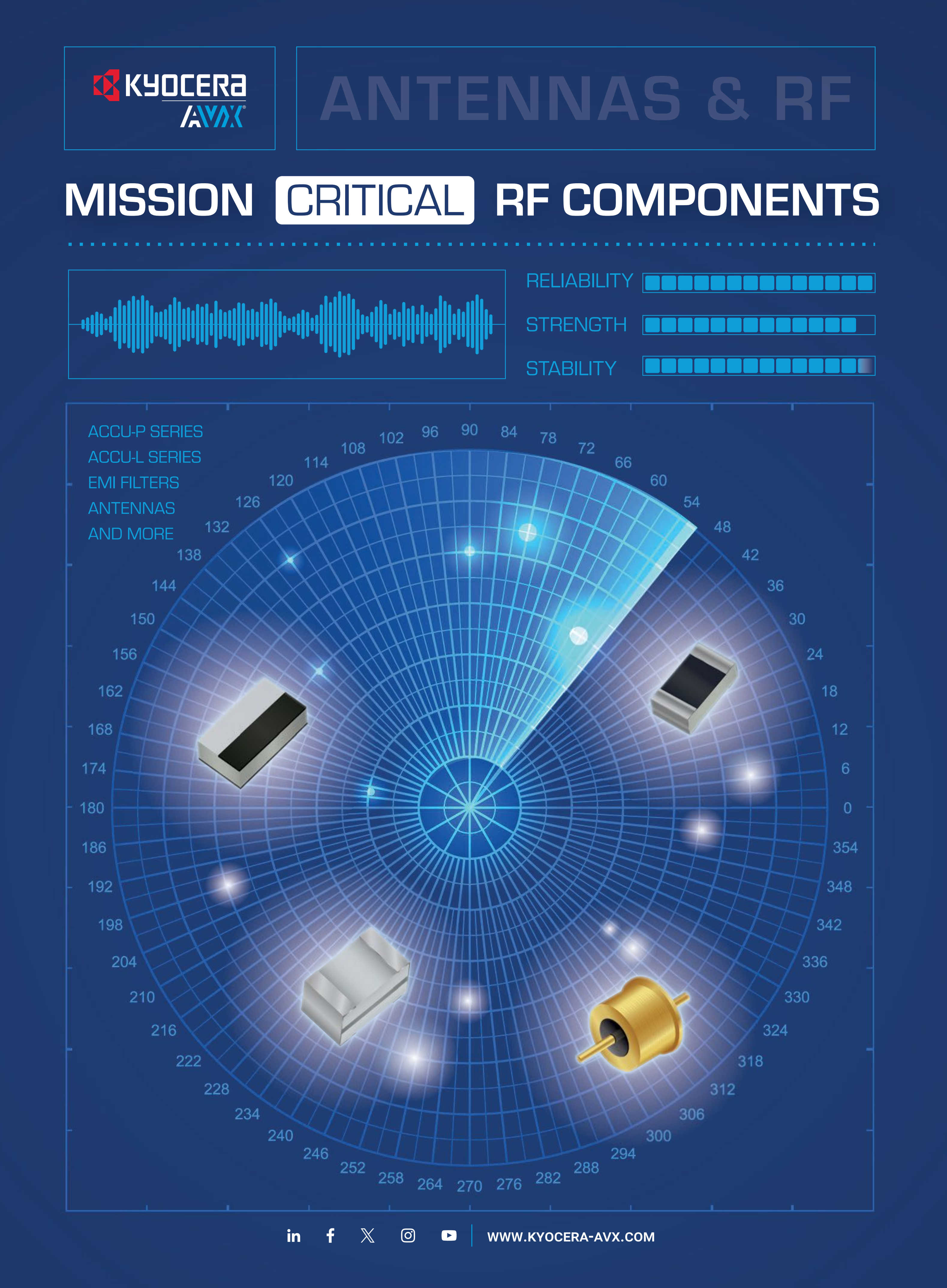
KYOCERA AVX
ANTENNAS & RF
MISSION CRITICAL RF COMPONENTS
RELIABILITY
STRENGTH
STABILITY
ACCU-P SERIES
ACCU-L SERIES
EMI FILTERS
ANTENNAS
AND MORE
WWW.KYOCERA-AVX.COM

OSCILLATOR TOPOLOGY

Figure 5 shows the topology and assembly of the feedback voltage-controlled oscillator (VCO). Both the active circuitry and the resonator reside in a split-block aluminum housing with WR-19 waveguides milled into the housing. The input and output of the MMIC circuit are connected by bond wires to microstrip lines that couple to the waveguide. A waveguide bandpass filter and fine and coarse phase shifters are also included. The EBG resonator connects to the WR-19 waveguides using HRS triangular tapers that protrude into the waveguide.

The active circuitry and the resonator can be tested individually. The two parts of the oscillator are joined by WR-19 flanges integrated into the housing. The total power consumption of the oscillator is 215 mW, its size is 157 × 88 × 29 mm and the weight is 442 g, including all connectors.

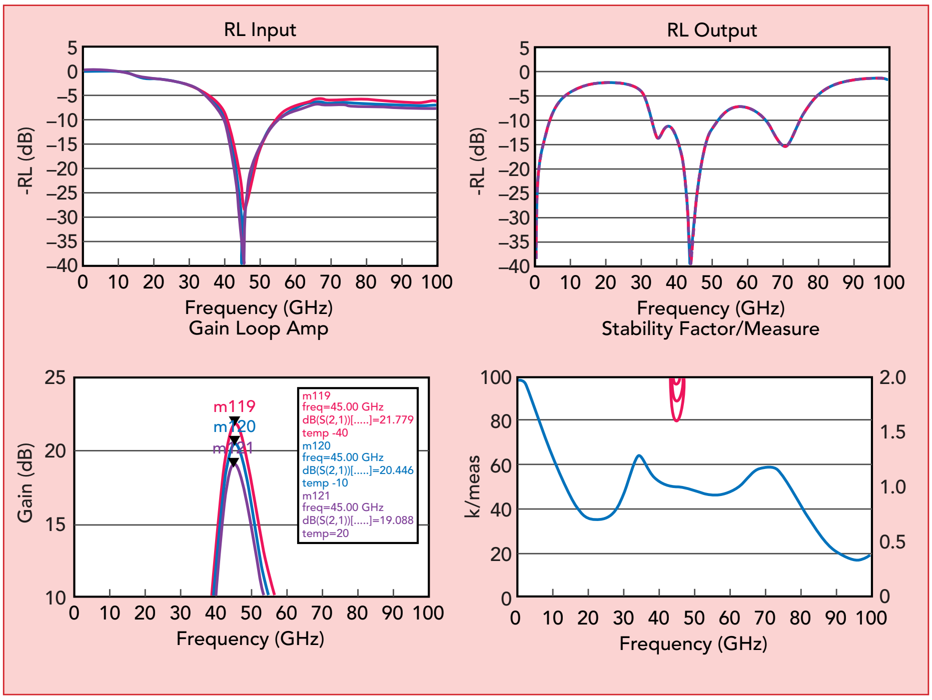

Fig. 7 **Simulated small-signal loop amplifier results. Input and output return loss (RL), Gain, Stability Factor k and Stability Measure (meas, right y-axis).**

MMIC LAYOUT AND DESIGN

The active circuit MMIC is designed using the IHP Microelectronics 130 nm SiGe BiCMOS SG13S process. The MMIC layout is shown in ***Figure 6***. The chip contains a two-stage loop amplifier consisting of a driver amplifier stage and a balanced power amplifier stage, a 10 dB coupler to couple a fraction of the oscillator power to the output, an electrical phase shifter and a coupling amplifier. The 10 dB coupler is realized by coupling transmission lines on the top two metal layers of the chip (TM1 and TM2). The coupling amplifier is realized as a standard common-emitter single-stage amplifier with 8 dB gain.

The loop amplifier uses a cascode design for the first and second stages. The loop amplifier shows good input and output matching as well as unconditional stability over the complete frequency and temperature range. The small-signal gain ranges from 19.1 dB at +20°C to 21.8 dB at -40°C. The small-signal results of the simulation are shown in ***Figure 7***.

The electronic phase shifter consists of a 90-degree hybrid coupler terminated by varactor diodes at two ports, as shown in ***Figure 8***. The simulated variation of transmission phase and insertion loss in response to varying the tuning voltage is displayed in ***Figure 9***. The total simulated phase variation is 32 degrees. The insertion loss of more than 4.5 dB is rather high due to the varactor diode loss. Measurement on test chips of the structure showed


RF-LAMBDA
THE LEADER OF RF BROADBAND SOLUTIONS
EUROPE
DEUTSCHLAND
RF-LAMBDA EUROPE
RF SWITCHES
MM / MICROWAVE DC-90GHz
RF-Lambda
RFSP160TA0020G-S
F:0.05-20GHz
SN:16010600274
160 CHANNELS
mm/Microwave
0.05-20GHz
Filter Bank Switch Matrix
For Phase Array Radar Application Satellite communication.
PN: RFSP32TA5M43G
SP32T SWITCH 0.5-43.5GHz
PN: RFSP16TA5M43G
SP16T SWITCH 0.5-43.5GHz
www.rflambda.com
sales@rflambda.com
1-888-976-8880
1-972-767-5998
San Diego, CA, US
Plano, TX, US
Ottawa, ONT, Canada
Frankfurt, Germany

good match of the measured characteristics with the simulation results.

WAVEGUIDE FILTER AND MECHANICAL PHASE SHIFTERS

The waveguide filter and the mechanical phase shifters were characterized in a dedicated milled test structure consisting of a WR-19 waveguide. The circuits are shown in ***Figure 10*** where the filter is the first structure on the left of the housing, circled in yellow. The fine phase shifter is in the middle, circled in green and the coarse phase shifter is the last structure on the right, circled in blue.

The waveguide filter serves to suppress the oscillation of other resonator or enclosure modes. The fifth-order filter was designed so that the center frequency can be varied between approximately 45.0 and 45.9 GHz with M1.4 polyether ether ketone (PEEK) screws. The measurement results of the filter from 44 to 46 GHz are shown in ***Figure 11(a)***. ***Figure 11(b)*** shows the passband in more detail and ***Figure 11(c)*** shows the wideband performance of the filter.

The tuning range of the electronic phase shifter is only 32 degrees. To augment this range, additional mechanical phase shifters were incorporated to ensure that the feedback loop can be adjusted for a multiple of 360 degrees total phase shift, ensuring oscillator startup. To achieve sufficient precision, two mechanical phase shifters were cascaded. For coarse adjustment, a WR-19 waveguide was partially filled with Teflon (permittivity = 2.1) to vary the electrical length. As shown in Figure 10, the Teflon pieces were tapered to improve impedance match. The length of these Teflon pieces varied from 16 to 36 mm in 2 mm steps. The measured phase shift between two adjacent lengths is approximately 60 degrees and the impact on insertion loss is less than 0.7 dB.

The fine phase shifter consists of three PEEK screws whose length within the waveguide can be varied. The measured phase difference be-

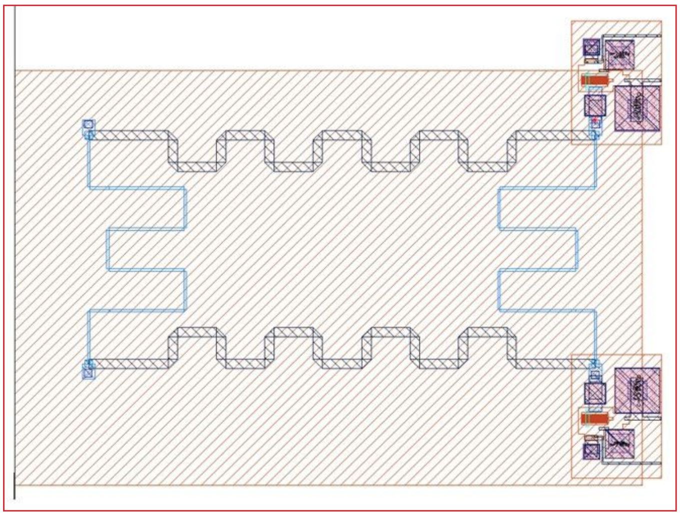

Fig. 8 Electrical phase shifter chip layout.

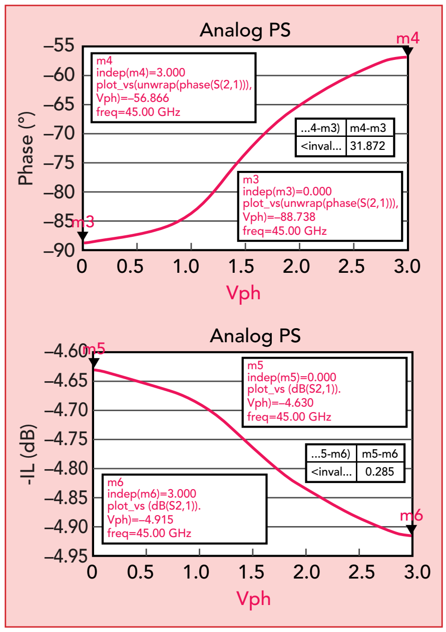

Fig. 9 Simulated phase shifter phase and amplitude variation.

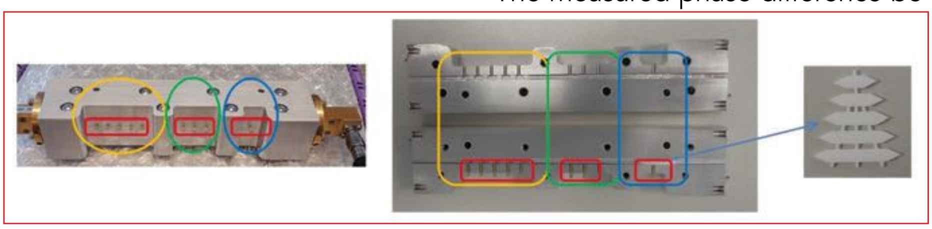

Fig. 10 Side view of test structure and the coarse phase shifter Teflon pieces.

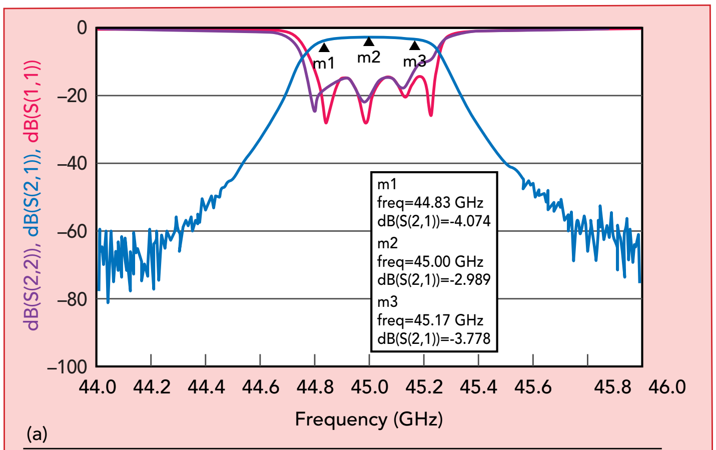

tween the minimum and maximum screw settings is 47 degrees. The measured tuning accuracy is better than 0.5 degrees. The change of the insertion loss is less than 0.2 dB within the total tuning range.

PHASE NOISE AND ELECTRONIC TUNING RANGE

An operating temperature of -10°C was chosen owing to the temperature dependence of the resonator quality factor. ***Figure 12*** shows measured phase noise levels of -95, -120 and -143 dBc/Hz obtained at offset frequencies of 1000, 10,000 and 100,000 Hz, respectively. The oscillator output power is -1.2 dBm and the electrical tuning range of the oscillator is 239 kHz. For

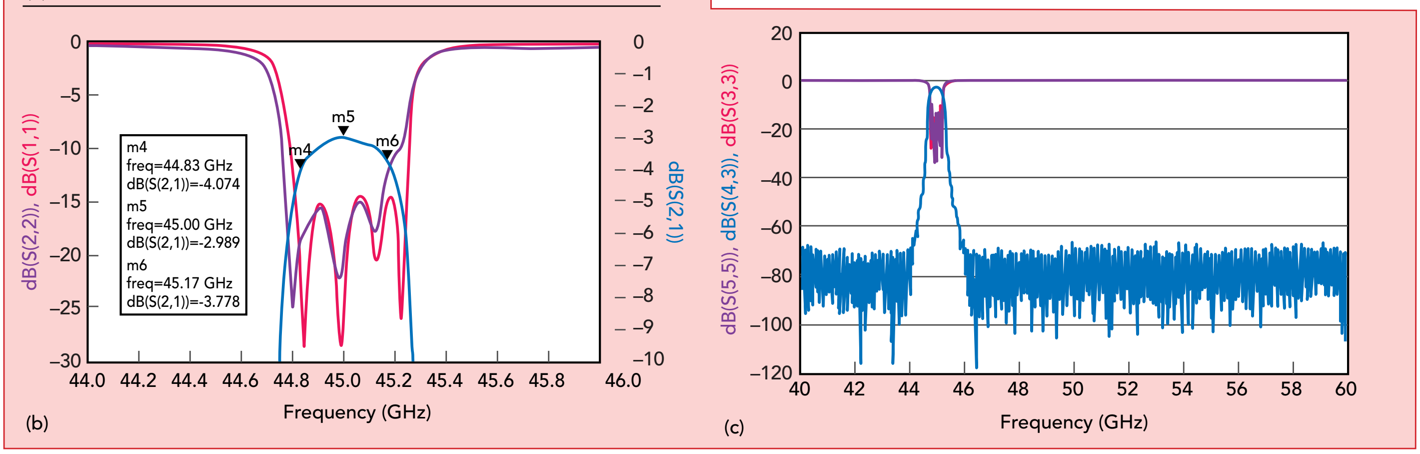

Fig. 11 **(a) Complete filter response. (b) Filter passband response. (c) Wideband response.**

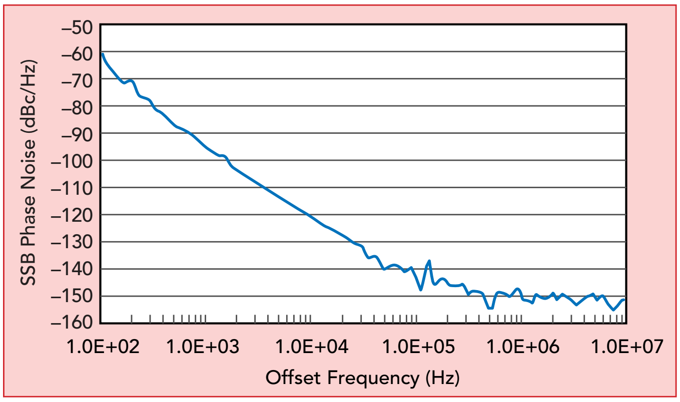

Fig. 12 Measured oscillator SSB phase noise at -10°C.

stable operation, the temperature stability needs to be better than 239 kHz/2.3 MHz/°C = 0.1°C.

CONCLUSION

This article describes the design and testing of a low noise mmWave oscillator employing an HRS resonator with a reduced dielectric filling factor. The authors believe that the phase noise values are the lowest published at this frequency range for electronic feedback oscillators without noise degeneration. The oscillator is lightweight with a small form factor and low power consumption. Future work will concentrate on improving the electronic frequency tunability to relax the requirements on temperature stability and to enhance the technology readiness level for space applications. ■

ACKNOWLEDGMENT

This work was funded by the European Space Agency (ESA-ESTEC) under the ESA Contract No. 4000130082/20/NL/HK.

References

1. J. Chen, D. Kuylenstierna, S. E. Gunnarsson, Z. Simon He, T. Eriksson, T. Swahn and H. Zirath, "Influence of White LO Noise on Wideband Communication," *IEEE Transactions on Microwave Theory and Techniques*, Vol. 66, No. 7, 2018.
2. D. B. Leeson, "A Simple Model of Feedback Oscillator Noise Spectrum," *Proceedings of the IEEE*, 54 (2): 329–330, doi:10.1109/PROC.1966.4682.
3. J. Krupka, W. Karcz, P. Kaminski and L. Jensen, "Electrical Properties of As-grown and Proton-irradiated High Purity silicon," *Nuclear Instruments and Methods in Physics Research B 380*, 2016, pp.76–83.
4. W. J. Otter, S. M. Hanham, N. M. Ridler, G. Marino, N. Klein and S. Lucyszyn, "100 GHz Ultra-high Q-factor Photonic Crystal Resonators," *Sensors and Actuators A 217*, 2014, 151–159.
5. Y. Akahane, T. Asano, B.-S. Song and S. Noda, "High-Q Photonic Nanocavity in a Two-dimensional Photonic Crystal," *Nature*, Vol. 425, October 2003.
6. E. Lia, I. Ghosh, S. M. Hanham, B. Walter, F. Bavedila, M. Faucher, A. P. Gregory, L. Jensen, J. Buchholz, H. Fischer, U. Altmann and R. Follmann, "Novel mmWave Oscillator Based on an Electromagnetic Bandgap Resonator," *IEEE Microwave and Wireless Technology Letters*, Vol. 33, No. 6, June 2023, pp. 863–866, doi: 10.1109/LMWT.2023.3268090.

INSULATED WIRE
INCORPORATED

When system engineers call for ultra-reliable, high performance military grade cables & connectors, the obvious choice is...

Today's advanced military platforms depend on the quality, selection, support and service that are the hallmarks of IW's product lines. We offer a range of jacket materials, armoring, and a wide variety of connectors including SMA, TNC, N, SC, 2.4 mm, and 7 mm to provide highly reliable, application specific solutions.

CALL US TODAY
with your project specs and we'll show you the most reliable way to get connected in the industry.

AS9100 Rev. D & ISO9001:2015 certified.

SEE US AT

AOC Symposium, National Harbor, MD Dec 11-13th

Booth #916

SCAN THIS CODE
TO FIND OUT HOW YOU CAN GET CONNECTED

We're how the microwave industry **gets connected!**

www.insulatedwire.com
t + 1 631 4724070
e nysales@insulatedwire.com

INVITED PAPER

Revving Up Automotive Safety: Advances in UWB for In-Cabin Sensing

Christian Bachmann, Amirashkan Farsaei and Chris Marshall
imec, Leuven, Belgium

Car manufacturers continuously explore and assess innovative technologies that could provide them with a competitive edge. Ultra-wideband (UWB) technology, a short-range wireless communication protocol, is one example. UWB already supports premium automotive features such as secure keyless car entry.

But UWB's potential extends far beyond simple tasks. Thanks to its fine-ranging capabilities, the technology could also facilitate in-cabin radar sensing, making UWB an important enabler of in-cabin gesture recognition applications. Alternatively, its in-cabin radar sensing capabilities could be used to support child presence detection (CPD) solutions that issue an alert if an infant is left unattended in a parked vehicle.

Researchers and technology providers are actively investigating UWB requirements to accommodate these features. A team of researchers at imec recently announced the availability of a low-power UWB chip that uses a pulse-shaping mechanism to improve the technology's ranging precision. Complementing this effort, they also demonstrated the added value of advanced signal processing algorithms for real-time, highly accurate car occupancy detection and breathing rate estimation.

ULTRA-WIDEBAND TECHNOLOGY: A POTENTIAL LIFESAVER

Drivers are regularly warned not to leave small children unattended in parked cars because of their heightened susceptibility to hyperthermia and heatstroke. If a car is exposed to the sun, in-cabin temperatures can reach a critical level in just 15 minutes. Leaving windows ajar does little to reduce this risk. Despite all awareness campaigns, nearly 1,000 children have died due to pediatric vehicular heatstroke since 1998 in the U.S. alone.[1] These deaths could have been prevented with appropriate warning systems in place. The good news is that such warning mechanisms are on the brink of becoming a reality, as initiatives like the European New Car Assessment Program (Euro NCAP) spur car manufacturers to integrate CPD solutions as a standard feature.[2]

Early CPD systems mainly relied on ultrasound but these systems suffered from accuracy limitations caused by external vibrations and noise. Radar technology, particularly at 60 GHz, offers a viable alternative. It is less prone to external disturbances and provides accurate results. The disadvantage is that mmWave radar solutions are currently less suited for mass deployment due to their cost.

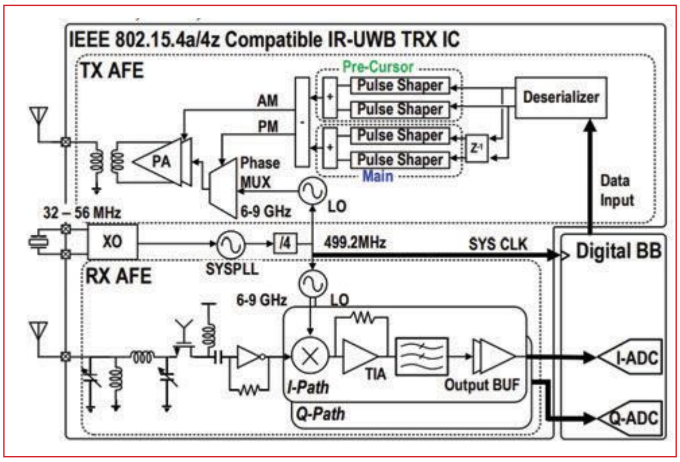

Fig. 1 **Architecture of imec's IR-UWB 3Rx-1Tx transceiver.** ***Source:*** **imec.**

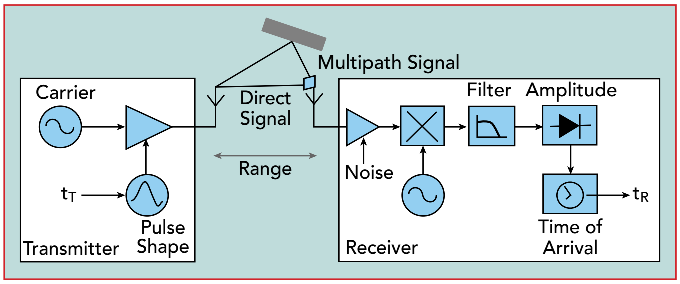

Fig. 2 **Block diagram of a UWB transmitter and receiver.** ***Source:*** **imec.**

Cost is an area where UWB radar can provide benefits. UWB already has the advantage of being integrated into premium cars to support features such as keyless entry. This makes it a technology familiar to the automotive sector. Additionally, operating within the 6 to 10 GHz frequency range, UWB radar easily penetrates car seats. It is also inherently capable of detecting even the slightest movements, such as an infant's chest rising and falling with each breath. Lastly, it comes at a lower cost than mmWave radar technology.

Technology vendors are already demonstrating and promoting the added value of UWB radar as a life-saving technology, even though practical implementations are not yet commercially available. Still, it is already clear that any viable solution will need to possess a transceiver architecture, allowing simultaneous transmission and reception. It should also prioritize extremely low power consumption to ensure seamless support for CPD systems running on electric car batteries. Achieving outstanding ranging precision will be a critical success factor as well.

POWER CONSUMPTION OF THE IR-UWB TRANSCEIVER

Researchers at imec recently developed an IEEE 802.15.4z-compliant impulse radio (IR) UWB transceiver with low power consumption. The team believes that this is a key milestone to the realization of in-cabin UWB radar-on-chip applications. The IR-UWB transceiver uses a cost-efficient silicon implementation and operates over a frequency range of 6 to 9 GHz, consuming 8.7 mW/21 mW in continuous Tx/Rx mode.[3] The imec researchers believe that is the lowest power consumption among state-of-the-art IEEE 802.15.4z radios. The block diagram of this transceiver is shown in ***Figure 1***.

Fabricated in 28 nm CMOS technology and occupying a silicon area of 1.33 mm, the chip's low power consumption results from an optimized, low-power and interference-resilient Rx architecture coupled with a digital polar transmitter architecture. A distributed, two-stage, all-digital phased locked loop (PLL) further reduces the chip's power consumption and contributes to a reduced measurement time for localization.

PULSE-SHAPING ENHANCES UWB'S RANGING PRECISION

The availability of a low-power solution will be essential to making CPD and other in-cabin sensing solutions a reality, but equally important is the technology's ranging precision. To support object localization and target ranging, UWB positioning systems rely on the time of flight (ToF) of RF pulses. Following a pulse's transmission at a channel center frequency of around 6 GHz, a receiver filters and measures the signal's time of arrival (ToA) to estimate the range distance between the transmitter (TX) and the receiver (RX).

To make this technique work inside a vehicle will be challenging. The in-car environment is prone to signal distortions caused by reflections from the floor, roof, windows and seats. These reflections result in multipath signals, making it more difficult to accurately measure the direct path signal and reliably estimate the target's location and distance. ***Figure 2*** shows a block diagram of an UWB TX and RX measuring the ToA of an RF pulse in a cluttered environment characterized by multipath signals. A multipath environment not only features a direct path line of sight (LOS) signal that should be measured to obtain a target's distance and location; it also comes with non-line of sight (NLOS) signal components, reflecting off surfaces and scattering from objects. These multipath components make it more difficult to measure the direct path and reliably estimate an object's distance and location.

To offset the impact of multipath components, pulse-shaping strategies are used to make the pulse as short as possible. The rapid change in amplitude improves the precision with which the signal's ToA can be measured. The short duration of the pulse helps in measuring the direct path LOS well before the NLOS multipath signals arrive. The design of a pulse shape comes with quite some flexibility: as long as UWB standards and specifications are met, the shape of the pulse, as well as the design of the TX and RX circuitry, are largely left to the system and product developers to optimize.

An important element to consider is that the UWB's frequency range has been divided into channels to manage interference between users. The TX must meet a spectrum mask, limiting the bandwidth and constraining the signal and ToA measurement. The RX also has a channel filter with limited bandwidth to remove potential interference in neighboring channels. In other words, the benefit of short pulse duration should be balanced against the occupied spectrum. As the pulse gets shorter, the spectrum gets wider and pulse-shaping mechanisms must account for this important limitation.

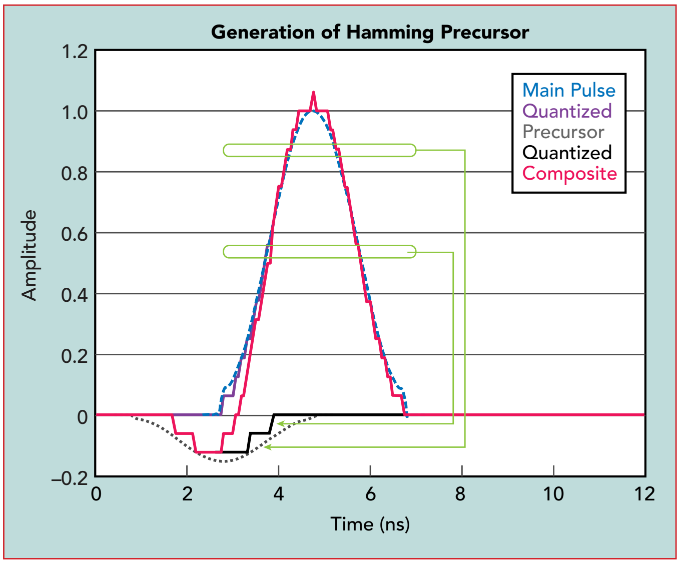

▲ Fig. 3 **Hamming pulse with a precursor.** ***Source:*** **imec.**

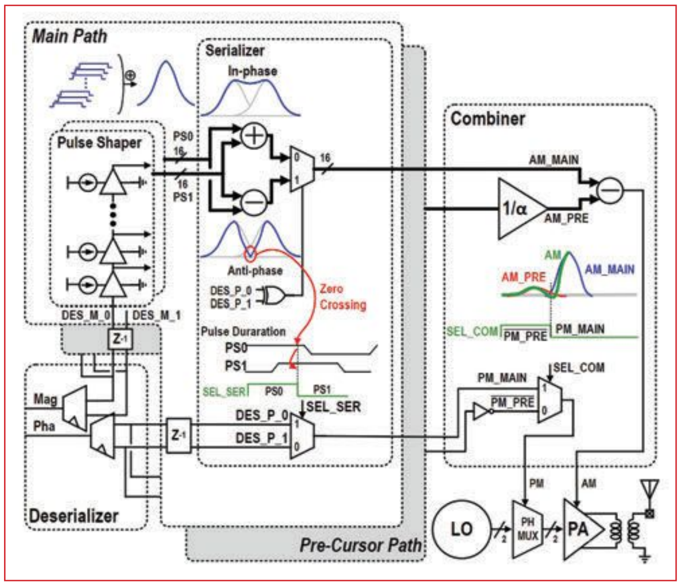

▲ Fig. 4 **TX circuit design to generate a pulse with an anti-phase precursor.** ***Source:*** **imec.**

A PULSE-SHAPING APPROACH USING AN ANTI-PHASE PRECURSOR

To accurately estimate the arrival time of a pulse, it is important to consider the leading edge of the pulse. This is especially true in indoor and in-cabin environments prone to multipath conditions where subsequent multipath components can potentially corrupt the trailing edge and to some extent, even the peak of the pulse. To address this, imec researchers propose creating an asymmetric pulse shape with a steep leading edge to disentangle the multipath components from the main signal. They propose doing this with an anti-phase precursor pulse with the opposite carrier phase.[4] This asymmetric pulse sharpens the pulse rise time, improves ToA measurement precision and decreases the interference from close multipath components while staying comfortably within the spectral mask for channelized signal compliance.

As a starting point, imec researchers used a pulse shape based on a Hamming waveform. The spectrum of this waveform has a good margin to the UWB spectrum mask requirement. The transmitted pulse shape consists of a main pulse and an auxiliary anti-phase pulse that is transmitted two nsec before the main pulse. This creates a short, negative-going precursor pulse that depresses the start of the main pulse and increases the slope of the rising edge up to the peak, all within the constraints of the spectral mask. The result is shown in ***Figure 3***.

GENERATING A PULSE WITH AN ANTI-PHASE PRECURSOR

To generate this anti-phase precursor for the pulse, imec researchers built a circuit based on their wideband transceiver implementation. The TX and RX are supplied by a locked frequency source using a cascaded PLL topology with a crystal oscillator to generate the 499.2 MHz system clock and 6 to 9 GHz local oscillator (LO) frequency. Second-stage LO PLLs generate the LO locally for the TX and the RX separately, reducing power consumption and simplifying the clock distribution.

The biggest challenges in the UWB TX design are the trade-offs between spectrum and low-power performance and dealing with inter-pulse interference (IPI). The IEEE 802.15.4a/z standards define the channel bandwidth and a chip/pulse rate of 499.2 MHz. This requires the pulse duration to be approximately 4 ns, exceeding the chip period. Unlike single pulse patterns in the preamble, IPI can be encountered in the payload data stream due to consecutive pulses at the chip rate.

imec's UWB TX design is shown in ***Figure 4***. It features a digital deserialization-serialization (DesSer) circuit to reduce the IPI. A two-bit amplitude and phase code at 499.2 MHz is first deserialized into two interleaved parallel paths running at 249.6 MHz. Each path employs the asynchronous pulse-shaper, producing 16 delayed sub-pulses, which together form a quantized Hamming pulse shape. The asynchronous shaping completely removes spectral images from which synchronous pulse-shaping systems suffer at the cost of a higher quantization noise floor. However, the quantization noise floor can be reduced by selecting sufficient quantization levels. The outputs of the two interleaved parallel asynchronous pulse-shapers are serialized by a digital serializer, either summing or subtracting them according to the polarity given by the phase code. Furthermore, the digital serializer extracts a new phase code signal, synchronizing it with the zero-crossing detection circuit, facilitating the phase transition without introducing spurious emissions.

An additional parallel path generates a smaller precursor pulse with opposite polarity. A similar DesSer circuit digitally combines the precursor and main pulse path before the power amplifier. Switching between the anti-phase precursor and main pulse is also synchronized by a zero-crossing detection circuit to avoid generating spurious emissions.

REALIZING AN IMPORTANT RANGING PRECISION IMPROVEMENT

Experiments using imec's IC implementation show that it effectively improves ToA measurement perfor-

SIGNAL MICROWAVE

Leading in Innovation

FPP Probe Series

- 100 ohm true odd mode differential
- 2 probe pins only – no ground pins
- Multiple bandwidths
  40 GHz bandwidth with 2.92 mm conn.
  50 GHz bandwidth with 2.40 mm conn.
  70 GHz bandwidth with 1.85 mm conn.
- Multiple probe pin pitches
  0.6 / 0.8 / 1.0 mm pin pitch
- New 110 GHz Probes with 1.00 mm connectors
- Multiple mounting configurations
  Standard 3 hole
  Straight 1 hole
  Custom mounting configurations available
- 1 year warranty

De-embedding Board

Probe 70 GHz s-parameters

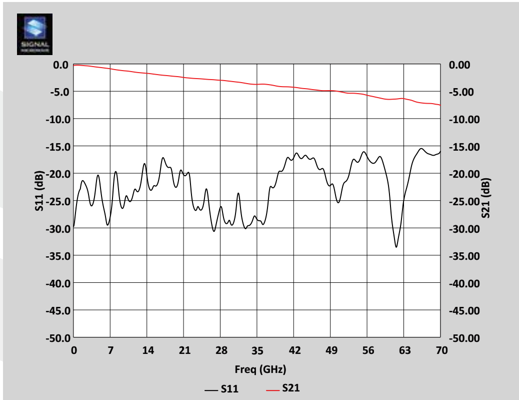

NEW AF70F70 & AM70F70 1.85 mm Blind Mate Interconnect System

The push-on interface is created by removing the threads and coupling nut of a 1.85mm interface pair. This allows for mating with very little force. See animation at www.signalmicrowave.com/adapters/video

- A new 1.85 mm interface blind mate connector system with 70 GHz bandwidth.
- Uses a float mount design for alignment and a spring to apply force.
- A better electrical performance alternative to current SMPM interface blind mate systems.

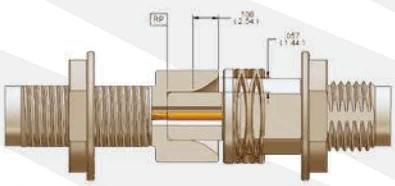

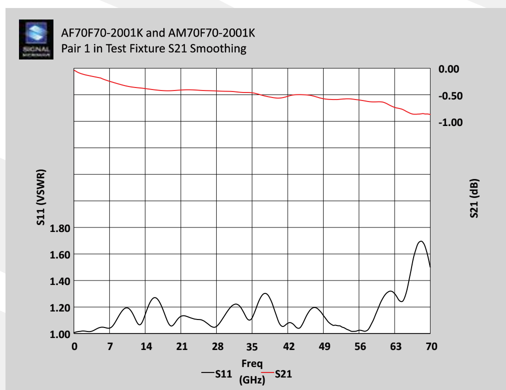

3D models for simulation available at no charge
to assist customers in their own development efforts.

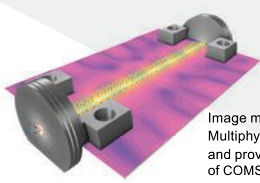

Image made using COMSOL Multiphysics® software and provided courtesy of COMSOL.

Signal Microwave, LLC
Tempe, Arizona
info@signalmicrowave.com
www.signalmicrowave.com
(480) 322-4992

SIGNAL MICROWAVE

mance and UWB ranging precision. ***Figure 5*** shows the performance improvement achieved by the TX while maintaining spectral compliance. The pulse mixing circuit, together with the resynchronization, maintains the sidelobe suppression of -35 dBc with and without precursor pulses. The addition of the precursor pulses reduces the rise time of the leading edge of the main pulse from 700 to 550 psec.

Using the precursor pulses has been shown to improve the precision of the difference in the ToA estimation by a factor of almost four. Care should be taken in extrapolating this difference result to general ranging performance due to limitations in measuring absolute ToA. However, the improvement is undoubtedly useful and arises from a combination of interrelated factors, including the pulse shape and the RX processing.

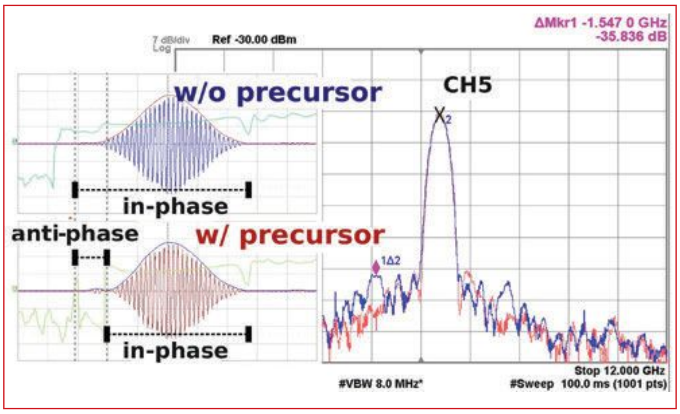

Fig. 5 **Transmitter output signal and spectrum with and without precursor.** ***Source:*** **imec.**

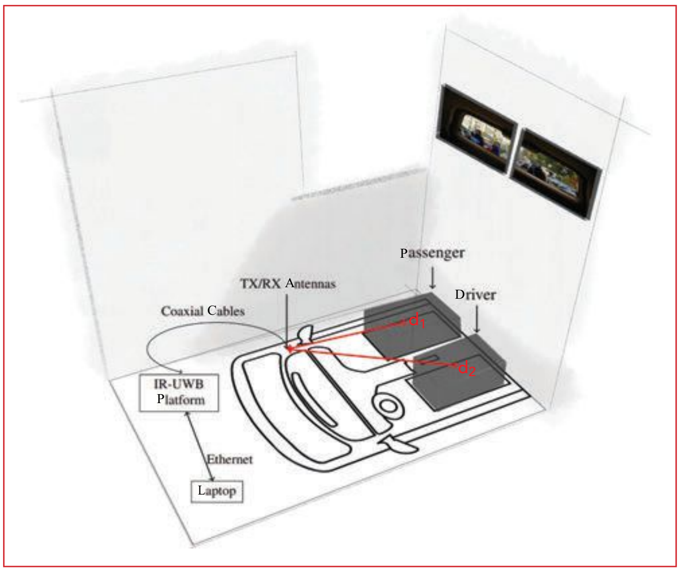

Fig. 6 **In-cabin demo setup.** ***Source:*** **imec.**

AN IEEE 802.15.4Z-COMPLIANT IR-UWB RADAR SYSTEM FOR IN-CABIN MONITORING

Building on this UWB transceiver design, imec researchers have developed an experimental IR-UWB radar system for real-time, in-cabin sensing.[5] The system operates at a bandwidth of 499.2 MHz to comply with the IEEE 802.15.4z standard. It provides occupancy detection and breathing rate estimation for individuals occupying the driver and/or front passenger seats, along with passenger gesture detection, all compelling automotive use cases.

The demo setup, simulating an in-cabin environment with a full-duplex, single-input, single-output (SISO) mono-static IR-UWB radar is depicted in ***Figure 6***. The antennas are strategically placed on the sides, tilted toward the ground and inclined more toward the driver's seat to include both seats in the main lobe of the antennas. The passenger and driver seats maintain a 45 cm edge-to-edge distance with the antennas positioned at 1.17 and 1.70 m from the center of the passenger and driver seats, respectively. Each TX and RX antenna is connected via 100 cm cables to the IR-UWB platform, which captures channel impulse responses (CIRs) every 10 msec, utilizing IEEE 802.15.4z-compliant SP0 packets. Following despreading and CIR accumulation, a captured CIR over fast time is estimated with a resolution of T_f = 1 nsec.

A crucial enabler to detect two closely located targets for a system with 499.2 MHz of bandwidth is advanced signal pro-

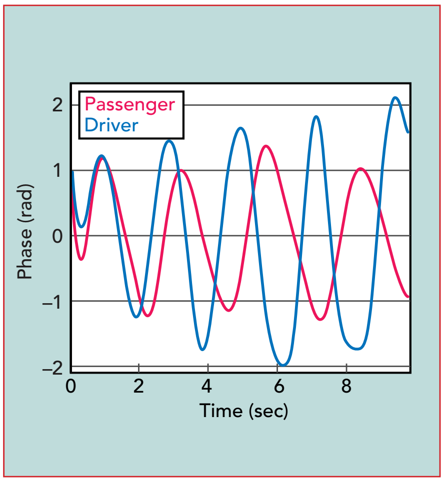

Fig. 7 Passenger and driver breathing signals. *Source:* imec.

cessing algorithms. This is especially true for an in-cabin environment where the driver and the passenger are in close proximity. With custom-built algorithms, imec researchers successfully achieved precise detection of both individuals, achieving a false alarm probability of more than 95 percent.

The researchers conducted two sets of experiments to evaluate the system's capability in estimating breathing rates. In the first scenario, their objective was to validate the system's accuracy in estimating breathing rates within a margin of less than 1 bpm. Employing a reference device with belt sensors to measure the subject's breathing rate, the reference device recorded a breathing rate of 11.96 bpm, while the demo setup estimated it at 11.71 bpm, confirming its accuracy within the desired threshold.

The researchers also successfully demonstrated the system's ability to estimate the passenger and driver's breathing rates simultaneously. This result is illustrated in ***Figure 7***, which shows the extracted breathing signals for both individuals. The researchers did observe that body movements and interference between targets can distort the measurements, which has them considering the development of specific algorithms to mitigate these factors in future work.

Algorithms also played a crucial role in the in-cabin detection of a predefined gesture. The experiments conducted by the imec team revealed that their classifier achieved 99.9 percent accuracy in correctly detecting false gestures and 90.5 percent for the reference gesture. According to imec researchers, these numbers can be further improved with additional data collection. For future work, they plan to gather more data and define more gestures to enhance the range of possible interactions between the human-vehicle interface.

While there are possible improvements, the imec experiments demonstrated the effectiveness of the proposed IR-UWB radar system. The results showcase the potential of using a UWB-based radar system to enhance automotive safety and comfort, particularly in CPD applications. Efforts like this one from imec will form the basis for improvements in vehicle in-cabin safety.

imec will present results on its ultra-wideband technology at the 2024 IEEE International Solid-State Circuits Conference.[6] ■

References

1. Heatstroke Deaths of Children in Vehicles, September 2023, Web: noheatstroke.org.
2. "Test and Assessment Protocol – Child Presence Detection," Euro NCAP, V. 1.1, November 2022, Web: cdn.euroncap.com/media/75474/euro-ncap-cpd-test-and-assessment-protocol-v11.pdf.
3. M. Song, et al., "An 8.7 mW/TX, 21 mW/RX 6-to-9GHz IEEE 802.15.4a/4z Compliant IR-UWB Transceiver with Pulse Pre-Emphasis Achieving 1.4mm Ranging Precision," *IEEE Symposium on VLSI Technology and Circuits*, June 2023.
4. C. Marshall, E. Allebes, A. Sheikh, M. Song, M. E. Soussi and Nick Winkel, "A UWB Pulse with Precursor for ToA Measurement," *International Conference on Indoor Positioning and Indoor Navigation*, September 2023.
5. A. Farsaei, B. Meyer, A. Sheikh, M. E. Soussi, P. Zhang, G. K. Ramachandra, J. Govers and M. Hijdra, "An IEEE 802.15.4z Compliant IR-UWB Radar System for In-Cabin Monitoring," *IEEE International Symposium on Personal, Indoor and Mobile Radio Communications*, September 2023.
6. 2024 IEEE International Solid-State Circuits Conference (ISSCC), Web: https://www.imec-int.com/en/5G-and-wireless-iot-communication/ultra-wide-band-uwb-technology.

INVITED PAPER

Wideband Butler Matrices and Their Potential Applications

Wei Liu
MIcable Inc., Fuzhou, China

The Butler matrix is a passive beamforming network that feeds a phased array of antenna elements. Traditionally, its accuracy over a wide bandwidth has been constrained by the limitations of components, resulting in a scarcity of wideband Butler matrices in the market that have high phase accuracy. This article explores the factors influencing Butler matrix bandwidth and performance and it will highlight the breakthrough technologies and products that have resulted in a series of Butler matrices achieving both wide bandwidth and high phase accuracy. In addition to discussing these advancements, the paper shares insights into potential applications, inviting readers to explore additional use cases for these products.

BEAMFORMING NETWORK

Beamforming networks are integral to phased array technology as they serve to feed the phased array of antenna elements. There are two primary approaches to realizing beamforming networks: active and passive.

Active Beamforming Networks

An active beamforming network is constructed with power combiners/dividers, digitally-controlled phase shifters and attenuators, as depicted in the block diagram in ***Figure 1***. A key advantage of this type of network lies in the ability to achieve continuous beam sweeping. This capability is facilitated by digitally-controlled phase shifters and attenuators that can provide a broad frequency bandwidth.

These types of devices are currently available in the market. These phase shifters and attenuators typically have a maximum of six bits with the digital control operating discrete phase or attenuation bits that range from the least significant bit value to the combination of all the bit values. The relative bandwidth of phase shifters and attenuators varies across the frequency bands of use, but it is not uncommon to see devices operating in S- and C-Band over a 2.4 to 5.1 GHz frequency range, which equates to a 75 percent bandwidth. Another popular band is the 6 to 18 GHz band, which equates to 100 percent bandwidth. MACOM and Analog Devices reference devices on their websites that operate in Ku-Band, at 24 to 29.5 GHz, equating to 23 percent bandwidth.

However, certain drawbacks come with this technology. The digitally-controlled phase shifters and attenuators necessitate complex control circuitry that includes digital-to-analog converters (DACs) and analog-to-digital converters (ADCs), along with logic control circuits. Additionally, a robust power supply network, effective heat dissipation and temperature-compensation circuits are required to maintain stable circuit performance. In addition to these challenges, information from current publications indicates that the bandwidth is presently limited to a maximum of 100 percent relative bandwidth.

Passive Beamforming Networks: The Butler Matrix

In contrast, a Butler matrix represents a completely passive beamforming feed network for phased array antenna elements. It contains an N × N matrix of hybrid couplers and a fixed number of phase shifters, where N is a power of two. The device features N input ports (beam ports) where power is applied and N output ports (element ports) connected to N antenna elements. It facilitates reciprocal signal transfer between any of the N input ports and any of the N output ports, enabling simultaneous operation as

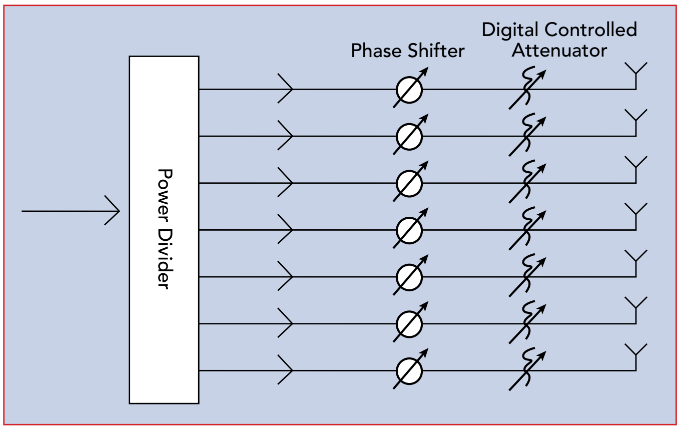

Fig. 1 Active beamforming feed network.

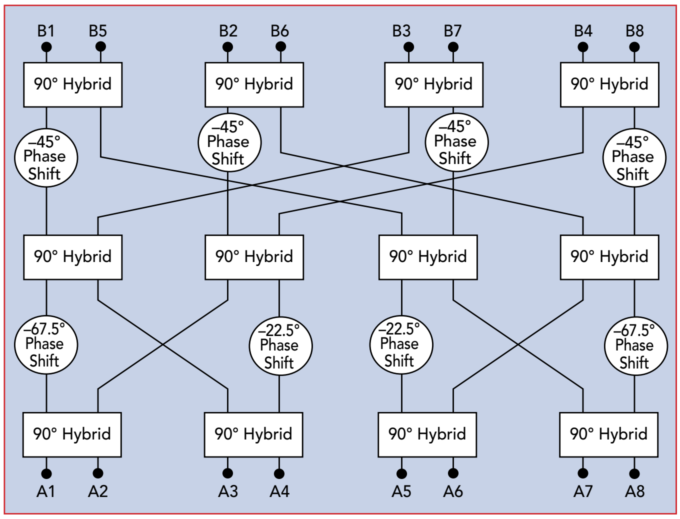

Fig. 3 8 × 8 Butler matrix configuration.

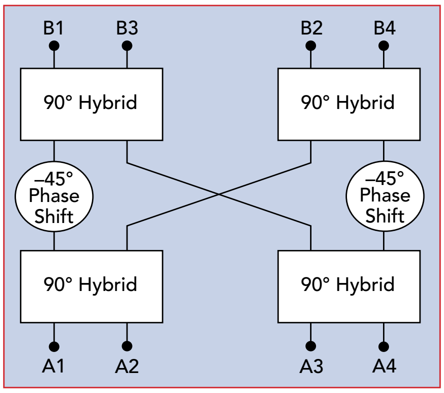

Fig. 2 4 × 4 Butler matrix configuration.

TABLE 1

4 X 4 BUTLER MATRIX PHASE RELATIONSHIPS

Input Output	A1	A2	A3	A4
B1	-45	-135	-90	-180
B2	-90	0	-225	-135
B3	-135	-225	0	-90
B4	-180	-90	-135	-45

both a transmission and receiving system. The power of two requirement in Butler matrices means that 4 × 4, 8 × 8 and 16 × 16 configurations are typical. ***Figure 2*** shows the 4 x 4 configuration and ***Table 1*** shows the phase relationships among the four output ports.

Figure 3 shows the 8 x 8 Butler matrix configuration. This configuration adds another stage of 90-degree hybrids, along with 67.5-degree and 22.5-degree fixed phase shift elements. ***Table 2*** shows the phase relationships among the eight output ports. Note that the phase relationship between output pairs remains the same.

Figure 4 shows a 16 × 16 configuration and there are now four hybrid stages. This configuration is notable because it uses a mixture of 180-degree and 90-degree hybrids and no phase shifters. The phase relationships for this topology are shown in ***Table 3***.

These visual representations offer insights into the matrix's structure and functionality. Compared to active phased array beamforming networks, the passive Butler matrix boasts a straightforward across-matrix configuration, ensuring accurate and stable performance, higher power handling for each path and cost effectiveness. However, it faces challenges in achieving wide bandwidth with higher phase control accuracy due to limitations in the bandwidth of its components. The factors influencing the bandwidth and performance of the Butler matrix are intricately linked to the design of its passive components, which are based on transmission lines. In the Butler matrix, connections between components are established through transmission lines, where the frequencies of electromagnetic waves have a linear relation with their phase. As shown in the circuit configurations, as the number of input and output ports increases in a Butler matrix, so does the complexity and potential lengths of the interconnections.

To illustrate, an absolute phase accuracy of ±5 degrees over a 0 to 360-degree range implies a maximum relative frequency bandwidth of 2.78 percent for a transmission line. Alternatively, for a 5 percent relative frequency bandwidth, the potential phase accuracy error could be ±9 degrees and for a 10 percent relative frequency bandwidth, the error could be ±18 degrees. In conventional terms, achieving more than 2.78 percent relative frequency bandwidth within 5-degree phase accuracy or obtaining below 18-degree phase accuracy over a 10 percent relative frequency bandwidth is considered challenging, if not impossible.

This underscores a crucial point: to achieve wide bandwidth, every

TABLE 2

8 X 8 BUTLER MATRIX PHASE RELATIONSHIPS

Input Output	A1	A2	A3	A4	A5	A6	A7	A8
B1	-112.5	-202.5	-135	-225	-112.5	-202.5	-180	-270
B2	-135	-45	-247.5	-157.5	-180	-90	-337.5	-247.5
B3	-157.5	-247.5	0	-90	-247.5	-337.5	-135	-225
B4	-180	-90	-112.5	-22.5	-315	-225	-292.5	-202.5
B5	-202.5	-292.5	-225	-315	-22.5	-112.5	-90	-180
B6	-225	-135	-337.5	-247.5	-90	0	-247.5	-157.5
B7	-247.5	-337.5	-90	-180	-157.5	-247.5	-45	-135
B8	-270	-180	-202.5	-112.5	-225	-135	-202.5	-112.5

component must support that wide bandwidth with the required phase accuracy and the electrical length error of each path must be meticulously controlled within a very narrow range. Any deviation in these characteristics leads to significant phase changes over a wide frequency range, presenting formidable technical challenges. It is these challenges that have, to date, prevented the emergence in the market of wideband Butler matrices or beamforming networks that also provide high phase accuracy.

MIcable is developing technology to address three areas that are essential for the development of wideband Butler matrices: wideband hybrids, wideband passive phase shifters and accurate phase-matching cable assemblies. Using simulation and optimization tools, coupled with advanced manufacturing processes, MIcable has successfully developed a series of high performance wideband products. Notable in the product portfolio are 0.6 to 18 GHz 90-degree hybrids with a 6-degree maximum phase error and a series of 2.4 to 7.25 GHz passive phase shifters. In addition, MIcable has shipped sets of eight cable assemblies that achieve ±2-degree phase matching among the cables in each group at 28 GHz.

POTENTIAL APPLICATIONS

There is substantial development effort and activity aimed at extending the capabilities of beamforming technology. Innovations in this technology offer advantages to a diverse set of opportunities in 5G, 6G, Wi-Fi, IoT, driverless cars, mobile communication, satellite communication, testing and radar applications. The realization of wideband high-accuracy Butler matrix beamforming networks will enable advances in a variety of applications.

Beamforming Feed Networks for Phased Array Antennas

There is an immediate application for beamforming feed networks in phased array antennas. MIcable Butler matrices can provide stable performance and a straightforward configuration over a frequency bandwidth of 0.6 to 7.25 GHz. Active feed networks struggle to achieve satisfactory performance over a frequency bandwidth this broad. Since the Butler matrix incorporates passive elements, it offers a cost-effective solution with higher than typical power handling capabilities. These devices can handle powers up to 20 W. This set of attributes makes the Butler matrix a compelling choice in these applications.

Channel Simulator in Massive MIMO Systems

Another promising application involves using Butler matrices as channel simulators in massive MIMO systems. They can simulate communication scenarios between IoT nodes, base stations and users. By integrating attenuators on each port, a new type of mesh network emerges with the ability to simulate both the amplitude and phase of signals, surpassing the capabilities of traditional mesh networks.

Object Detection and Allocation

Leveraging the reciprocal signal transfer capability

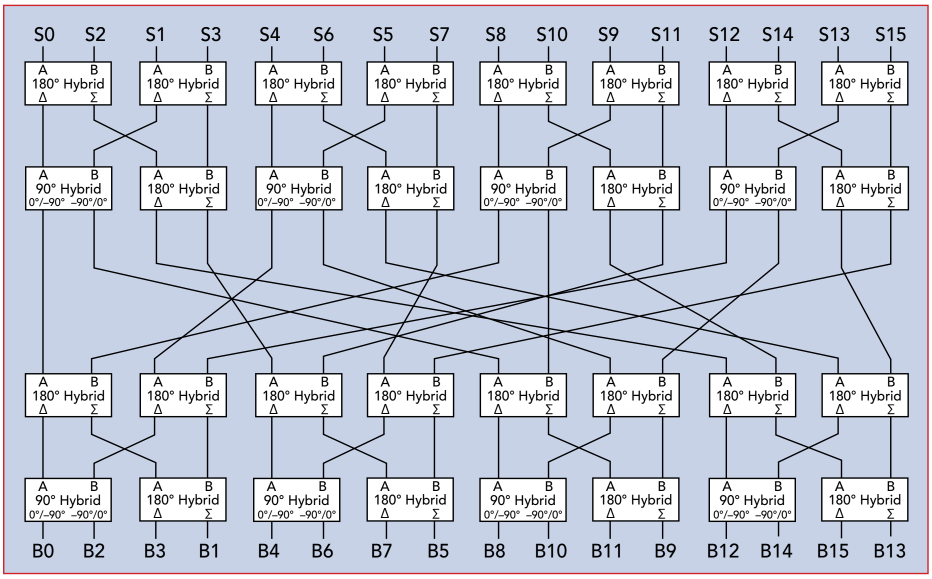

Fig. 4 16 × 16 Butler matrix configuration.

and the ability to feed all input ports simultaneously, Butler matrices can serve as plus and minus networks for signal detection and allocation. This expands the possibilities for detecting and allocating objects in various contexts.

Exploring More Applications

The versatility of wideband high-accuracy Butler matrix beamforming networks implies that more applications await discovery in various industries. As technology evolves, these networks are likely to find novel applications that cater to the specific needs of different sectors.

PRACTICAL EXAMPLES OF BUTLER MATRICES

By developing and integrating wideband hybrids, passive phase shifters and phase-matching cable assemblies, MIcable has produced a portfolio of wideband Butler matrices with high phase accuracy. The specifications of some typical Butler matrix products that have already been shipped are outlined in ***Table 4***. This table shows the broad variety of Butler matrices in MIcable's portfolio, along with the typical frequency bands and performance that these solutions provide.

ADDITIONAL BUTLER MATRIX CONFIGURATIONS

The table of catalog parts shows a variety of solutions ranging from ultra-high frequencies to Ka-Band frequencies. MIcable has developed a 0.6 to 5 GHz 8×8 Butler matrix. This wideband Butler matrix achieves a phase accuracy of ±11 degrees to ±14 degrees maximum, amplitude unbalance of ±1.0 to ±1.2 dB maximum, insertion loss of 12.3 to 14.5 dB maximum and input/output port VSWR of 1.4:1 to 1.5:1 maximum. This wide frequency coverage addresses the requirements of 5G Frequency Range 1.

MIcable has also developed a 2.4 to 7.25 GHz 8 × 8 Butler matrix. The 8 × 8 Butler matrix exhibits a phase accuracy ranging from ±6 to ±8 degrees maximum, amplitude unbalance of ±0.2 to ±0.4 dB maximum, insertion loss of 9.8 to 10.8 dB maximum and input/output port VSWR of 1.2:1 to 1.4:1 maximum. These results can be achieved across Wi-Fi frequencies of 2.4 to 2.5 GHz, 5.18 to 5.83 GHz and 5.9 to 7.25 GHz. These solutions become more attractive as Wi-Fi 6E/7E applications begin to gain production traction.

The latest addition to the MIcable Butler matrix portfolio is a 0.6 to 7.25 GHz 8 × 8 solution. This device offers ±14 degrees of phase accuracy. MIcable believes that the availability of wideband, high phase accuracy Butler matrices will enable

TABLE 3 16 X 16 BUTLER MATRIX PHASE RELATIONSHIPS

Input / Output	S0	S1	S2	S3	S4	S5	S6	S7	S8	S9	S10	S11	S12	S13	S14	S15
B0	180	90	0	-90	90	0	-90	180	0	-90	180	90	-90	180	90	0
B1	90	0	-90	180	90	0	-90	180	90	0	-90	180	90	0	-90	180
B2	90	0	-90	180	180	90	0	-90	-90	180	90	0	0	-90	180	90
B3	180	90	0	-90	0	-90	180	90	180	90	0	-90	0	-90	180	90
B4	90	90	90	90	0	0	0	0	-90	-90	-90	-90	180	180	180	180
B5	0	0	0	0	0	0	0	0	0	0	0	0	0	0	0	0
B6	0	0	0	0	90	90	90	90	180	180	180	180	-90	-90	-90	-90
B7	90	90	90	90	-90	-90	-90	-90	90	90	90	90	-90	-90	-90	-90
B8	90	180	-90	0	0	90	180	-90	-90	0	90	180	180	-90	0	90
B9	0	90	180	-90	0	90	180	-90	0	90	180	-90	0	90	180	-90
B10	0	90	180	-90	90	180	-90	0	180	-90	0	90	-90	0	90	180
B11	90	180	-90	0	-90	0	90	180	90	180	-90	0	-90	0	90	180
B12	180	0	180	0	90	-90	90	-90	0	180	0	180	-90	90	-90	90
B13	90	-90	90	-90	90	-90	90	-90	90	-90	90	-90	90	-90	90	-90
B14	90	-90	90	-90	180	0	180	0	-90	90	-90	90	0	180	0	180
B15	180	0	180	0	0	180	0	180	180	0	180	0	0	180	0	180

MiCable

NEW

SUPER BEND®

High Performance Millimeter Wave Cable Assemblies

67GHz 67GHz 67GHz

Really tight bend radius to save installation space & eliminate the need for costly right angle connectors without performance degradation

- **Low Loss** <5.7dB/m@67GHz
- **Low VSWR** <1.35:1@67GHz
- **High Shielding Efficiency** <-90dB
- Shielded with stainless steel braids with high mechnical strength & flexure durability

Test Report for 0.2M Cable Assemblies

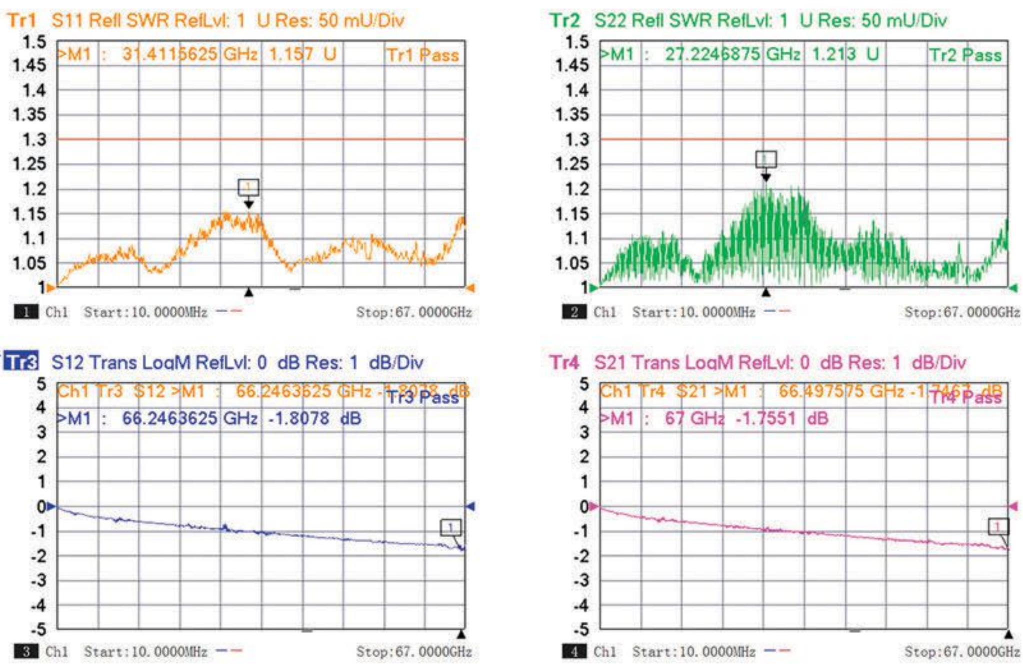

More Information-
Scan the QR Code

MIcable Inc.

www.micable.cn sales@micable.cn +86-591-87382856

TABLE 4 CATALOG BUTLER MATRICES

	Part Number	Frequency Range* (GHz)	VSWR :1 (Max.)	Insertion Loss** dB (Max.)	Amplitude Unbal. dB (Max.)	Amplitude Flatness dB (Max.)	Phase Accuracy Deg. (Max)	Isolation dB (Min.)	Dimension L x W x H (mm)
4x4	SA-07-4B006050	0.617-0.8.21	1.4	8.2	±1.1	±0.8	±10	16	152.4 x 141.4 x 43
		0.832-0.96	1.4	8.2	±1.1	±0.7	±9	16	152.4 x 141.4 x 43
		1.427-1.71	1.5	8.3	±0.9	±0.7	±9	15	152.4 x 141.4 x 43
		1.71-2.2	1.5	8.5	± 0.9	±0.8	±10	14	152.4 x 141.4 x 43
		2.496-2.69	1.5	8.7	± 0.9	±0.7	±9	13	152.4 x 141.4 x 43
		3.3-4.2	1.6	8.9	±1.0	±0.7	±12	13	152.4 x 141.4 x 43
		4.4-5	1.6	9.2	±1.0	±0.8	±12	13	152.4 x 141.4 x 43
	SA-07-4B020060	2-6	1.5	7.8	±0.9	±0.8	±8	14	101.6 x 122 x 16.5
		2.4-2.5	1.4	7.3	±0.5	±0.3	±4	15	101.6 x 122 x 16.5
		5.18-5.83	1.5	7.7	±0.6	±0.4	±5	14	101.6 x 122 x 16.5
	SA-07-4B020080	2.4-2.5	1.5	7.3	±0.5	±0.3	±4	14	101.6 x 106.7 x 16.5
		5.18-5.83	1.5	7.7	±0.6	±0.4	±5	13	101.6 x 106.7 x 16.5
		5.9-7.25	1.5	7.8	±0.7	±0.5	±6	13	101.6 x 106.7 x 16.5
	SA-07-4B020080E	2.4-2.5	1.4	7.5	±0.6	±0.5	±7	12	125.6 x 51.5 x 44.5
		5.18-5.83	1.5	7.9	±0.7	±0.6	±8	12	125.6 x 51.5 x 44.5
		5.9-7.25	1.5	8	±0.8	±0.7	±9	12	125.6 x 51.5 x 44.5
	SA-07-4B180400	18-40	2.0	12	±1.2	±2.0	±15	10	144.8 x 101.6 x 16.5
	SA-07-4B265295	26.5-29.5	1.9	11	±0.8	±0.8	±10	10	144.8 x 101.6 x 16.5
	SA-07-4B405435E	40.5-43.5	2.0	13.7	±1.0	±1.0	±16	7	169 x 58.7 x 54
8x8	SA-07-8B006050	0.617-0.821	1.6	12.7	±1.5	±1.2	±16	15	324 x 304.8 x 43.2
		0.832-0.96	1.6	12.7	±1.5	±1.1	±14	15	324 x 304.8 x 43.2
		1.427-1.71	1.6	13.1	±1.3	±1.1	±15	14	324 x 304.8 x 43.2
		1.71-2.2	1.7	13.3	±1.3	±1.2	±15	13	324 x 304.8 x 43.2
		2.496-2.69	1.7	13.7	±1.3	±1.1	±14	12	324 x 304.8 x 43.2
		3.3-4.2	1.7	14.5	±1.4	±1.1	±20	12	324 x 304.8 x 43.2
		4.4-5	1.7	14.9	±1.4	±1.2	±20	12	324 x 304.8 x 43.2
	SA-07-8B0200060	2-6	1.6	12.0	±1.2	±1.2	±12	12	205.7 x 233.8 x 16.5
		2.4-2.5	1.5	11.4	±0.7	±0.5	±8	13	205.7 x 233.8 x 16.5
		5.18-5.83	1.6	12.0	±0.9	±0.6	±10	12	205.7 x 233.8 x 16.5
	SA-07-8B0200080	2.4-2.5	1.5	11.2	±0.6	±0.4	±8	13	205.7 x 205.7 x 16.5
		5.18-5.83	1.5	11.6	±0.8	±0.5	±10	12	205.7 x 205.7 x 16.5
		5.9-7.25	1.55	11.8	±0.9	±0.7	±12	12	205.7 x 207.7 x 16.5
	SA-07-8B0200080E	2.4-2.5	1.6	11.4	±0.6	±0.5	±12	12	229.7 x 106.7 x 44.5
		5.18-5.83	1.6	11.8	±0.8	±0.6	±14	12	229.7 x 106.7 x 44.5
		5.9-7.25	1.6	12.0	±0.9	±0.8	±16	12	229.7 x 106.7 x 44.5
	SA-07-8B060180	6-8	1.7	12.0	±1.0	±0.7	±12	9	205.7 x 157.5 x 16.5
		6-18	1.8	14.5	±1.3	±2.0	±15	8	205.7 x 157.5 x 16.5
		8-12	1.7	13.0	±0.9	±0.8	±12	9	205.7 x 157.5 x 16.5
		12-18	1.8	14.5	±1.0	±1.0	±14	8	205.7 x 157.5 x 16.5
16x16	SA-07-16B017022	1.7-2.2	1.4	15.0	±0.8	±0.8	±4	14	2U
	SA-07-16B0200600	2.3-2.7	1.6	17.0	±1.2	±0.8	±12	10	2U
		3.3-3.8	1.6	18.0	±1.2	±0.8	±12	9	2U
		4.4-5	1.7	19.0	±1.2	±0.8	±14	8	2U
	SA-07-16B020060E	2.3-2.7	1.6	17.5	±1.6	±1.2	±16	10	2U
		3.3-3.8	1.6	18.5	±1.6	±1.2	±16	9	2U
		4.4-5	1.7	19.5	±1.6	±1.2	±18	8	2U
32x16	SA-07-3216B017022	1.7-2.2	1.5	18.4	±0.9	±1.0	±5	13	3U
	SA-07-3216B033042E	3.3-4.2	1.6	20.0	±1.2	±1.4	±10	12	3U

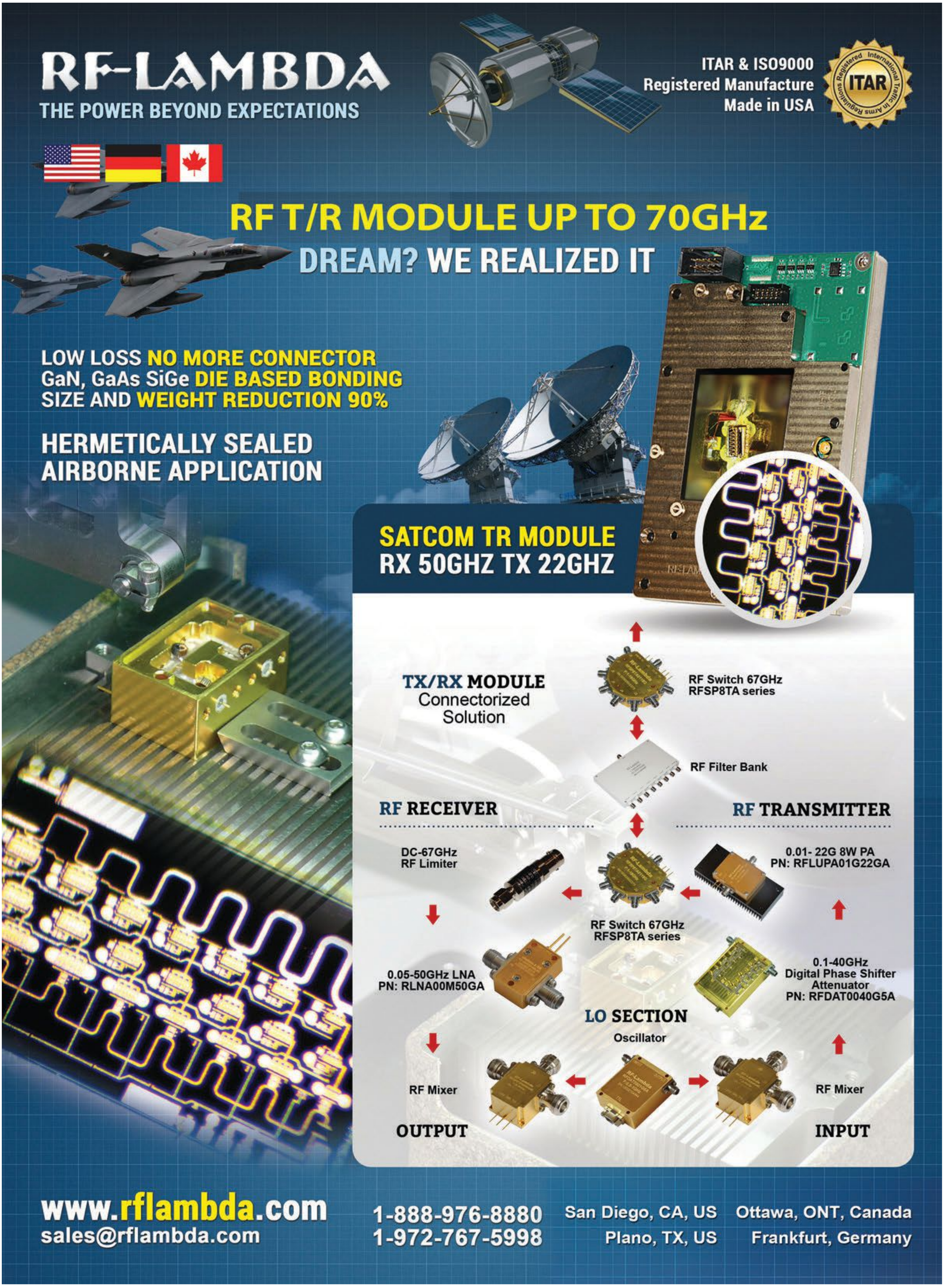
RF-LAMBDA
THE POWER BEYOND EXPECTATIONS
ITAR & ISO9000
Registered Manufacture
Made in USA
ITAR
Registered International Traffic in Arms Regulations
RF T/R MODULE UP TO 70GHz
DREAM? WE REALIZED IT
LOW LOSS NO MORE CONNECTOR
GaN, GaAs SiGe DIE BASED BONDING
SIZE AND WEIGHT REDUCTION 90%
HERMETICALLY SEALED
AIRBORNE APPLICATION
SATCOM TR MODULE
RX 50GHZ TX 22GHZ
TX/RX MODULE
Connectorized
Solution
RF Switch 67GHz
RFSP8TA series
RF Filter Bank
RF RECEIVER
RF TRANSMITTER
DC-67GHz
RF Limiter
0.01- 22G 8W PA
PN: RFLUPA01G22GA
RF Switch 67GHz
RFSP8TA series
0.05-50GHz LNA
PN: RLNA00M50GA
0.1-40GHz
Digital Phase Shifter
Attenuator
PN: RFDAT0040G5A
LO SECTION
Oscillator
RF Mixer
RF Mixer
OUTPUT
INPUT
www.rflambda.com
sales@rflambda.com
1-888-976-8880
1-972-767-5998
San Diego, CA, US
Plano, TX, US
Ottawa, ONT, Canada
Frankfurt, Germany

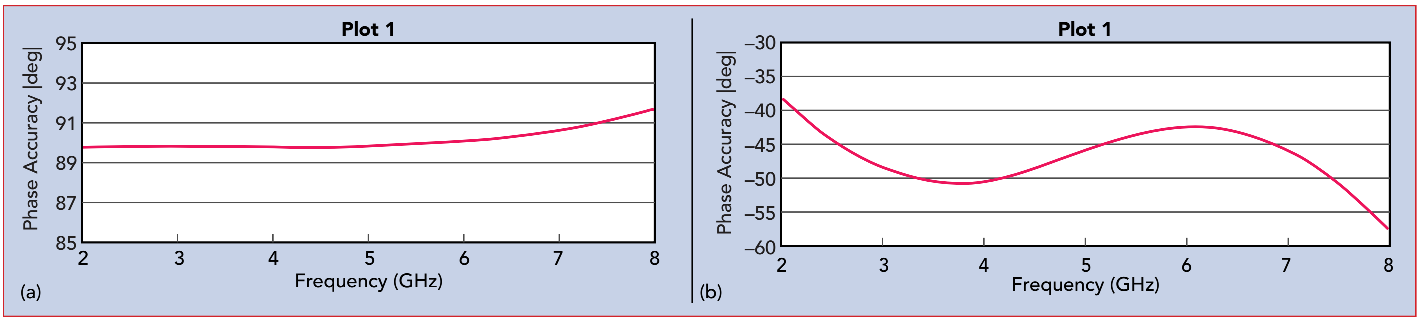

Fig. 5 (a) Phase accuracy of 2.4 to 7.25 GHz 90° hybrid. (b) Phase accuracy of 2.4 to 7.25 GHz 45° phase shifter.

the passive beamforming architecture in more applications.

BUILDING BLOCK PERFORMANCE

As described, there are distinct advantages to using a passive beamforming approach to feeding an antenna array. The Butler matrix provides an excellent solution for these passive beamforming needs, but the viability of this solution depends on the performance of the passive elements. As the desired application bandwidth increases, solving the wideband performance challenge of these passive devices becomes increasingly important.

As an example of the design goals for the building blocks of the wideband Butler matrices, ***Figure 5a*** shows the design simulation for the phase accuracy performance of the 2.4 to 7.25 GHz 90-degree hybrid. ***Figure 5b*** shows a similar analysis of the phase accuracy performance for the 45-degree phase shifter bit. Similar charts exist for the 22.5-degree and 67.5-degree phase shifter bits, but they are not presented in the interest of brevity.

As the frequency bandwidth increases, it is not surprising to see the phase accuracy degrade, but the performance is still more than sufficient to meet the needs of the Butler matrix. ***Figure 6a*** shows the simulated phase accuracy of the 0.5 to 5 GHz 90-degree hybrid building block. ***Figure 6b*** shows the simulated phase accuracy for the 67.5-degree phase shifter bit, the highest required phase shift value.

Measured Results

The simulated results show the performance of the fundamental Butler matrix building blocks, but the better guideline is the actual performance. ***Figure 7a*** shows the input port VSWR for the 2.4 to 7.25 GHz 8

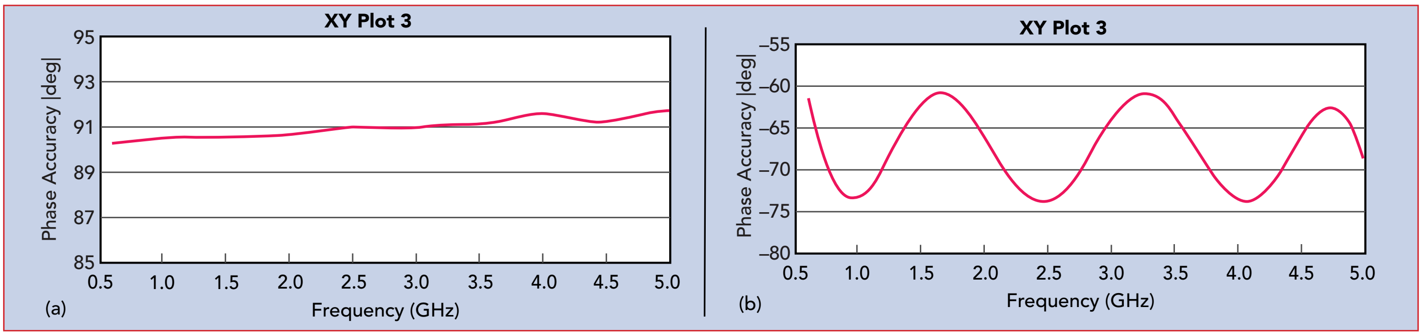

Fig. 6 **Phase accuracy of 0.5 to 5 GHz 90° hybrid. (b) Phase accuracy of 0.5 to 5 GHz 67.5° phase shifter.**

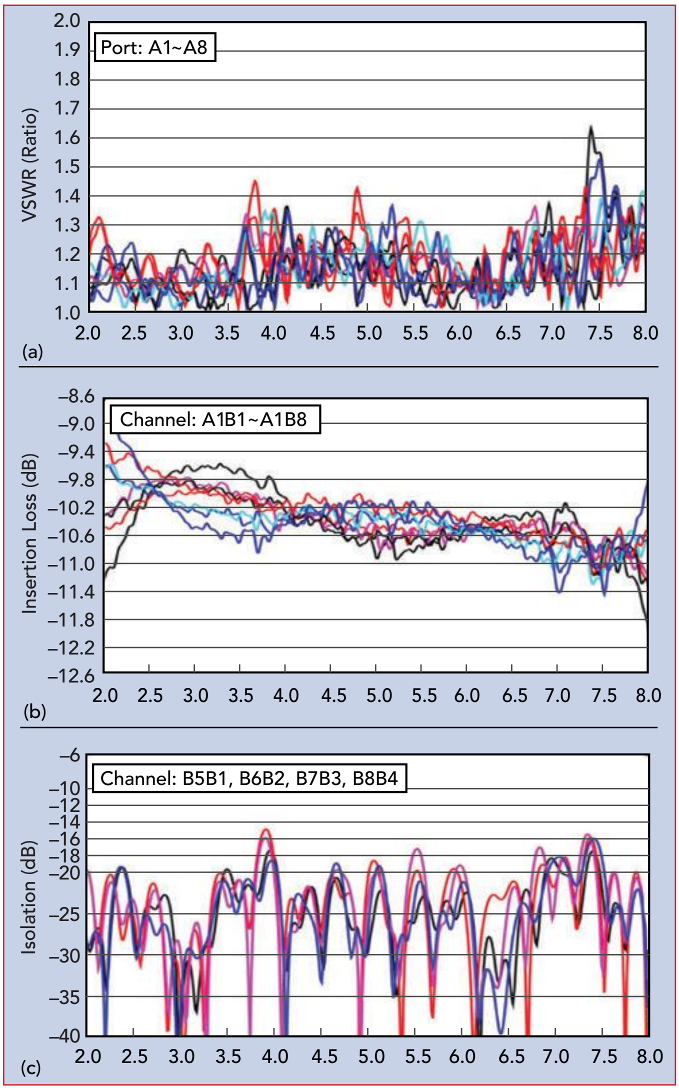

Fig. 7 **(a) Input port VSWR. (b) Insertion loss from input A1. (c) Port isolation.**

× 8 Butler matrix. ***Figure 7b*** shows the insertion loss for the same device and ***Figure 7c*** shows some representative isolation plots for ports of the 8 × 8 Butler matrix.

The S-parameter information for the Butler matrix is important, but the function of the device is to route signals to antenna ports that require beamforming and beam steering. As we have described, phase and amplitude imbalance and accuracy become of paramount importance for these applications. ***Figure 8a*** shows the amplitude balance for one input of the 2.4 to 7.25 GHz 8 x 8 Butler matrix as compared to all the output ports.

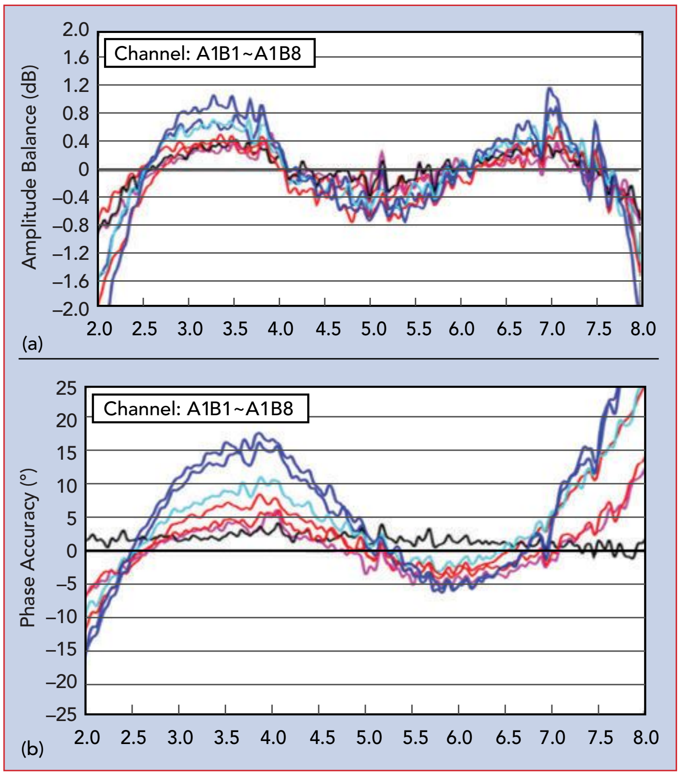

Fig. 8 **(a) Amplitude balance A1 input to outputs. (b) Phase accuracy A1 input to outputs.**

Figure 8b shows the phase accuracy for the same input of the Butler matrix to all the output ports.

CONCLUSION

A growing number of applications are relying on phased array antennas to increase capacity, data rates and capabilities. These systems may use active beamforming and beam steering architectures to achieve their performance goals, but these architectures may create issues with cost, power consumption and complexity. Passive beamforming can achieve the same performance objectives and alleviate some of the issues that active beamforming creates. Until recently, the passive building blocks required for a Butler matrix were not capable of the bandwidth and phase accuracy performance necessary to make these solutions attractive to a wide variety of applications. This paper describes the product portfolio, development efforts and results from new products that address the bandwidth and phase accuracy performance that had limited the wider adoption of Butler matrices. ■

INVITED PAPER

Over-the-Air Techniques for Measuring Integrated RF Electronics and Antennas

Anouk Hubrechsen and Teun van den Biggelaar
ANTENNEX B.V., Eindhoven, The Netherlands

With higher frequencies, the integration of antennas and RF electronics means that many measurements now must be performed over the air. This article addresses the challenges of testing integrated antenna systems in e.g. phased array, antenna-on-chip and antenna-in-package configurations. This article details the latest over-the-air (OTA) measurement techniques for metrics such as noise figure, out-of-band emissions and radiated power spectral density.

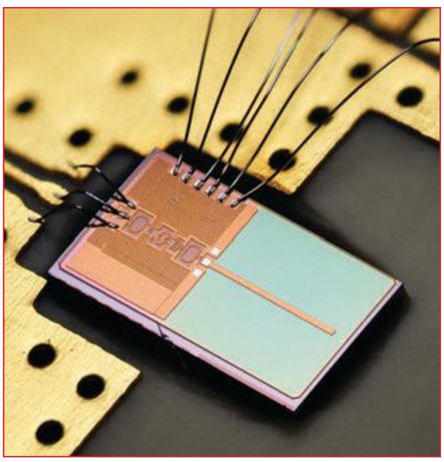

Fig. 1 **30 GHz monopole antenna integrated with an LNA bonded to an evaluation board.**[1]

INTEGRATION OF ANTENNAS AND RF ELECTRONICS

An ongoing trend in the mmWave regime is towards highly integrated wireless system designs. These efforts are being undertaken to reduce costs and increase efficiency. This integration often means that the antenna and the RF electronics cannot be separated, creating a new dimension in testing RF front-end performance.

Some of the most integrated designs involve antennas-on-chip or antennas-in-package, which are becoming especially popular in high frequency applications, such as automotive radar. ***Figure 1*** shows a 2 × 1 mm, 30 GHz monopole antenna integrated with a low noise amplifier (LNA) in SiGe BiCMOS technology. This integration has the added benefit of co-designing the impedance of the LNA and antenna to optimize efficiency and noise figure, but a challenge lies in the manufacturing and testing of such a system.

Traditionally, LNAs are measured on a wafer probe station using conducted techniques. However, with this new configuration, there is no straightforward port available to feed RF power to the input of the LNA for a traditional conducted method. Since the antenna is the only port that is connected to the LNA, it is evident that characterizing the electronics in this system requires OTA methods. This motivates a reassessment of measurement techniques to determine the best way to evaluate the noise figure, system gain and compression point for such a system.

PHASED ARRAY ANTENNAS

These challenges become even more complex when using phased array configu-

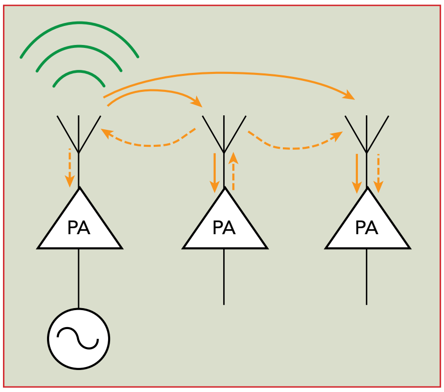

Fig. 2 **Mutual coupling in an antenna array.**

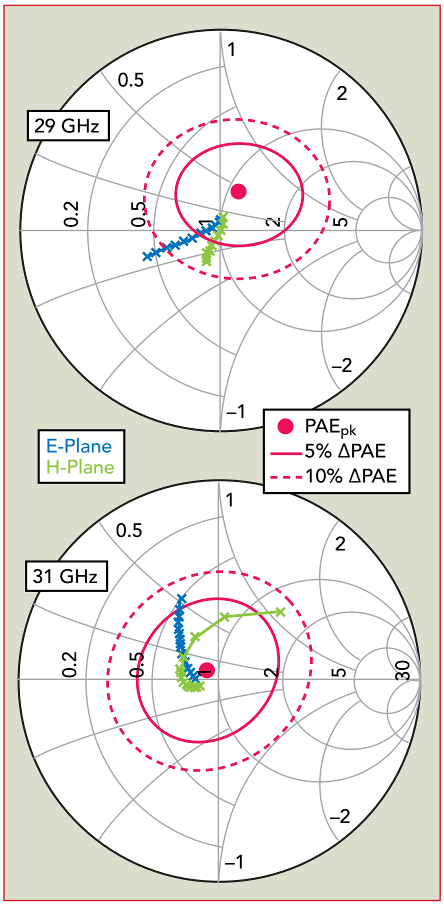

Fig. 3 **Simulation results including simulated PAE circles.**[2]

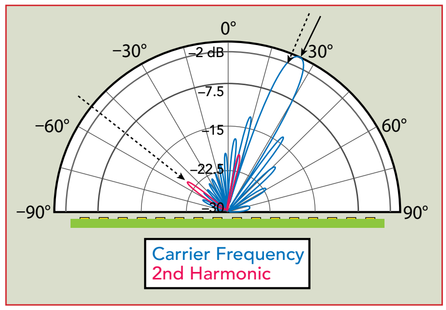

Fig. 4 **Possible measurement errors when measuring a single direction.**

Fig. 5 **ANTENNEX reverberation chamber.**[4]

rations. If multiple antennas operate nearby, RF power is coupled from one element to another, as depicted in ***Figure 2***. The mutual coupling between the individual antenna elements will alter the load impedance for different scan angles and therefore interact with the power amplifiers (PAs) in a transmitting system. Similarly, the coupling changes the source impedance of LNAs for different scan angles in a receiving system. This means that when the array is used to perform beamforming, the loading conditions change, impacting the array's performance for each beamforming setting.

An example of the impact of beamforming is shown in ***Figure 3***. The figure shows the active impedance of a Ka-Band stacked patch antenna connected to a PA in an infinite array environment for different scan angles of 0 to 70 degrees in the E- and H-planes.[2] Under different beamforming conditions and frequencies, the active impedance changes significantly. Consequently, this can cause a reduction of over 10 percent in power-added efficiency (PAE). Similar effects occur in receiving systems that can impact the noise figure accordingly.

This simulation assumed that all paths are identical and that all relevant RF parameters like material loss, dielectric constant and surface roughness, are known. In addition, there will be differences between the paths, and antenna elements on the edge of a finite array will be affected differently as compared to the center elements. Manufacturing tolerances must be considered at mmWave frequencies. The unpredictability of all these effects can make the deviations in efficiency and noise figure even larger between simulation and measurement. Testing many different settings becomes essential to understanding the overall performance of the system and the only way to do so for RF electronics with integrated antennas is OTA.

TRADITIONAL OTA TESTING METHODS

Typically, OTA testing is performed in an anechoic chamber, which is known for its ability to precisely determine the direction of radiation as it measures one direction at a time. The radiation in all other directions is ideally absorbed by RF absorbers on the chamber walls. For many metrics, like ACLR, P1dB, system gain, out-of-band emission and noise figure that relate to an overall radiated power spectral density, a full sphere needs to be sampled and this is a time-consuming process. Often, a measurement at a single angle is performed. This inherently includes the antenna gain and can lead to measurement errors.

Some sources of measurement error in a single direction are visualized in ***Figure 4***. This figure shows a simulated normalized array radiation pattern for a 16-element linear array pointed towards 25 degrees. The direction of the maximum radiation is generally not known, a priori and precise alignment is not trivial. The main lobe is likely missed when measuring only one direction. A misalignment as small as 3 degrees results in a 2 dB error, as indicated by the dashed arrow in Figure 4. Additionally, it is insufficient to measure some metrics in only one direction. This is the case with harmonics. Figure 4 shows the second harmonic and with the same phase shift as the carrier frequency, the radiated power is assumed to be 20 dB lower. Since the harmonic is twice the frequency, the beam is steered in a different direction. This makes it important to perform a full spherical scan and sample very densely around the device under test (DUT), to ensure that all contributions are captured. This is obviously a very time-consuming task.

REVERBERATION CHAMBER

An alternative for OTA testing is the reverberation chamber, shown in ***Figure 5***, which acts as the dual of an anechoic chamber.[3,4] The reflective walls of the reverberation chamber ensure that radiation in

Fig. 6 **Pharrowtech 60 GHz PTK1060 and mode stirrers.**[5]

all directions is captured, which reduces risk in the measurement process. The sensitivity to positional sampling and the issue of missing the second harmonic illustrated in Figure 4 is eliminated. Unlike spatial sampling in anechoic chambers, sampling in a reverberation chamber involves changing the environment around the DUT. This method requires significantly less sampling compared to a spatial scan, reducing measurement time. This method results in accurate and fast OTA measurements for RF electronics in integrated antenna systems, including the transition to the antenna, making it particularly valuable for mmWave tests. As an example, a radiated power spectral density measurement of a 60 GHz integrated antenna module across a 1 GHz bandwidth with 1 MHz resolution takes just 15 seconds, with less than 0.4 dB measurement uncertainty. The downside to this method is that extracting the radiation direction is more complex due to the highly reflective environment.

SETTING UP THE CHAMBER

The reverberation chamber works by mode-stirring, which means altering the electromagnetic environment within the chamber. This process involves mode stirrers, which are complex metallic shapes designed so that a small movement can create a significant change in the field distribution within the chamber. The mode stirrers can be seen in the chamber shown in ***Figure 6***, along with the Pharrowtech 60 GHz PTK1060.

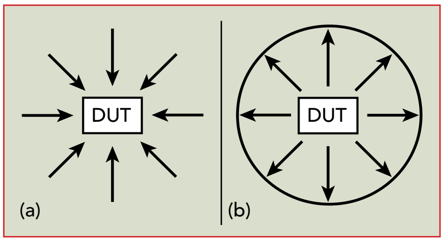

Fig. 7 **Ideal reverberation chamber for (a) receiving and (b) transmitting DUT.**

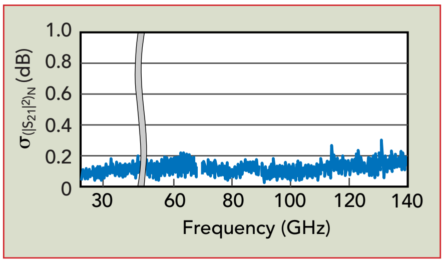

Fig. 8 **Standard deviation of reverberation chamber measurements.**

When measurements are performed over more than 100 different mode-stirrer positions, the field distribution within the chamber is, on average, uniform and isotropic. Increasing the number of measured positions of the mode stirrers reduces measurement uncertainty. The uncertainty due to the number of mode-stirrer positions is typically on the order of $1/\sqrt{N}$ where N is the number of different positions of the mode stirrers. These positions need to be carefully chosen such that the measured samples have a low correlation between them.

Having a uniform field inside the chamber makes the measurement essentially independent of the positioning of the DUT. This is particularly advantageous at mmWave frequencies because it simplifies the measurement procedure and reduces measurement uncertainty. In a sense, the reverberation chamber is the OTA equivalent of a coaxial connector, acting as an integrating sphere for transmitting devices and uniformly illuminating receiving devices from all directions, as shown in ***Figure 7***. This capability allows for rapid and accurate measurement of all the metrics related to the overall received or transmitted power.

To demonstrate the DUT positioning independence, transferred power through the chamber $\langle|S_{21}|^2\rangle_N$ was averaged over N=100 mode-stirrer positions at nine different antenna locations. Each measurement was taken on a different day with a new calibration. The standard deviation between all measurements is on the order of 0.1 dB at 26 GHz and only 0.2 dB at 140 GHz. This data is shown in ***Figure 8*** and it shows the precision and operational bandwidth of the reverberation chamber.

CHAMBER LOSS CALIBRATION

Chamber losses for a regular setup are on the order of 25 to 40 dB in the 26 to 100 GHz range. This loss is comparable to the reduction in received power in a line-of-sight measurement at the same frequency range in an anechoic chamber with 20 dBi antennas at 2 m. Like anechoic chamber measurements, the losses in the reverberation chamber often need to be measured and de-embedded.

The characterization of the chamber loss is typically a separate measurement. This measurement is generally performed with a vector network analyzer connected to two reference antennas and needs to be performed for every new DUT because the DUT imposes different loading conditions on the chamber. Since many measurements can be performed using a spectrum analyzer, multiple instruments are often required to perform a measurement and the setup must be manually rebuilt between measurements. To overcome this issue, the ANTENNEX reverberation chamber contains an integrated signal generator that acts as a calibration module to characterize and calibrate chamber losses. For a transmitting device, the same spectrum analyzer configuration can be used for the chamber loss calibration and the measurement of the DUT without any setup alterations.

RADIATED POWER SPECTRAL DENSITY MEASUREMENTS

Measuring the radiated power spectral density is straightforward when the chamber is set up and calibrated.[6] ***Figure 9*** illustrates a typical setup. The DUT transmits a modulated or CW signal that is attenuated by the chamber losses. A receiving antenna with a spectrum analyzer receives the signal. The ra-

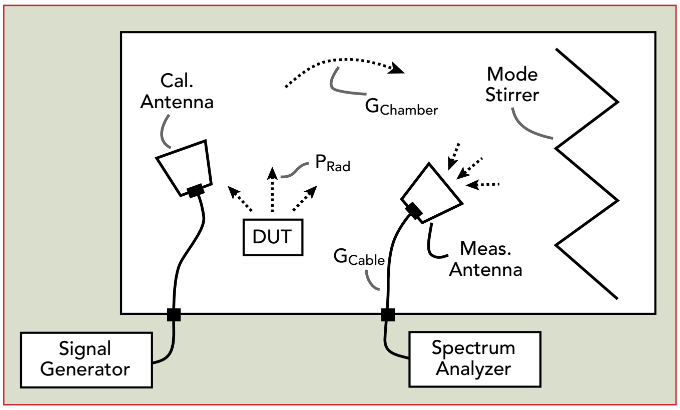

Fig. 9 **Typical total radiated power setup in the chamber.**

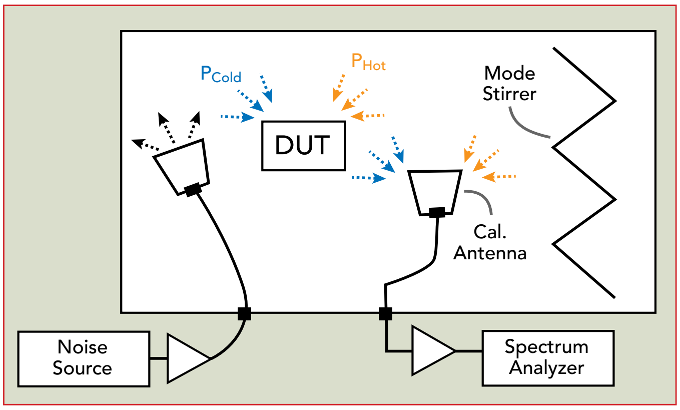

Fig. 10 **OTA noise figure measurements in a reverberation chamber.**

diated power spectral density (PSD) can be calculated using the simple link budget analysis (in dB) shown in Equation 1:

$$PSD = \langle P_{R,SA}\rangle_N - G_{Cable} - \eta_{ant} - G_{Chamber} \qquad (1)$$

Frequency-dependent losses from the chamber, cables and antenna can be measured and calibrated as mentioned earlier. In Equation 1, $\langle P_{R,SA}\rangle_N$ is the received power at the spectrum analyzer averaged over N mode-stirrer positions. A similar procedure can be used to characterize a DUT in receiving mode when the device has a detector, like an analog-to-digital converter (ADC), integrated or when it has an RF output.

In a reverberation chamber, the radiated PSD can easily be measured over a wide frequency band in less than a minute. This enables tests of metrics like out-of-band emissions, spectral regrowth, efficiency, system gain and more for many beamforming settings. This capability creates many possibilities in electromagnetic compatibility testing where the reverberation chamber has long been a staple for measurements below 18 GHz. For instance, it allows the characterization of radiated emissions from an RFIC that is not intended to radiate harmonics from lower frequency antenna systems.

In this example, the DUT is a standalone. Often DUTs need different inputs like data, RF or DC power. To enable all these inputs to the DUT, a dedicated panel that can be equipped with different feedthrough components is placed inside the chamber.

MANAGING REFLECTIONS

The reverberation chamber is a highly reflective environment, making it inevitable that a portion of the power returns to the antenna. When the antenna is properly positioned, the power returning to the DUT is the radiated power at a given frequency minus the chamber loss. When that power level is too high, the chamber loss can also be increased by loading the chamber with RF absorber. This will impact uniformity, but this can be compensated by measuring at different antenna locations.

Incorrect antenna positioning can cause high-magnitude reflections to return to the DUT, potentially affecting the device's performance. This condition is similar to the effects of mutual coupling, especially when the main beam is pointed towards a wall or a corner. To address this, the ANTENNEX chamber has mode stirrers that are optimized to reduce direct reflections. As seen in Figure 6, there is a scattering structure located at the top of the chamber. When the antenna array is directed upward, the scattering structure minimizes reflections directly back to the DUT. The antenna should also not be placed too close to the chamber walls or mode-stirring mechanisms, as objects close to the antenna can change the impedance and reduce its efficiency.

THE REVERBERATION CHAMBER AS A WIRELESS NOISE SOURCE

The ability to create a uniform field in the chamber can also be used to create different noise power levels. This means that the chamber acts as a wireless noise source.[7,8] Similar to a conducted Y-factor method, a receiving DUT can be exposed to both hot and cold noise powers. An example of a setup for OTA noise figure measurements using the chamber is illustrated in ***Figure 10***. By measuring the noise power at the output of the DUT with an internal ADC or with a detector connected to an RF output, the noise figure can be estimated.

This measurement also requires calibration of the chamber with an additional receive antenna, which is used to estimate the hot and cold noise power levels. In this calibration, the noise figure and gain of the detector are removed with a conducted Y-factor method. A measured result of a single antenna with an attenuator and an LNA is shown in ***Figure 11***, which shows good agreement with a conducted reference.

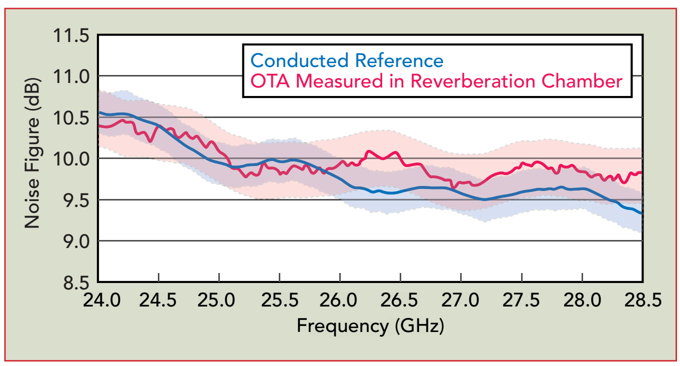

Fig. 11 **OTA noise figure measurement.**

CONCLUSION

Higher levels of integration in mmWave systems increase testing complexity. Reverberation chambers enable fast and accurate measurements of various metrics linked to both RFICs and antennas. This makes these chambers a valuable tool in the toolbox of both antenna and RF electronics engineers. By utilizing the reflective properties of a reverberation chamber, measurement time can be greatly reduced for several types of OTA measurements compared to traditional approaches. The inherent broadband behavior of the metallic walls and mode stirrers allows low uncertainties to be achieved over a wide bandwidth. By containing the radiation inside the reverberation chamber rather than the walls of the anechoic chamber absorbing a large portion of the energy, all the radiated information remains inside the chamber. This opens a realm of possibilities in other areas, like assessing the baseband signal quality with error vector magnitude measurements or measuring radiation patterns. ■

ACKNOWLEDGMENTS

The authors would like to thank Tim Stek and Roel Budé from ANTENNEX B.V. and Martijn de Kok from the Eindhoven University of Technology for contributing to this article.

References

1. Z. Chen, Q. Liu, B. Smolders, P. Baltus and H. Gao, "30-GHz Co-designed Low-Noise Amplifier and Antenna-on-Chip for Wireless Applications," *IEEE International Symposium on Radio-Frequency Integration Technology (RFIT)*, Nanjing, China, 2019, pp. 1–3, doi: 10.1109/RFIT.2019.8929159.
2. M. de Kok, S. Monni, M. van Heijningen, A. Garufo, A. B. Smolders and U. Johannsen, "A Review of PA-Antenna Co-design: Direct Matching, Harmonic Tuning and Power Combining," *52nd European Microwave Conference (EuMC)*, Milan, Italy, 2022, pp. 536–539, doi: 10.23919/EuMC54642.2022.9924344.
3. A. Hubrechsen, K. A. Remley and S. Catteau, "Reverberation Chamber Metrology for Wireless Internet of Things Devices: Flexibility in Form Factor, Rigor in Test," *IEEE Microwave Magazine*, Vol. 23, No. 2, Feb. 2022, pp. 75–85, doi: 10.1109/MMM.2021.3125464.
4. The Wireless Connector™, ANTENNEX B.V., Web: www.antennex.tech.
5. PTK1060 EVK, Pharrowtech, Web: www.pharrowtech.com.
6. A. Hubrechsen et al., "Total Radiated Power Measurement at 100 GHz in a Reverberation Chamber," *17th European Conference on Antennas and Propagation (EuCAP)*, Florence, Italy, 2023, pp. 1–4, doi: 10.23919/EuCAP57121.2023.10132953.
7. A. Hubrechsen, T. Stek and A. B. Smolders, "Simplified Over-the-Air Noise Figure Measurement Method for Reduced Uncertainty," *IEEE/MTT-S International Microwave Symposium - IMS 2023*, San Diego, Calif., 2023, pp. 911–914, doi: 10.1109/IMS37964.2023.10188197.
8. T. Stek, A. Hubrechsen, D. S. Prinsloo and U. Johannsen, "Over-the-Air Noise Figure Characterization of mm-Wave Active Integrated Antennas Using a Reverberation Chamber," *IEEE Transactions on Microwave Theory and Techniques*, Vol. 71, No. 3, March 2023, pp. 1093–1101, doi: 10.1109/TMTT.2022.3217149.

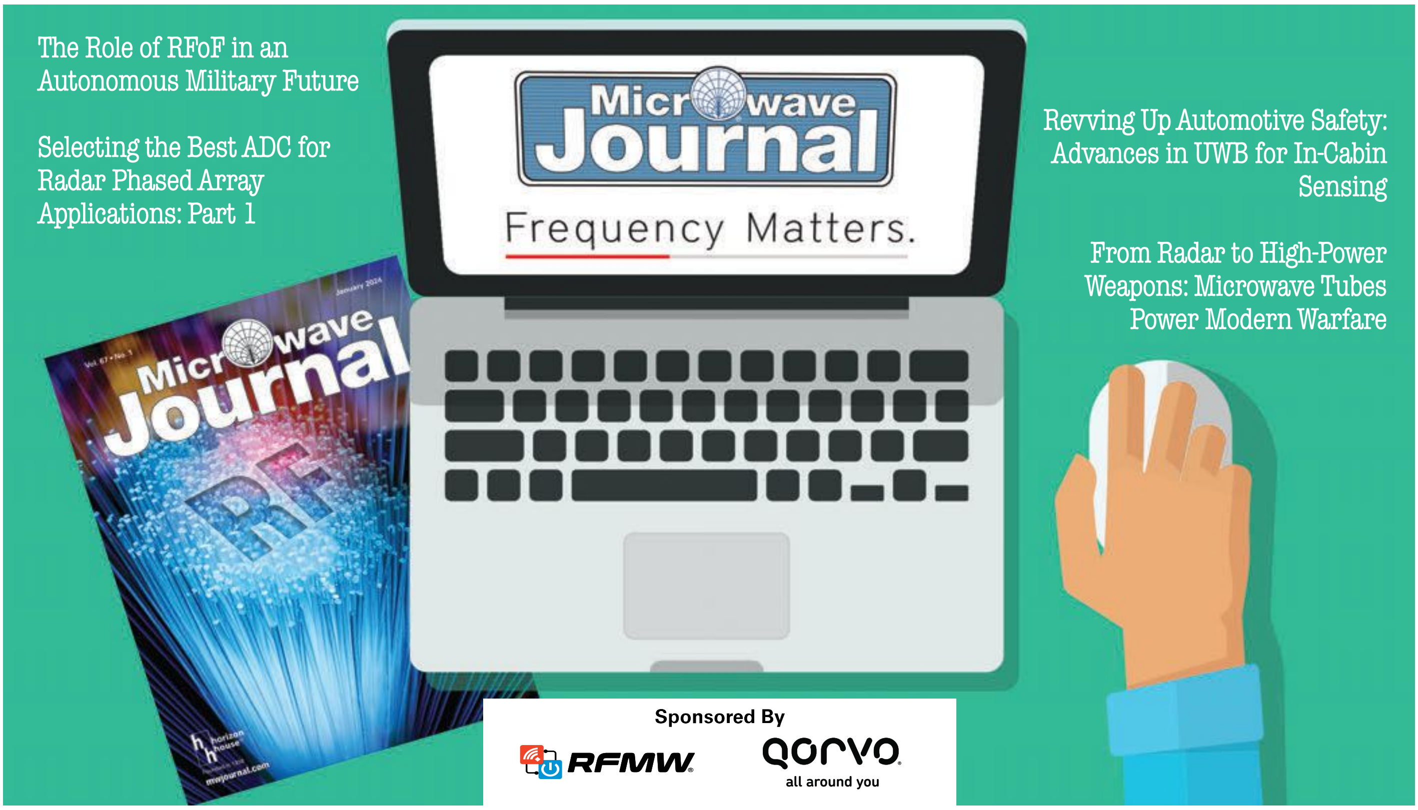

LN2 Calibrated Noise Source Family Aids in Noise Figure Measurements

Eravant, formerly Sage Millimeter Inc.
Torrance, Calif.

TABLE 1
ERAVANT NOISE SOURCE MODELS

Model	RF Port	Frequency (GHz)	ENR (dB)
STZ-05240318-KM-0T2	2.92 mm	0.5 to 40	18
STZ-05250318-2M-0T2	2.4 mm	0.5 to 50	18
STZ-05267313-VM-0T2	1.85 mm	0.5 to 67	18
STZ-42-0T2	WR-42	18 to 26.5	18
STZ-28-0T2	WR-28	26.5 to 40	18
STZ-22-0T2	WR-22	33 to 50	18
STZ-19-0T2	WR-19	40 to 60	13
STZ-15-IT2	WR-15	50 to 75	15
STZ-50375320-12-IT2	WR-15	50 to 75	20
STZ-12-IT2	WR-12	60 to 90	15
STZ-60396320-12-IT2	WR-12	60 to 96	20
STZ-10-IT2	WR-10	75 to 110	15
STZ-75311420-10-IT2	WR-10	75 to 110	20
STZ-65312415-10-IT2	WR-10	65 to 116	15
STZ-06-IT2	WR-06	110 to 170	15
STZ-14420412-05-IT2	WR-05	140 to 200	12

Noise sources play a pivotal role in various test and measurement applications. Primarily, they serve as reference signals to measure internally generated noise levels in components, subsystems and systems. These sources are adept at providing wideband stimulus signals for built-in test functions in radar and communication systems and they contribute to assessing the linearity and stability of high-power amplifiers. They are integral components in the calibration circuitry of microwave radiometers and radio astronomy receivers. The noise source injects a predetermined and known amount of noise power into the receiver. This injected noise power enables testing the receiver output power to determine gain and calibrate its variance. The noise source can be toggled on and off to supply two different injected power levels. This creates two corresponding output power levels, facilitating the gain and noise figure measurements of the receiver. This comprehensive process

Fig. 1 **Eravant Liquid Nitrogen (LN2) calibrated noise source.**

enables the complete calibration of the receiver system. ***Table 1*** shows Eravant's noise source offerings.

With the advancements in mmWave and sub-terahertz technologies, there is a growing demand for noise sources operating at frequencies beyond W-Band (75 to 110 GHz). Presently, discussions around 6G at D-Band (110 to 170 GHz) are burgeoning, leading to the development of numerous systems tailored for various applications. The assessment of gain and noise figures for these systems is crucial for validation and testing. Consequently, D-Band noise sources garner increased attention from academic and industrial circles. Yet, commercial noise sources capable of covering the complete set of sub-terahertz frequency bands are presently not widely available. Addressing this market need, Eravant has introduced the STZ series of noise source products, offering a diverse range to meet various test and measurement requirements within the frequency range of 0.5 to 220 GHz. An example of this series is depicted in ***Figure 1***.

Typically, coaxial connector-based noise sources are available for frequencies below 67 GHz, while waveguide versions cater to the 18 to 220 GHz range. The excess noise ratios (ENRs) of these STZ models range from 12 to 20 dB. For the waveguide noise sources, the typical ENR flatness is ±2 dB across the entire operating bandwidth. The ENR calibration for waveguide models uses the LN2-based true cold/hot termination method. All models necessitate a nominal supply voltage of +28 VDC. All models are equipped with either a Faraday isolator or an internal attenuator to offer high return loss and isolate the port impedance variations. This ensures a consistent, flat ENR across

TABLE 2

D-BAND STZ ELECTRICAL SPECIFICATIONS

Parameter	Minimum	Typical	Maximum
Input Frequency	110 GHz		170 GHz
ENR		15 dB	
ENR Flatness		±3 dB	
AM Modulation Rate		1 kHz	
Return Loss		15 dB	
DC Voltage		+28 VDC	
DC Current		45 mA	
Specification Temperature		+25°C	
Operating Temperature	0°C		+50°C

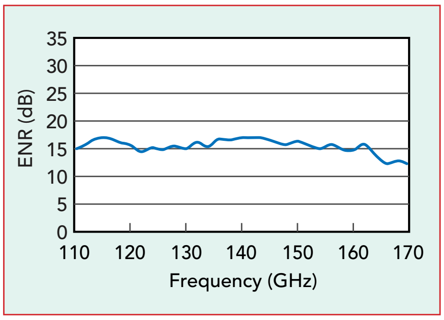

Fig. 2 **Calibrated D-Band STZ ENR.**

frequency bands. The STZ series includes different RF ports and operates across various frequency bands as detailed in Table 1.

These noise sources support TTL-level input for on/off control signals and can accommodate modulation rates of up to 1 kHz. In addition, a manual toggle switch is provided to turn the noise source on and off. The specifications for the D-Band STZ model are detailed in ***Table 2*** and calibrated ENR over the band is depicted in ***Figure 2***, with the device achieving a typical ENR of 15 dB.

Eravant not only offers calibrated noise sources but also provides noise source calibration services. Eravant has adopted the Y-factor method to determine the ENR of a noise source under test. To ascertain the noise temperature of the device under test (DUT) requires a reference noise source with a known noise temperature. This method utilizes a liquid nitrogen-cooled termination as the cold state of the reference noise source with a noise temperature of 77K and a room temperature termination as the hot state with a noise temperature of 290K. Noise power readings from the reference noise source are collected by the noise figure measurement system at its hot and cold states, normalizing the noise figure of the measurement system. By gathering noise power readings from the noise source under test in its on and off states, the ENR of the DUT can be calculated, completing the calibration process. The effective noise temperatures of these terminations are meticulously regulated and measured with high precision to ensure the accuracy and reliability of noise source calibrations.

Signal analyzers and noise figure analyzers that are currently available lack the direct capability to measure noise power within the mmWave and sub-THz frequency ranges. To facilitate noise figure measurements in these frequency ranges, integrating down-converters within the measuring system is essential. Eravant offers full waveguide band down-converters extending the operating frequency of the analyzers up to 220 GHz and typically providing a conversion gain from 20 to 30 dB.

Eravant provides a comprehensive solution set for mmWave and sub-THz frequency challenges. Critical to these solutions are noise sources. In addition to noise sources with flat ENRs, Eravant offers calibration services for waveguide-banded noise sources. Eravant also supplies down-converters for precise noise figure and gain measurements up to 220 GHz.

VENDORVIEW

Eravant, formerly Sage Millimeter Inc.
Torrance, Calif.
www.eravant.com

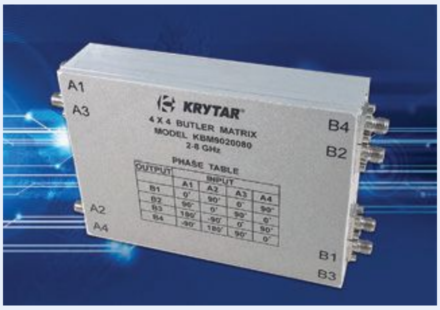

Butler Matrix Family Covers 0.5 to 40 GHz

KRYTAR's Butler matrix family includes 13 models providing operating performance over the 0.5 to 40 GHz frequency range. These Butler matrices rely on KRYTAR's 90-degree and 180-degree hybrid couplers to provide good phase accuracy, amplitude imbalance, stability and repeatability performance. This family offers phase imbalance values of ±3 to ±15 degrees, amplitude imbalance values of ±0.4 to ±1.6 dB, isolation values of 10 to 16 dB minimum, insertion loss values of 8.0 to 13.5 dB maximum and VSWR values of 1.2:1 to 2.0:1 maximum, depending on frequency range. All models include SMA female or 2.4 mm female connectors for higher frequency performance. KRYTAR also offers complete engineering services for custom designs that meet or exceed critical performance and/or packaging specifications.

A KRYTAR Butler Matrix can be utilized as a beamforming network to feed phased array antenna elements to control RF beamforming and beam steering. The Butler matrix advantage over other beamforming methods is the simplicity of use in a variety of applications. KRYTAR's Butler matrices target antenna array beamforming in applications like 5G NR, Wi-Fi 6 and Wi-Fi 6E, mmWave, MIMO radio links, radio direction finding, multipath simulation and performance evaluation.

For nearly 50 years, KRYTAR, Inc., located in the heart of Silicon Valley, has been specializing in the design and manufacture of broadband mmWave, microwave and RF components and test equipment for commercial and military applications. The KRYTAR product line covers DC to 110 GHz and includes directional couplers, directional detectors, 3 dB hybrids, MLDD power dividers, detectors, terminations, coaxial adapters and beamformers. KRYTAR microwave components are manufactured in full compliance with the EU RoHS-6 Environmental Requirements.

VENDORVIEW

KRYTAR, Inc.
Sunnyvale, Calif.
Toll Free: +1-877-734-5999
krytar.com/products/beamformers/butler-matrix

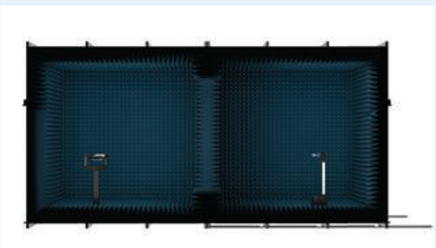

Split-Chamber Antenna Tester Doubles Capacity

Extending the line of AC1224 walk-in antenna test chambers, mmWave Test Solutions has debuted a split-chamber version of the large AC1224-360. This new split version is reconfigurable from one large single chamber to two half-chambers, doubling the test capacity whenever needed. The end walls of each of the two half-chambers have removable center sections, opening an 8 x 8 ft. aperture between them. One half-chamber moves on linear rails to efficiently move them apart for reconfiguration.

Panel sizes of only 1.2 x 1.8 m (4 x 6 ft.) allow the chamber parts to be hand-carried through narrow pathways or on stairs to build an AC1224 in areas where traditional full-size chambers cannot go. Furthermore, all AC1224 antenna test chambers are assembled from the inside out and require almost no workspace around them during assembly, making this test chamber ideal for labs, offices and basements with highly constrained building space.

Like the standard 12 x 12 ft. modular AC1224-360, the AC1224 chamber can be ordered with extended depth by adding more modules. The chambers ship with 115 mm (4.5 in.), 300 mm (12 in.) absorbers or a mix of both. These chambers are ideally suited for radar, microwave and mmWave antenna test applications.

The AC1224-360 is available immediately and ships worldwide. The DUO and UNO positioners from mmWave Test Solutions all fit the AC1224 chambers. Visit the mmWave Test website for further technical details on chambers and positioners.

mmWave Test Solutions
Copenhagen, Denmark
www.mmwavetest.com

European Synthetic Aperture Radar Operates in X-Band

SAR-AESA-X, a pulsed radar imaging solution operating in X-Band, integrates advanced synthetic aperture radar (SAR) signal processing and AESA phased array technology. With an operating bandwidth of 2 GHz in X-Band and a pulse repetition frequency range from 100 kHz down to 10 kHz, the SAR-AESA-X produces an effective isotropically radiated power of 82 dBm and achieves a fine range and cross-range imaging resolution of 20 cm. With antenna dimensions of 45 x 25 x 20 cm and a total system weight of 20 kg, the SAR-AESA-X is compact and lightweight and draws 300 W of power.

Besides the technical specifications, the SAR-AESA-X sensor can be used in a wide range of application scenarios. The SAR-AESA-X targets applications from intelligence gathering and reconnaissance to surveillance and monitoring. Its capabilities allow the possible applications to extend to the detection of underground explosives, combating drug trafficking and other illegal activities, search and rescue operations, forest fire monitoring, disaster scenarios, emergency response and geographic mapping.

In addition to its adaptability to many applications, the SAR-AESA-X covers imaging ranges of up to 50 km. It offers varying image resolution modes from 3 x 3 m down to 0.2 x 0.2 m, with adaptive swath settings at 1 km, 5 km, 10 km and 20 km. It operates in strip-map, spotlight and GMTI modes and features electronic beam stabilization to ensure stable imaging even in dynamic environments. The SAR-AESA-X also excels in scenarios where GPS reception is not available, providing robustness in harsh environments.

Besides radar antennas, PIDSO focuses on all types of antennas, like blades and buttons and RF systems like tracking antennas and smart arrays.

PIDSO GmbH
Vienna, Austria
pidso.com/en/products/pidso-antennas

COMSOL Releases Version 6.2 of COMSOL Multiphysics®

COMSOL announced the release of COMSOL Multiphysics® version 6.2, adding data-driven surrogate model functionality for efficient standalone simulation apps and multiphysics-based digital twins.

COMSOL
www.comsol.com

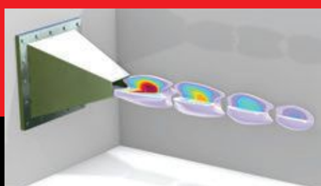

IW Moves Microwave Products Division

Insulated Wire Inc. (IW) announced that the Microwave Products Division has relocated to Ronkonkoma, N.Y. Now close to their headquarters at Bayport, N.Y., the IW Microwave Products team will continue to provide high-quality and high performance RF/microwave cable assemblies and accessories.

Insulated Wire Inc.
https://insulatedwire.com

INSULATED WIRE INCORPORATED

Keysight Opens Technology Center in Germany

Keysight announced the grand opening of their brand-new Technology Center in Germany. This state-of-the-art facility is set to further enable electric vehicle test solutions by providing cutting-edge testing equipment to meet the growing demands of the automotive industry.

Keysight Technologies, Inc.
www.keysight.com

MegaPhase 25TH ANNIVERSARY

MegaPhase Celebrates 25 Years of Excellence

Over the past 25 years, MegaPhase has achieved numerous milestones, culminating in 22 major product lines, five U.S. patents, 19 space programs and over 50 military programs.

MegaPhase
www.megaphase.com

Passive Plus Releases New Catalogs & Brochures

Passive Plus (PPI) has launched a series of catalogs and brochures, representing PPI's complete product offerings. Individual component information, such as series datasheets, S-Parameter data and Modelithics' Modeling Data, can also be found on the website.

Passive Plus
www.passiveplus.com

Pixus Releases New Products & Services Brochure

Pixus announced a new brochure for SOSA aligned/OpenVPX platforms and other key product lines. The new brochure includes backplanes, enclosure platforms, instrumentation cases, specialty boards/modules, handle and panel sets and other components.

Pixus Technologies
www.pixustechnologies.com

NEW PRODUCTS

FOR MORE NEW PRODUCTS, VISIT WWW.MWJOURNAL.COM/BUYERSGUIDE
FEATURING VENDORVIEW STOREFRONTS

DEVICES/ COMPONENTS/MODULES

Single Pole 25 Throw Solid-State Switch

American Microwave Corporation offers Model Number: MSN-MSN-0518-25T-30DB-HERM-1JV, a single pole 25 throw solid-state switch. The switch is a new and custom design by AMC. This model has a frequency range of 0.5 to 18 GHz. It also has an insertion loss of 7.5 dB maximum, an isolation of 60 dB minimum and measures 13.25 × 2.65 × 0.40 in.

American Microwave Corporation
www.americanmic.com

HP Series Filters

KYOCERA AVX has released a new series of miniature highpass thin-film filters engineered to provide excellent high frequency performance in a variety of space constrained microwave and RF applications in the telecommunications, automotive, consumer electronics and military markets. The new HP Series highpass thin-film filters are based on proven multilayer integrated thin-film technology that enables the quick adjustment of RF parameters and development of custom filters.

Kyocera AVX
www.kyocera-avx.com

Surface-Mount 90° Hybrid

VENDORVIEW

Mlcable released the new 0.5~6 GHz high power surface-mount 90-degree hybrid. It has low insertion loss, low VSWR and 100 W power handling capability with excellent stability and heat dissipation ability in a small package. It is suitable for power amplifier, power combining network, antenna feed network, modulator and phase shifter applications.

Mlcable
www.micable.cn

Wide Notch Bandwidth – Band Reject Filters

Micro Lambda Wireless Inc. has developed a new yttrium iron garnet based filter that provides superior notch depths over the 6 to 18 GHz and 6 to 20 GHz frequency ranges. This new filter provides a tunable notch of 80 MHz minimum at 40 dBc down. The 3 dB bandwidth is 250 MHz maximum with typical passband insertion loss of 2.2 dB. YIG-based notch filters for EW and ECM.

Micro Lambda Wireless Inc.
www.microlambdawireless.com

5 to 2000 MHz, 12 dB Coupler with Low Loss

The MRFCP8752 is a broadband 75 Ω coupler that provides excellent performance for signal level monitoring in DOCSIS 4.0 applications. Utilizing a 12 dB coupling factor, this component provides CATV system designers a low loss < 1.1 dB, flatness of ±0.5 dB and excellent return loss of 22 dB over most of the band. The MRFCP8752 is in a standard surface-mount package (.250 × .280) with standard pinouts for "drop in" performance. Contact MiniRF at 408-228-3533 for additional technical information, pricing and availability. Smaller packaging options may also be offered.

MiniRF
www.minirf.com

Broadband Baluns

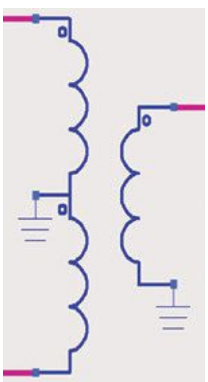

A balun is one of the primary components used in mmTron high speed converter interfaces to transform between differential and single-ended signals. When we surveyed the market for a balun to use, we were not satisfied with the performance, size and physical layout of what we found. So, we designed our own MMIC baluns and have added them to our growing list of products. We think they set new records for bandwidth, insertion loss and amplitude/phase matching.

mmTron
www.mmtron.com

RF Resistors & Loads

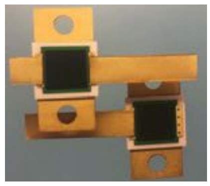

Remtec now offers RF resistors and loads up to 6 GHz to handle power up to 500 W, while maintaining excellent thermal properties. Produced using thick film screen-printed resistors on ceramic substrates — including alumina, aluminum nitride or beryllium oxide — based on customer designs, frequency range, configuration and thermal dissipation goals. Remtec brings 35+ years of cutting-edge thick film processing, screen printing, plating and laser trimming experience to the task and is well-positioned to help bring overseas production (re-onshoring) to the U.S.

Remtec
www.remtec.com

24.25–30.5 GHz RF Front-End

VENDORVIEW

Richardson RFPD Inc. announced the availability and full design support capabilities for a new RF front-end module from United Monolithic Semiconductors. The CHC6054-QQA is a high-power front-end (HPFE) incorporating transmit and receive paths and a transmit/receive switch. It operates in the 24.25 to 30.5 GHz frequency range and is designed for telecom radio systems applications. The new HPFE typically exhibits an Rx gain of 18 dB with a low noise figure of 3.2 dB, and a Tx gain of 28 dB with +31 dBm saturated output power.

Richardson RFPD Inc.
www.richardsonrfpd.com

CABLES & CONNECTORS

Remoting Over Fiber

Antenna remoting over fiber enables greater flexibility to locate an antenna away from a radio head. Coax cables or waveguides have RF losses and are cumbersome to install. RF over fiber enables "virtual cable" installation over flexible, easily deployed fiber. Such an antenna remoting solution was deployed and validated by the US Navy. The Common Data Link (CDL) is a secure communications protocol, established by the U.S. DOD, for transporting signals, intelligence and imagery.

Optical Zonu
www.opticalzonu.com

NewProducts

AMPLIFIERS

100 W SSPA

VENDORVIEW

Exodus AMP2053B-1 is a rugged solid-state power amplifier (SSPA) incorporating advanced technology for 6 to 12 GHz high-power testing applications. broadband (C- and X-Bands), class A/AB design for all industry standards, > 100 W minimum with 50 dB gain. Excellent power/gain flatness, forward/reflected power monitoring in both dBm and watts, VSWR, voltage/current and temperature sensing for superb reliability and ruggedness. The nominal weight is 27 kg in a compact 4U chassis, 7 H × 19 W × 22 D in.

Exodus Advanced Communications
www.exoduscomm.com

5G Amplifiers

VENDORVIEW

Fairview Microwave introduces its ground-breaking series of 5G amplifiers. Tailored to cater to the demands of modern projects, these amplifiers encapsulate the best of innovative technology, ensuring top-tier performance across the 5G spectrum without straining budgets. The all-new amplifiers come in compact coaxial packages, addressing a vast frequency spectrum ranging from 10 MHz up to 8 GHz.

Fairview Microwave
www.fairviewmicrowave.com

5 GHz MMIC LNA

VENDORVIEW

Mini-Circuits' model TSS2-53LNB+ is a low noise amplifier (LNA) with bypass switching for high-level input signals. The MMIC amplifier has 1.3 dB or better typical noise figure from 0.5 to 5.0 GHz with 21 dB typical gain at midband. A good fit for 5G backhaul radio systems, the amplifier features high dynamic range with typical third-order intercept of +47 dBm IP3 in bypass mode. The 50 Ω amplifier is supplied in an eight-lead QFN style package measuring 2 × 2 mm.

Mini-Circuits
www.minicircuits.com

Amplifier SLKaQ-38-15

Spacek Labs' amplifier, model SLKaQ-38-15 has excellent performance characteristics from 26.5 to 50 GHz. Ideal for 5G frequency range 2 applications. With a noise figure of 3.8 dB and output P1dB of 15 dBm typical, the unit has a nominal gain of 38 dB minimum, 43 dB typical. VSWR is 1.5:1 typical while using 2.4 mm connectors. Bias voltage +8 to +12 VDC at 0.3A. Without a heat sink, the amplifier size is 1.13 × 0.93 × 0.31 in.

Spacek Labs, Inc.
www.spaceklabs.com

SOURCES

Tight Stability Oscillators

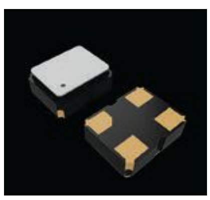

Abracon's ASxTDV Continuous Voltage™ tight stability oscillators (XOs) are an expansion of the Continuous Voltage™ Oscillators family and are cutting-edge electronic components that have found their way into a wide range of applications across various industries. These oscillators provide tight stability and precise frequency control, making them indispensable

New**Products**

in today's technology-driven world. These quartz-based oscillators offer precise timing with low jitter and phase noise, thanks to their cutting-edge small form factor ASIC technology.
Abracon
www.abracon.com

ANTENNAS

GNSS and GPS Patch Antennas

Amphenol RF introduces embedded GNSS and GPS antennas into their growing antenna solutions. These passive and active internal antennas offer a lightweight, compact option for applications that rely on accurate location detection for navigational purposes. Ceramic antennas such as these can be surface mounted to a printed circuit board or connectorized for better positioning. GNSS and GPS antennas are designed to receive radio signals transmitted on specific frequencies by satellites. GNSS antennas use signals from global navigation satellites whereas GPS antennas utilize primarily North American satellites.
Amphenol RF
www.amphenolrf.com

3D Mobile PRO 3-Axis Testing Antenna

Saelig Company Inc. has introduced the Aaronia IsoLOG 3D Mobile PRO three-axis testing antennas for RF measurements up to 8 GHz. The 3D Mobile PRO is an extremely light and small isotropic antenna, compatible with any spectrum analyzer, for making X/Y/Z axis RF measurements, or in chop-mode, to make rotating measurements around an X/Y/Z axis, for frequencies up to 8 GHz. Ready for rapid use, it offers a plug and play solution for 3D measurements in fast time frames.
Saelig Company Inc.
www.saelig.com

TEST & MEASUREMENT

60 GHz Ranging Sensor

VENDORVIEW

Model SSP-60318-D1 is an E-Band ranging sensor for medium-range measurements of a moving target's speed, distance and direction of travel. Operating from 59.75 to 60.25 GHz, the sensor module has a single transmit/receive waveguide port. The transmitted power is +18 dBm and the receiver conversion loss is 14 dB. Using a supply voltage of +8 VDC at 750 mA, the sensor includes a varactor-tuned oscillator, isolator, amplifier, directional coupler, circulator and balanced I/Q mixer.
Eravant
www.eravant.com

Calibration Kits and Extensions

VENDORVIEW

Pasternack announced a series of waveguide calibration kits expertly designed for WR-90, WR-75, WR-62, WR-34, WR-28 and WR-22. They offer features including waveguide-to-coax adapters, matched waveguide terminations and multiple precision waveguide sections. To meet customers' varied requirements, optional waveguide straight sections have been introduced, available for separate procurement. With choices between robust aluminum and sturdy brass constructions based on waveguide dimensions, Pasternack ensures longevity and optimal performance.
Pasternack
www.Pasternack.com

MXO 5 Next-Generation Oscilloscope

VENDORVIEW

Rohde & Schwarz presents the R&S MXO 5 oscilloscopes, available with four or eight channels. Building on next-generation MXO-EP processing ASIC technology developed by Rohde & Schwarz and introduced with the R&S MXO 4, the new eight-channel R&S MXO 5 oscilloscopes take measurement performance to the next level.
Rohde & Schwarz
www.rohde-schwarz.com

FEATURED e-Books

Check out this month's featured eBooks, online at
mwjournal.com/ebooks

RF and Microwave Circuit Design: Theory and Applications

By Charles E. Free and Colin S. Aitchison

RF and Microwave Circuit Design is a textbook that truly stands out for anyone delving into the realm of microwave engineering or working as a practicing professional. It's more than just a book; it's a comprehensive guide that is exceptionally useful for teaching senior-level undergraduate or first-year graduate courses in microwave engineering circuits and systems.

One of the standout features of this book is its unwavering focus on microwave circuit design without becoming entangled in the complexities of electromagnetic theory. The book provides a thorough treatment of microwave engineering topics, covering everything from transmission lines to modern microwave measurements, making it a well-rounded resource.

The derivation of the Smith Chart is explained with utmost clarity in Chapter 1. The inclusion of several practical examples demonstrating the use of the Smith Chart cements its importance as a teaching tool. This book is a goldmine for educators, enabling them to offer practical insights to their students. It not only explains concepts but also challenges learners to apply their knowledge.

For those working in planar circuit design, this book is a treasure trove. Its practical orientation makes it an ideal resource for engineers and students looking to excel in the field of microwave circuit design. I found the chapter dedicated to modern microwave measurements to be excellent. It covers microwave connectors, probes and VNAs, making it an indispensable guide for students and professionals engaged in microwave measurements. The book does an excellent job covering all common microwave components including amplifiers, filters, circulators, control circuits and oscillators. Many aspects of microwave receiver design are also covered in the final chapter.

When evaluating a textbook for the purposes of a microwave engineering course, it must be compared to David Pozar's *Microwave Engineering*. I find that *RF and Microwave Circuit Design* leans toward a more practical approach. It's grounded in the requirements of making a successful modern-day microwave engineer and includes additional topics highly relevant to contemporary microwave engineering practice.

In conclusion, *RF and Microwave Circuit Design* is a gem for educators, students and professionals in microwave engineering. It comes highly recommended for teaching senior-level undergraduates and first-year graduate students, offering a practical perspective that's hard to find in other textbooks. The companion website with teaching slides is the cherry on top.

ISBN 13: 978-1-119-11463-5
528 pages
To order this book, contact:
Wiley (September 2021)
wiley.com/en-us

Advertising**Index**

Sales Representatives

Eastern and Central Time Zones
Carl Sheffres
Group Director
(New England, New York, Eastern Canada)
Tel: (781) 619-1949
Cell: (781) 363-0554
csheffres@horizonhouse.com

Michael Hallman
Associate Publisher
(NJ, Mid-Atlantic, Southeast, Midwest, TX)
Tel: (301) 371-8830
Cell: (781) 363-0338
mhallman@mwjournal.com

Pacific and Mountain Time Zones
Brian Landy
Western Reg. Sales Mgr.
(CA, AZ, OR, WA, ID, NV, UT, NM, CO, WY, MT, ND, SD, NE & Western Canada)
Tel: (831) 426-4143
Cell: (831) 713-9085
blandy@mwjournal.com

Submitting ad material?
Visit: www.adshuttle.com/mwj
(866) 774-5784
outside the U.S. call
+1-414-566-6940

Ed Kiessling
(781) 619-1963
ekiessling@mwjournal.com

International Sales
Richard Vaughan
International Sales Manager
Tel: +44 207 596 8742
rvaughan@horizonhouse.co.uk

Zena Coupé
Tel: + 44 207 1506737
Cell: +44 7887 874074
zena@expomedia.biz

Germany, Austria, and Switzerland (German-speaking)
Brigitte Beranek
Tel: +49 7125 407 31 18
bberanek@horizonhouse.com

France
Gaston Traboulsi
Tel: +44 207 596 8742
gtraboulsi@horizonhouse.com

Korea
Jaeho Chinn
JES MEDIA, INC.
Tel: +82 2 481-3411
corres1@jesmedia.com

China
Shanghai
Linda Li
ACT International
Tel: +86 136 7154 0807
lindal@actintl.com.hk

Wuhan
Phoebe Yin
ACT International
Tel: +86 134 7707 0600
phoebey@actintl.com.hk

Shenzhen
Annie Liu
ACT International
Tel: +135 9024 6961
anniel@actintl.com.hk

Beijing
Cecily Bian
ACT International
Tel: +86 135 5262 1310
cecilyb@actintl.com.hk

Hong Kong
Floyd Chun
ACT International
Tel: +852 28386298
floydc@actintl.com.hk

Taiwan, Singapore
Simon Lee
ACT International
Tel: +852 2838 6298
simonlee@actintl.com.hk

Japan
Katsuhiro Ishii
Ace Media Service Inc.
Tel: +81 3 5691 3335
amskatsu@dream.com

Corporate Headquarters: 685 Canton Street, Norwood, MA 02062 • Tel: (781) 769-9750

PROPRIETARY TECHNOLOGIES

LTCC Filter Innovations

The Industry's Widest Selection

LEARN MORE

Ultra-High Rejection

- Rejection floor down to 100+ dB
- Excellent selectivity
- Built-in shielding
- 1812 package style
- Patent pending

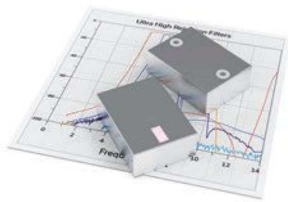

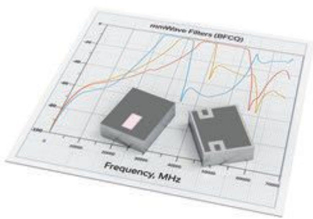

mmWave Passbands

- Passbands to 50+ GHz
- The industry's widest selection of LTCC filters optimized for 5G FR2 bands
- Growing selection of models for Ku- and Ka-band Satcom downlink
- 1812 & 1008 package styles

Substrate Integrated Waveguide

- First commercially available SIW LTCC filter in the industry
- Narrow bandwidth (~5%) and good selectivity
- Internally shielded to prevent detuning
- 1210 package style

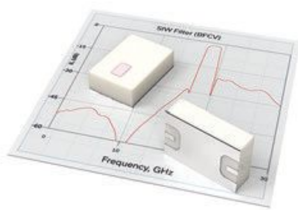

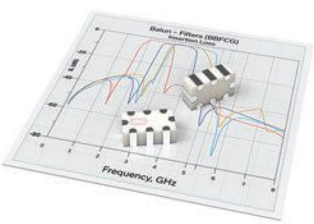

Integrated Balun-Bandpass Filters

- Combine balun transformer and bandpass filter in a single device
- Saves space and simplifies board layouts in ADCs, DACs and other circuits
- 1210, 1008 & 0805 package styles

Mini-Circuits®

FABS and LABS

Antenna Research Associates: When Every Second Counts




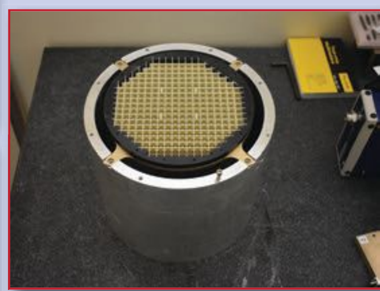

Antenna Research Associates (ARA) has a six-decade long history of producing many of the world's most notable antennas, including the first to be placed atop the Empire State Building in New York City. R. Wayne Masters and John H. Dunlvay who founded the Laurel, Md., company in 1963, were industry pioneers who made significant contributions to advancing antenna and electromagnetic systems technology throughout their careers.

ARA's first products were small antennas for long-range, high frequency communications, produced for a customer base surrounding the Fort Meade area of Maryland. Building upon early successes, the company quickly became a forerunner in broadband antenna systems for surveillance, spectrum management and TEMPEST testing. In the 1970s and 1980s, ARA added new capabilities and products, including VSAT antennas, satcom products, military and commercial radar systems and antenna systems for mobile and tactical communications. In the 1990s, ARA's product expansion focused on military products including high gain horn arrays, high gain broadband omnidirectional antennas for jamming, body wearable antennas and quick deployment antennas.

In 2014, ARA's current CEO Logen Thiran, along with a group of institutional investors, began accelerating the company's growth once again. Through a combination of organic growth and acquisition over the past 10 years, ARA has expanded to more than 220 employees in four ISO 9001:2015-certified fully NIST-compliant facilities totaling nearly 150,000 square feet in three states. The company has remained true to its roots with a customer mix that is 95 percent defense, five percent commercial, along with 95 percent U.S. and five percent international companies.

Thiran's ultimate plan for ARA, to become a leading supplier of C5ISR products and technologies to the aerospace and defense community, is nearing the finish line with the recent acquisitions of two Massachusetts companies, AQYR Technologies and SI2 Technologies. The innovative technology of AQYR and SI2 added product offerings and capabilities to ARA have expanded its communications and electromagnetic systems expertise and product portfolios for a broader set of target markets.

ARA has evolved far beyond its legacy antenna products and provides advanced apertures integrating signature mitigation technologies, as well as a wide range of advanced arrays, including AESA and PESA systems. ARA's expertise also extends to terminals that incorporate antennas with a portfolio of multi-band, multi-mission VSAT terminals. The current market verticals for ARA's integrated solutions are satcom, radar, electronic warfare and milcom; but the company is steadily growing and pursuing new opportunities in hypersonic, advanced aircraft, missiles and munitions, counter UAS-technologies and space applications.

The key benefit to customers and stakeholders is that while ARA is rapidly expanding its product portfolio and broadening its target market, it remains a non-traditional contractor with a small-business, entrepreneurial mindset that focuses on the immediate and long-term needs of its customers. It is agile and can produce both small and large quantities of customized products. An example, on one end of the vertical integration chain, ARA now has internal additive manufacturing capabilities that enable 2D and 2.5D printing on flexible substrates and curved surfaces. On the other end of that chain, ARA maintains multiple outdoor test ranges and anechoic chambers with test capabilities from 20 MHz to 50 GHz.

Warfighters know that every second counts, and ARA's versatility and unique mix of economical high volume production, groundbreaking technology development and subsystem integration is ready to answer the call.

https://ara-inc.com

ECO 150XA-6
REAL-TIME SPECTRUM ANALYZER
Tx
Rx1

DIGITAL RF POWER METERS

Optimal Accuracy ✦ 40 dB Dynamic Range ✦ No Calibration Required

Simultaneously Monitor: Forward Power, Reverse Power, Load VSWR, & Temperature

ACCURACY

- Multi-Octave Solutions provide accuracy within ± 5% of a Customer Lab Standard (± 2% Typical).

CALIBRATION

- No On-Site Calibration Required.
- Calibration Routine completed internally to each Power Sensor.
- Traceable to National Institute of Standards & Technology (NIST).

ALARMS & RELAYS

- Alarm Thresholds of Forward & Reverse Power.
- Full VSWR Monitoring/Alarm Capability.
- Full Temperature Monitoring/Alarm Capability.
- Six General Purpose Inputs & 2 Form-C Relays to External Devices

FIRMWARE

- Windows Application includes an ergonomic tab-based access system for easy setup and operation of the Power Meter.
- Multi-Window Display for access to up to five Meters on screen.
- VSWR Indication & Reflected Power on main Power Sensor display.
- MIB File available for use with SNMP software.
- LabVIEW Driver Available.

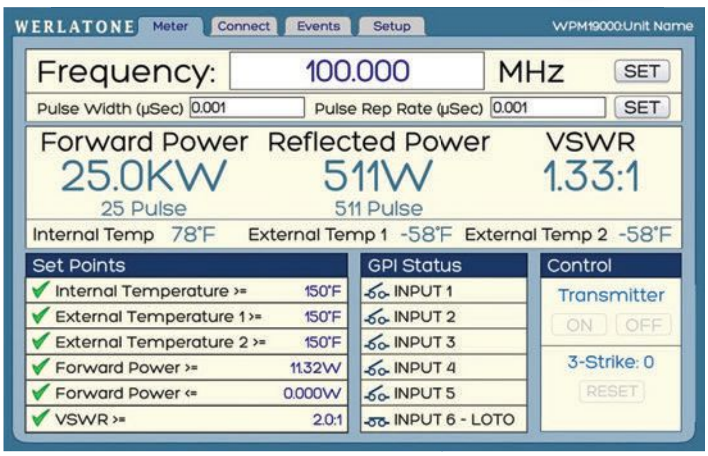

Werlatone, Inc. 17 Jon Barrett Road Patterson, NY 12563 845-278-2220 sales@werlatone.com www.werlatone.com